

Doctoral Thesis

**Development of single-cell analysis systems
for discerning neural circuits
in the mammalian brain**

Wenshu Luo

Doctor of Philosophy

Department of Genetics

School of Life Science

The Graduate University for Advanced Studies (SOKENDAI)

Department of Developmental Genetics

National Institute of Genetics

2015

Contents

Abbreviations.....	1
Summary.....	4
Introduction	7
Results.....	9
Discussion	24
Experimental procedures	32
Acknowledgements	49
References	51
Figure legends	58
Figures	72

ABBREVIATIONS

α 2-Chn: α 2-isoform of α -chimaerin

β -gal: β -galactosidase

AAV: adeno-associated virus

CST: corticospinal tract

DAPI: 4',6-diamidino-2-phenylindole

DG: dentate gyrus

DiI: 1,1'-dioctadecyl-3,3,3',3'-tetramethylindocarbocyanine perchorate

DIO: double-floxed inverse open reading frame

E: embryonic day

FSF: FRT-STOP-FRT

GAP43: growth associated protein 43

IUE: in utero electroporation

KD: knockdown

KI: knock-in

KO: knockout

L: layer

LSL: loxP-STOP-loxP

MADM: mosaic analysis with double markers

mir30: microRNA30

nls: nuclear localization signal

NGS: normal goat serum

NMDAR: N-methyl-D-aspartate receptor

NS: non-significant

OE: overexpression

P: postnatal day

PASME: promoter-assisted sparse-neuron multiple-gene labeling using in utero electroporation

PB: phosphate buffer

PBS: phosphate buffered saline

PCR: polymerase chain reaction

PFA: paraformaldehyde

PSD-95: postsynaptic density protein 95

RNAi: RNA interference

RNZ: Rosa26-loxP-STOP-loxP-nlsLacZ

RSR: Rox-STOP-Rox

SEM: standard error of the mean

shRNA: small hairpin RNA

SLICK: single neuron labeling with inducible Cre-mediated knockout

SnRFP: Supernova RFP

SnAmcyan: Supernova Amcyan

SnGFP: Supernova GFP

TRE: tetracycline response element

TALENs: target transcription activator-like effector nucleases

tTA: tetracycline transactivator

XFP: red, green, yellow, or cyan fluorescent proteins

SUMMARY

The assembly of neural circuits that is responsible for higher brain function relies on tightly interconnected neurons, which are diverse in molecular, morphological, physiological and functional properties. Approaches for imaging isolated single neurons would help researchers to characterize the complex organization of neural circuits in the mammalian brain. For this purpose, the Supernova system was developed (Mizuno, Luo et al., 2014). This system consists of two vectors: tetracycline response element (TRE)-Cre and CAG-loxP-STOP-loxP-RFP-ires-tTA. In the cells transfected with the Supernova vector set, leakage of TRE drives the weak expression of Cre and, subsequently, RFP and tTA in a very small population of cells. Then only in these cells, the expression of RFP was facilitated by the positive feedback of the tTA-TRE cycles. I evaluated sparseness and brightness of the Supernova-mediated labeling. I quantitatively examined the sparseness of the Supernova labeling and showed that Supernova vectors introduced by in utero electroporation at embryonic day (E) 14.5 labeled less than 10% of transfected neurons in the cortex at postnatal day 16. I also revealed that more than half of Supernova-labeled neurons exhibited high intensity of neuronal labeling, by which I could clearly observe the whole dendritic morphologies.

In the subsequent studies, I refined and expanded the Supernova system in several aspects. First, I developed the Flpe/FRT-based Supernova system, which consists of TRE-Flpe and CAG-FRT-STOP-FRT-RFP-ires-tTA. By comparing the Flpe/FRT-based and original Cre/loxP-based Supernova systems in cortical neurons transfected, I found that the Flpe/FRT-based system shows much more excellent properties in sparseness and brightness than the Cre/loxP-based one. Importantly, the Flpe/FRT-based system

achieved neuronal labeling with essentially no background (few darkly labeled neurons). By taking advantage of these features, I was able to image the whole cellular morphology of a single callosal projection neuron in the intact young adult mouse brain. In addition to the Flpe/FRT-based Supernova system, I constructed a Dre/Rox-based Supernova system. I showed that both of these two systems could be used for neuronal labeling even in Cre expressing transgenic mice. Second, I developed an adeno-associated virus (AAV)-based Supernova system and successfully used it to visualize isolated single hippocampal CA1 pyramidal neurons. This system makes the Supernova labeling even more flexible to use than the in utero electroporation-based system, because the AAV-based system has no brain region limitation and is suitable for labeling in cells in elder mice.

The original Cre/loxP-based Supernova system was designed to enable labeled-cell-specific gene knockout when it is combined with a floxed mouse line, in which the essential region of the target gene was flanked by two loxP sites. To evaluate the efficiency, I transfected the Cre/loxP-based Supernova vectors into hippocampal CA1 neurons in $\alpha 2$ -Chimaerin ($\alpha 2$ -Chn) flox/flox mice by in utero electroporation. I found that almost all of Supernova-labeled neurons showed a deletion of $\alpha 2$ -Chn protein expression and this deletion was observed only in Supernova-labeled neurons. These results indicate the high-efficiency of the Supernova system for labeled-cell-specific knockout of endogenous genes.

In order to save time and efforts for generating floxed mice, methods that can manipulate target gene expression in individual cells in wild-type mice would be required. For the purpose, I combined the RNA interference technique with the Supernova system. By electroporation of constructed Supernova-mediated expression vectors carrying small hairpin RNA against target genes, I efficiently reduced the

expression level of reporter genes in sparsely labeled cortical neurons in two lines of Cre-reporter mice. Moreover, I also adapted target transcription activator-like effector nuclease (TALEN)-based genome editing technology to Supernova system and successfully inhibited the expression of an endogenous gene, $\alpha 2$ -Chn, in wild-type hippocampal CA1 pyramidal neurons. To my knowledge, this is the first report for manipulation of an endogenous gene in identified individual cells in wild-type individuals.

In summary, the original and improved Supernova systems are general methods to label a sparse population of cells with high fluorescent intensity and essentially little background, and enables simultaneous gene manipulation in these labeled cells. Thus, Supernova systems are promising tools to elucidate the cellular and molecular mechanisms underlying neural circuit development and function at single cell levels.

INTRODUCTION

The neural circuits in the mammalian central nervous system possess an intricate pattern. Each neural circuit is composed of densely packed neurons, which are diverse in molecular, morphological, physiological and functional properties. During development, these varieties of neurons are interconnected with each other to form neural circuits that are responsible for higher brain function in adulthood. These processes are sophisticated and are considered to be results from the interplay between intrinsic genetic programs and extracellular signals (Parrish et al., 2007; Scott and Luo, 2001; Wong and Ghosh, 2002).

For understanding the cellular mechanisms underlying the neural circuit formation, approaches for imaging neurons at a single cell level are imperative. Historically, many approaches for observing the cellular morphologies of individual neurons have been used. Golgi staining, a silver staining method that proceeds on fixed tissue, enables the first systematic analysis of the organization of nervous system at a single cell level (Golgi, 1873). Methods for observing the cellular morphologies of single neurons can also be achieved by intracellular injection of tracers, such as horseradish peroxidase (HRP), neurobiotin or biocytin and fluorescent dyes (Dacey and Lee, 1994; David and Aguayo, 1981; Honig and Hume, 1989; Horikawa and Armstrong, 1988). Later, taking advantage of the transgenic mouse technology, genetically directed neural labeling was developed based on selective expression of a fluorescent protein under the control of a cell-type specific promoter which restricts the labeling in a defined small subset of neurons (Feng et al., 2000). Another general strategy for sparse labeling relies on selective transfection of genes encoding for fluorescent proteins into a sparse population of neurons by in utero electroporation (IUE) or viral infection (Ako et al., 2011; Dhande et al., 2011; Kim et al., 2013; Kim et al., 2012). Either of these

approaches is suffered by its own limitations (see discussions) and a more flexible tool, which enables sparse and bright neuron labeling, is required.

To understand the molecular mechanisms underlying the development, maintenance and plasticity of neural circuits, genetic manipulation in mice, such as generating global knockout mice and conditional knockout mice, has become the most popular way (Iwasato et al., 2000; Iwasato et al., 1997). However, these approaches usually accompany with disruption of neural circuits in a large scale. Genetic analysis on single neurons that are surrounded by the masses of wild-type cells would help researchers to identify the cell-autonomous function of a target gene. The observation of the competition between mutant and wild-type cells in dynamic biological processes, such as dendritic refinement of cortical neurons during the postnatal development (Mizuno et al., 2014), would further facilitate elucidation of the cellular and molecular mechanisms that underlie neural circuit formation. Recently, two systems were reported that allow the generation of single isolated mutant cells, which are simultaneously labeled by fluorescent proteins for investigating their morphology and physiological properties among the mass of wild-type cells (Young et al., 2008; Zong et al., 2005). Both of these two systems are based on generation of transgenic mice, which is time-consuming and inflexible for using (e.g. one cannot change the color of fluorescent protein easily) and has limitation of utilization.

Here, I report a novel system, termed “Supernova”, which enables 1) single-cell labeling with high fluorescent intensity, little background, no cell-type specificity and no area limitation, and 2) labeled cell-specific gene knockout in floxed transgenic mouse as well as labeled cell-specific gene knock-down or genome editing in wild-type mice.

RESULTS

The Supernova system enables high intensity single-cell labeling

One of my primary goals is to develop a system which enables visualization of the detailed cellular morphology of an isolated single neuron in the mammalian brain during postnatal development. With this goal, the Supernova system was developed (Mizuno et al., 2014). This system consists of two vectors: tetracycline response element (TRE)-Cre (TRE-Cre) and CAG-loxP-STOP-loxP-RFP-ires-tTA-WPRE (LSL-RFP-tTA) (Figure 1A, upper panel). The Supernova system relies on stochastic leaky gene expression of TRE in the absence of tetracycline transactivator (tTA) stimulation. The strategy is that, in the cells transfected with these vector set, leakage of TRE drives the weak expression of Cre and, subsequently, tTA in a very small population of cells. Thus, only in these cells, the expression of RFP is facilitated by the positive feedback of the tTA-TRE cycles (Figure 1B).

To examine the efficiency of tTA-TRE positive feedback, I compared the sparseness and brightness of cells labeled by Supernova RFP (SnRFP) and those of cells labeled by SnRFP Δ tTA (Figure 2), in which the CAG-loxP-STOP-loxP-RFP-WPRE (LSL-RFP) vector was used instead of the LSL-RFP-tTA vector. I introduced either of SnRFP and SnRFP Δ tTA vectors into layer 4 (L4) cortical neurons by IUE at E14.5 (Figure 2B). The CAG-GFP vector was co-transfected to label the transfected cells. I made coronal sections from postnatal day 16 (P16) brains and took the images of the sections using confocal microscope with low laser power to avoid the saturation of both RFP and GFP signals of labeled cell bodies (Figure 2B). First, I counted numbers of RFP-positive and GFP-positive neurons, and found that only $8.18\% \pm 0.92\%$ (n=4 mice) and $8.60\% \pm 1.21\%$ (n=4 mice) of GFP-labeled neurons (transfected neurons) expressed RFP

in SnRFP and SnRFP Δ tTA labeling, respectively (Figure 2C). These results showed that both SnRFP and SnRFP Δ tTA labeling achieved similar sparse labeling. Thus, the sparseness of Supernova labeling was primarily determined by the efficacy of initial TRE leakage-induced Cre expression. Transfection of the LSL-GFP-tTA vector with the CAG-GFP vector produced only GFP positive neurons (data not shown), confirming that the RFP expression by LSL-RFP-tTA is Cre-dependent. I next compared the brightness of RFP labeling. I quantified the RFP intensity of cell bodies of SnRFP and SnRFP Δ tTA labeled neurons. The intensity of GFP signals in the same neurons was used to normalize the electroporation efficiency (Figure 2B). I found that the average brightness of cell bodies of RFP positive neurons labeled by the SnRFP (n = 86 cells, 4 mice) was significantly higher than that of RFP positive neurons labeled by SnRFP Δ tTA (n = 124 cells, 4 mice; p = 0.041) (Figure 2D). In addition, I also evaluated the brightness of RFP labeled neurons based on how much their dendrites would be visible. I took the images of the same sections again using relatively high laser power to visualize the dendritic morphology of SnRFP and SnRFP Δ tTA labeled neurons (Figure 3A). I quantified the ratio of RFP^{high} neurons, in which whole dendritic morphology can be clearly identified by RFP (Figure 3A arrows). I found that 53.69% \pm 4.47% (n= 3 mice, 65 cells in total) of the SnRFP-labeled neurons was RFP^{high} neurons. By contrast, in the neurons labeled by SnRFP Δ tTA, the percentage of RFP^{high} cells was significantly lower (24.87% \pm 1.33%, p<0.01, n=3 mice, 79 cells in total). These results indicated that the tTA-TRE cycles amplified the expression of RFP (Figure 2D, 3B).

I examined the developmental time course of Supernova-mediated fluorescent neural labeling. I co-transfected SnRFP and CAG-GFP vectors into cortical neurons by IUE at E14.5 and the brains were fixed at E16.5, P0, P4 and P8 (Figure 4). The expression of SnRFP was already observed two days after

transfection (at E16.5). The leading processes of the migrating neurons in the developing cortex could be observed (Figure 4A, arrow). I quantified the ratio of SnRFP-positive neurons to GFP positive neurons at P0, P4 and P8. The ratios were similar, with $4.50\% \pm 0.40\%$ (n=3 mice) at P0, $4.73\% \pm 0.33\%$ (n=4 mice) at P4 and $5.63\% \pm 0.75\%$ (n=5 mice) at P8 (Figure 4B, 4C).

In order to increase the color variation of Supernova labeling, genes encoding other fluorescent proteins such as Amcyan and GFP (together termed XFPs) were cloned into Supernova vector sets (Figure 5A). The cortical neurons labeled by different fluorescent proteins are shown in Figure 5B, 6, 7. Briefly, I delivered Supernova XFPs into neurons in distinct cortical layers through IUE at different embryonic stages. For the transfection control, CAG-RFP or CAG-GFP vector, which was widely used for regular labeling, was co-transfected (Figure 5B, 6, 7). Figure 5B showed the images of coronal sections made from P8 brains that were electroporated with SnXFP and CAG-RFP or CAG-GFP, confirmed the sparse labeling. Higher magnification images were shown in Figure 6. The high intensity of fluorescent labeling by Supernova system was confirmed by clear visualization of the complete dendritic branching of labeled neurons (Figure 6, 7 upper panel), dendritic spines (Figure 7, lower panel), and axons crossing long distance (Figure 8). Figure 7 showed the dendritic spines of SnAmcyan-labeled L5 pyramidal, SnGFP-labeled L4 spiny stellate, and SnRFP-labeled L2/3 pyramidal neurons, in 1 month-old mice. For the axon labeling, I examined the corticospinal tract (CST), the longest axonal trajectory in the mammalian central nervous system. CST axons are originated in L5 of the motor cortex, cross into the contralateral side of the medulla and down through the entire length of the spinal cord (Gianino et al., 1999; Liang et al., 1991) (Figure 8A). To visualize individual CST axons, I electroporated SnRFP vectors into the right motor cortex at E13.5. The

CAG-GFP vector was co-expressed to label CST axons from transfected neurons (Figure 8B). I analyzed the projections of the CST axons in the spinal cord. In the coronal sections of the cervical enlargement of P5 mouse spinal cord, individual SnRFP-labeled axons were clearly identified (Figure 8C).

The Flpe/FRT-based Supernova system achieves extremely low background of neuron labeling

Supernova system based on another recombination system, Flpe/FRT, was also constructed (Figure 9A upper panel). To confirm the efficiency of tTA-TRE feedback of Flpe/FRT-based Supernova system, I electroporated Flpe/FRT-based Supernova RFP (Flpe/FRT-SnRFP) and Flpe/FRT-SnRFP Δ tTA vector sets into L4 cortical neurons by IUE at E14.5. The CAG-GFP vector was co-transfected to label the transfected neurons (Figure 9B). Figure 10 showed higher magnification images taken by confocal microscope with low laser power. I quantified the number of RFP-labeled cells and GFP-labeled cells. At P16, 1.67% \pm 0.17% (n=5 mice) of GFP positive neurons were labeled by Flpe/FRT-SnRFP, while only 0.48% \pm 0.10% (n=5 mice) of GFP positive neurons were labeled by Flpe/FRT-SnRFP Δ tTA (Figure 10B). Without tTA-TRE enhancement, the weak expression of RFP was almost invisible (Figure 10A lower panel, arrowhead). Next, I quantified the RFP signal intensity of Flpe/FRT-SnRFP and Flpe/FRT-SnRFP Δ tTA labeled neurons. I found that the average brightness of cell bodies of RFP positive neurons labeled by the Flpe/FRT-SnRFP (n= 155 cells, 4 mice) was about 8 times higher than that of Flpe/FRT-SnRFP Δ tTA labeled neurons (n=81 cells, 4 mice, p<0.001) (Figure 10C). These data indicated that, as the Cre/loxP-based Supernova system, the tTA-TRE cycles effectively facilitated the RFP expression in Flpe/FRT-SnRFP labeled neurons.

To achieve sparse labeling, a DNA solution containing a Supernova vector set with 5ng/ μ l

TRE-Flpe vector was usually used (Figure 9B upper panel, 10A upper panel). Based on the design of Supernova system, the number of labeled cells is supposed to be adjusted by the concentration of TRE-Flpe vector. I prepared the Flpe/FRT-SnGFP vector set containing 5ng/ μ l and 500ng/ μ l TRE-Flpe vector and electroporated into L2/3 cortical neurons by IUE at E15.5. The CAG-RFP was co-transfected to label transfected neurons (Figure 11A). I quantified the GFP-positive cells and RFP-positive cells at P8. I found that, when 5ng/ μ l was used as the final concentration of TRE-Flpe vector, 1.43% \pm 0.09% (n=5 mice) of RFP positive neurons were labeled by Flpe/FRT-SnGFP, while the final concentration of TRE-Flpe vector increased to 500ng/ μ l, almost all of RFP positive neurons (98.71% \pm 2.46% , n=5 mice, P<0.001) were labeled by Flpe/FRT-SnGFP (Figure 11B). These data indicated the sparseness of Supernova labeling can be adjusted by changing the amount of the TRE-Flpe vector in the DNA solution for electroporation.

Next I compared the Flpe/FRT-based Supernova labeling with Cre/loxP based Supernova labeling. I introduced Flpe/FRT-SnRFP and Cre/loxP-SnRFP vector sets into L2/3 cortical neurons, separately, by performing IUE at E15.5. I co-transfected the CAG-GFP vector to label the transfected cells (Figure 12). I quantified the sparseness as the ratio of RFP-labeled neurons to GFP-labeled neurons. At P6, 14.84% \pm 3.27% (n=4 mice) of GFP positive neurons were labeled by Cre/loxP-SnRFP, while only 1.95% \pm 0.23% (n=4 mice) of GFP positive neurons expressed Flpe/FRT-SnRFP, indicating that Flpe/FRT-based Supernova labeling reveals excellent property in sparseness (Figure 12C). I evaluated the brightness of RFP labeled neurons based on visibility of their dendrites. Strikingly, most Flpe/FRT-SnRFP labeled neurons (90.00% \pm 7.93%, n=4 mice) were RFP^{high} neurons, while only half of the Cre/loxP-SnRFP labeled cells (55.99% \pm 3.60%, n=4 mice) showed high fluorescent intensity (Figure 12D). In other words, differing

from Cre/loxP-based Supernova labeling, an extremely high level of RFP was expressed in most of Flpe/FRT-SnRFP labeled neurons. Indeed, I showed that Flpe/FRT-SnRFP-mediated neuronal labeling is suitable for the visualization of detailed cellular morphology including dendritic spines of hippocampal CA1 pyramidal neurons (Figure 13) and interhemispheric (callosal) connections of L2/3 pyramidal neurons (Figure 14, See also next section). These data indicated that Flpe/FRT Supernova system achieved high intensities of fluorescent neural labeling with little background. These features of Flpe/FRT-based Supernova system are most useful for neural imaging in living animals, in which the outstanding sparseness and brightness are required.

The Flpe/FRT-based Supernova labeling is bright enough to visualize intact neural connectivity at single cell resolution in whole brain

For understanding the organization of complex nervous system, mapping the architecture of neural circuits is the basis and has been one of the most challenging projects for neuroscientists. A common way for quantitative reconstruction of neuronal circuits has been to slice brains into thin sections, followed by confocal imaging to gain a high resolution images and 3D reconstruction within a limited volume. The advent of the two-photon microscope broke the limits, which increased the accessible imaging depth into hundreds of micrometers in the intact brain. By combination of newly developed optical clearing technologies (e.g. *Scale*, *SeeDB* and *CLARITY*), the imaging depth of transparent tissues further increases into more than 2 millimeter (Chung et al., 2013; Hama et al., 2011; Ke et al., 2013; Tomer et al., 2014).

Here, I successfully visualized and reconstructed the whole cellular morphology of single L2/3

callosal projection neurons in the intact P12 mouse brain by combination of Supernova labeling and SeeDB technique (Ke et al., 2013) (Figure 14). Briefly, I labeled L2/3 cortical neurons with Flpe/FRT-SnRFP via IUE at E15.5. After the perfusion and fixation, I cleared the brains by proceeding SeeDB (Figure 14A). Two-photon microscopy was used to capture the images from the dorsal surface of the brain (Figure 14B, right panel). To reconstruct the whole cellular morphology of single L2/3 callosal projection neuron, totally 23×1 blocks (1 block = $607.28 \mu\text{m} \times 607.28 \mu\text{m}$, $Z_{\text{max}} = 1.5\text{mm}$ from the surface) images were taken from the electroplated side to contralateral side where the axons projected. Figure 14C shows the Z-stacked images of labeled neuron. A frontal view of dendrites and callosal axon termini of a SnRFP labeled cortical neuron is shown on the bottom (Figure 14D). Using a three-dimensional software, I successfully reconstructed the dendritic and axonal morphology of a labeled neuron (Figure 14D).

The Flpe/FRT and Dre/Rox-based Supernova systems enable single cell labeling in Cre expressing mice

Our original Supernova vector, which is designed based on Cre/loxP recombination, cannot be used for sparse labeling in Cre expressing transgenic mice, while Flpe/FRT-based Supernova should be used (Figure 15A). To confirm that, I introduced the vectors of Flpe/FRT-based SnGFP (Flpe/FRT-SnGFP) into cortical neurons of Emx1Cre knock-in mouse, which shows Cre-mediated recombination in all excitatory neurons of the cerebral cortex (Figure 15A, C upper panel, D left panel, E) (Iwasato et al., 2000; Iwasato et al., 2008; Iwasato et al., 2004). As a recombination indicator, I co-expressed CAG-LSL-RFP-WPRE. As Figure 15C upper panel showed, the complete dendritic morphology can be clearly observed by Flpe/FRT-SnGFP

labeling. On the other hand, it cannot be observed by Cre-induced neural labeling with CAG-LSL-RFP-WPRE, because too many neurons were labeled.

Moreover, I also constructed Supernova vector sets using another site-directed recombination system, Dre/Rox (Anastassiadis et al., 2009) (Figure 15B, C lower panel). Furthermore, I increased the color variation of Flpe/FRT-based Supernova labeling and Dre/Rox-based Supernova labeling with both GFP and RFP version (Figure 15C-D). I also showed that the fluorescent intensity expressed by Flpe/FRT-based SnRFP and Dre/Rox-SnRFP was maintained to be high even in the adult mouse brain (3-month-old), which was sufficient to visualize the dendritic spines (Figure 15D).

Expression of multiple proteins simultaneously in the same individual neuron

Co-expression of multiple genes simultaneously in the same individual neuron would provide effective ways to characterize the mechanisms underlying neural circuit formation. One example is co-expression of a fluorescent protein and a calcium indicator into individual neurons and in vivo imaging of neuronal morphology and neural activity by two photon microscope. The correlation analysis between morphological variety of labeled neuron and its neural activity changes would supply valuable information for understanding the neural circuit development and function.

The Supernova systems can achieve co-expression of multiple genes in the same cell by simply increasing the number of LSL-GeneX-tTA vectors in Cre/loxP-based or FSF-GeneX-tTA vectors in Flpe/FRT-based Supernova vector sets (Figure 16A, 16C). To test the co-expression efficiency, I performed quantification on confocal images of the P4 mouse brain, in which cortical neurons were transfected with

Cre/loxP-SnGFP and Cre/loxP-based Supernova nuclear localization signal (nls)-RFP (nlsRFP) by IUE at E15.5. I found that $93.05\% \pm 1.01\%$ (n=4 mice) of nlsRFP-positive cells expressed GFP signal (Figure 16B). In reverse, $80.78\% \pm 5.10\%$ (n=4 mice) of GFP-labeled neurons expressed nlsRFP, while $96.43\% \pm 3.57\%$ (n=4 mice) of GFP^{high} neurons, in which all dendritic morphologies were visualized by GFP, were nlsRFP-positive cells (Figure 16B).

For Flpe/FRT-based Supernova co-expression system, I examined the overlap of GFP and RFP signals in cortical neurons transfected with Flpe/FRT-SnGFP and Flpe/FRT-SnRFP (Figure 16D). At P8, all of RFP-labeled cells expressed GFP (51/51 cells, n=5 mice). In reverse, over 95% of GFP-positive cells also expressed RFP (51/53 cells, n=5 mice).

These results demonstrate that Supernova system allows selective expression of distinct proteins in a small subset of defined neurons.

AAV-mediated Supernova enables sparse labeling at single cell level

Viral infection is another powerful method for gene expression in targeted cells. This method is suitable for labeling of cells in adult animals or cells in the organs that IUE-based gene expression cannot be applied for.

I chose adeno-associated virus (AAV) for Supernova labeling, because it is the least toxic among all viral vectors and leads to high levels of and long-lasting gene expression (Kaplitt et al., 1994; Peel and Klein, 2000). However, due to the limitation of insert size of the AAV vector, which is only about 5000 nucleotides (Ehrengruber et al., 2001), the construct design used for IUE-based Supernova vectors

could not be used. Instead of loxP-STOP-loxP cassette, I used the strategy of double-floxed inverse open reading frame (DIO)(Sohal et al., 2009) to reduce the size of Gene X expression vector (Figure 17). Briefly, the AAV-mediated Supernova system consists of two vectors: aav-TRE-Cre, Cre-expression vector which is driven by the leakage of TRE and aav-DIO-RFP-tTA, Cre-dependent expression vector that carries a loxP/lox2722-flanked inverted inactive RFP-P2A-tTA (Figure 17A). In a very small portion of the cells that have these two vectors, the leakage of TRE drives very weak expression of Cre, which subsequently reorients the target gene and then excises one of two lox sites from each pair. As the result, the vector contains only an incompatible pair of the lox sites that no longer shows response to Cre (Figure 17A). I injected the constructed viral vectors into the hippocampus of P10 mice. The coronal sections were prepared 20 days after transfection (Figure 17B). I successfully obtained the clear image of hippocampal neurons, which were sparsely labeled, and whose cellular morphologies were clearly visible (Figure 17C).

Cre/loxP-based Supernova system enables labeled cell-specific gene knockout in floxed mice

Besides labeling, another unique and important feature of Cre/loxP-based Supernova system is that it can achieve simultaneous gene manipulation in the labeled cell. As described above, in Supernova system, an extremely high level of Cre is expressed only in sparsely labeled neurons, which would be enough to induce the excision of a floxed fragment from chromosome. To examine the efficiency and specificity of Cre-mediated recombination, I transfected Cre/loxP-SnRFP into L2/3 cortical neurons of CAG-loxP-CAT-loxP-GFP reporter transgenic mice, which express GFP under the Cre-dependent excision of loxP-CAT-loxP cassette (Figure 18A). In P8 brain section, almost all of SnRFP-labeled neurons (359/397 cells, n=3 mice)

expressed GFP. Notably, all of RFP^{high} neurons were labeled by GFP (291/291 cells). On the contrary, all GFP positive neurons were labeled by SnRFP (359/359 cells; Figure 18B). These data indicate that Cre-dependent genomic recombination was highly specific to SnRFP-labeled neurons.

Next, I characterized the efficiency of Supernova system in knocking out of an endogenous gene using floxed mice, in which an essential region of the target gene is flanked by two loxP sites. I chose α 2-chamerin (α 2-Chn) as the target gene, because hippocampal CA1 pyramidal neurons ubiquitously express very high level of α 2-Chn during early postnatal period, and its expression can be clearly visualized by immunohistochemistry (Hall et al., 2001; Iwata et al., 2014). I introduced Cre/loxP-SnRFP into hippocampal neurons of α 2-Chn^{flox/flox} mice by IUE at E14.5 (Figure 19). The brains were dissected at P14, when the α 2-Chn signals are strongest in CA1 region (Figure 149 left panels) (Hall et al., 2001; Iwata et al., 2014). DAPI staining was performed to visualize the hippocampal cells. I quantified the ratio of α 2-Chn positive cells to DAPI visualized cells in RFP-negative cells (control cells) and RFP positive cells (SnRFP labeled neurons, α 2-Chn KO cells) (Figure 19B right panels, two example image sets were shown). In hippocampal CA1 region, 97.70% \pm 0.09% (n=3 mice) of RFP-negative cells expressed α 2-Chn, while only 5.93% \pm 3.00% (n=3 mice) of RFP-positive neurons showed α 2-Chn signals (Figure 19C). Note that, in α 2-Chn^{flox/flox} mice, most of CA1 pyramidal neurons with high intensity of SnRFP labeling, in which the shape of cell body could be clearly identified, showed deletion of α 2-Chn proteins (n= 80 cells / total 86 cells, 3 individuals). These results further suggest the high recombination specificity and efficiency of the Supernova system.

Next, I electroporated Cre/loxP-SnRFP into CA1 neurons of α 2-Chn^{flox/flox} and α 2-Chn^{flox/+}

mice (Figure 20A, B). I quantified $\alpha 2$ -Chn intensity in both SnRFP-labeled cells and RFP-negative cells (control cells) in $\alpha 2$ -Chn^{flox/flox} and $\alpha 2$ -Chn^{flox/+} mice. I found that, compared to control cells, $\alpha 2$ -Chn protein level was significantly reduced in RFP-positive cells in $\alpha 2$ -Chn^{flox/+} mice ($\alpha 2$ -Chn heterozygous cells) and those in $\alpha 2$ -Chn^{flox/flox} mice ($\alpha 2$ -Chn KO cells). I also observed the significant difference of $\alpha 2$ -Chn protein level between $\alpha 2$ -Chn heterozygous and $\alpha 2$ -Chn KO cells (Figure 20C).

All of the data shown above provided the compelling evidence that Supernova system is suitable for conditional gene knockout in combination with floxed mouse.

RNAi-mediated Supernova system enables labeled cell-specific gene knockdown in wild type mice

To achieve sparsely labeled cell-specific manipulation of endogenous gene expression without using floxed mouse, I modified the Supernova system. Small hairpin RNA (shRNA) can be transfected into cortical neurons by IUE-mediated transfection of CAG promoter/microRNA30-based inducible RNAi vector (CAG-LSL-mir30) (Matsuda and Cepko, 2007). By combining this strategy and the Supernova system, I successfully knocked-down target genes in sparse cortical neurons in two reporter transgenic mouse lines (Figure 21, 22).

One was the CAG-loxP-CAT-loxP-GFP reporter transgenic (GFP reporter) mice, which express GFP when the loxP-CAT-loxP cassette was excised by Cre-dependent recombination (Kawamoto et al., 2000) (Figure 21B). I electroporated Sn-nlsRFP together with CAG-LSL-mir30 (GFPshRNA scramble sequence) or CAG-LSL-mir30 (GFPshRNA) into L4 cortical neurons in GFP reporter mice by IUE at E14.5 (Figure 21A-C). I quantified the intensities of GFP signals in cortical neurons expressed with

GFPshRNA and GFPshRNA scramble sequence. I used nlsRFP signal to normalize the electroporation efficiency. I found that the relative GFP intensity in neurons electroporated with GFPshRNA was significantly lower than that in neurons expressed with GFPshRNA scramble sequence (GFPshRNA: n =3 mice, total 14 cells; GFPshRNA scramble control: n=3 mice, total 23cells) (Figure 21D).

The efficiency of target gene knockdown was further confirmed in another reporter mouse line, Rosa26-loxP-STOP-loxP-nlsLacZ (RNZ) mouse, which expresses nlsLacZ by Cre-mediated recombination (Kobayashi et al., 2013) (Figure 22B). I constructed CAG-LSL-mir30 (LacZshRNA) and CAG-LSL-mir30 (LacZshRNA scramble sequence) and transfected them into RNZ reporter mouse cortex by IUE, together with SnAmcyan (Figure 22A, C). The level of LacZ expression was visualized by β -gal immunohistochemistry (Figure 22C). I quantified the fluorescent intensity ratio of anti- β -gal to Amcyan and found that, as expected, the ratio in LacZshRNA expressing neuron was significantly lower than that in LacZshRNA scramble sequence expressing neuron (n=5 mice for each group, total 148 cells) (Figure 22D).

TALEN-mediated Supernova system enables labeled cell-specific gene manipulation in wild-type mice

As described in the previous section, knocking-down an endogenous gene in individual neurons *via* an RNAi-mediated Supernova system was successful. However, its efficiency may not be sufficient for investigating individual gene function in single cells, because, in both reporter mouse lines, the expression levels of reporter genes with knockdown were only about half of the normal expression levels (Figure 21-

22). In order to achieve more effective gene knockdown/knockout, I adapted target transcription activator-like effector nucleases (TALENs)-based genome editing technology to the Supernova system with the help of Dr. Ryohei Iwata. I successfully inhibited the endogenous gene, $\alpha 2$ -Chn, expression in CA1 pyramidal neurons of wild-type mouse. $\alpha 2$ -Chn TALEN was designed to target the exon 6 of $\alpha 2$ -Chn gene, because the effective disruption of $\alpha 2$ -Chn by deleting this region has been shown in $\alpha 2$ -Chn KO mice (Iwata et al., 2014) (Figure 23A). $\alpha 2$ -Chn TALENs consist of two constructs (Left and Right) having FokI nuclease domain fused to unique DNA binding domains for sites in the target genome (Figure 23). The $\alpha 2$ -Chn TALENs were constructed into Flpe-induced expression vector, and cotransfected into hippocampal CA1 neurons with Flpe/FRT-SnRFP (Figure 23B).

To assess the editing efficiency of the TALEN-based Supernova gene manipulation system, I transfected $\alpha 2$ -Chn TALENs together with Flpe/FRT-SnRFP into hippocampal CA1 pyramidal neurons by performing IUE at E14.5. At P14, I perfused and fixed the electroporated brain, sectioned them and stained these slices with an anti- $\alpha 2$ -chimaerin antibody. I also performed DAPI-staining to visualize cell body location (Figure 24A-B). Based on the confocal images, I divided the DAPI-visualized cells in hippocampal CA1 region into three groups depending on the intensity of anti- $\alpha 2$ -Chn signals: $\alpha 2$ -Chn^{high}, $\alpha 2$ -Chn^{low} and $\alpha 2$ -Chn^{negative}. $\alpha 2$ -Chn^{high} cells refer to cells that show high intensity of $\alpha 2$ -Chn signals, and the intensity of the signal are similar with that in surround RFP-negative cells (control cells). $\alpha 2$ -Chn^{negative} refers to cells in which the $\alpha 2$ -Chn signals would not be detected. $\alpha 2$ -Chn^{low} cells refer to cells, in which the $\alpha 2$ -Chn signals can be visualized, but the intensity of $\alpha 2$ -Chn signals are weaker than that in surround RFP-negative cells (control cells). I found that $75.96\% \pm 5.95\%$ (n=3 mice) of Flpe/FRT-SnRFP labeled cells were $\alpha 2$ -

Chn^{negative} cells. The rest was $\alpha 2$ -Chn^{low} cells, while there were no $\alpha 2$ -Chn^{high} cells. On the other hand, $\alpha 2$ -Chn^{high} and $\alpha 2$ -Chn^{low} cells were $95.06\% \pm 0.52\%$ (n=3 mice) and $3.22\% \pm 0.15\%$ (n=3 mice), respectively, of RFP-negative neurons. In other words, in cells that were transfected with Supernova $\alpha 2$ -Chn TALEN, the protein level of $\alpha 2$ -Chn was dramatically reduced, indicating the high efficiency of gene manipulation of TALEN-mediated Supernova system.

For excluding the possibility that the expression of $\alpha 2$ -Chn may be affected by high fluorescent protein expression, I electroporated Flpe/FRT-SnRFP into hippocampal CA1 neurons by IUE at E14.5. I prepared coronal sections from the P14 brains and stained these slices with an anti- $\alpha 2$ -chimaerin antibody (Figure 25). The expression of $\alpha 2$ -chimaerin protein in RFP-positive cells was confirmed (Figure 25, arrowhead).

DISCUSSION

The strategy to target a small subset of cells for exogenous gene expression (e.g. fluorescent protein) or endogenous gene manipulation is indispensable for understanding the cellular and molecular mechanisms responsible for neural circuit development and function. For this purpose, the Supernova system was developed (Mizuno et al., 2014). I demonstrated quantitatively that this original version of Supernova method can label only small populations of neurons brightly in the mouse brain (Figure 2, 4, 5). Extremely high fluorescent signals via Supernova labeling enabled visualization of the whole cellular morphologies of labeled neurons, including individual dendritic spines and axons (Figure 3, 6-8).

I improved and expanded the Supernova system in several aspects. First, I developed the Flpe/FRT-mediated-Supernova method, in which I used the Flpe/FRT recombination system instead of the Cre/loxP system used in the original version of the Supernova. I showed that this new Supernova system has excellent properties in sparseness and brightness, and that it achieved neural labeling with essentially no background (Figure 12). These features were critical for imaging neural morphology in living animal and mapping neuronal circuits in intact tissues (Figure 14). Second, I developed an AAV-based Supernova system (Figure 17), which makes Supernova labeling even more flexible, because AAV-based transfection has no area limitation and is convenient for labeling in cells in adulthood.

The original Cre/loxP-based Supernova system is designed to enable labeled cell-specific gene manipulation, when it is combined with lines of floxed mice, in which the essential region of target genes is flanked by two loxP sites. I evaluated the efficiencies of gene targeting quantitatively. I found that Cre/loxP-mediated Supernova system shows high efficiencies for labeled-cell-specific knockout of

endogenous genes (Figure 18-20).

For manipulating target gene expression in individual cells in wild-type mice, I utilized the RNA interference, and found that Supernova-mediated expression of shRNA efficiently reduced the expression level of endogenous genes (Figure 21-22). I also developed TALEN-mediated Supernova gene manipulation system. It had remarkable ability for the reduction of target protein expression in all transfected cells (Figure 23-24).

Taken together, these results indicated that the Supernova system is a general method to label a sparse population of cells and to manipulate a gene specifically in the labeled cells; thus, the Supernova system is a promising tool to elucidate the cellular and molecular mechanisms of neuronal circuit development and function at a single cell level.

Labeling single cell *in vivo*

The neurons in the mammalian brain are densely packed and tightly interconnected. For understanding the complex networking structure of the brain, methods to label a limited number of cells and to clearly image the whole structures of these cells are requisite.

A widely used approach for sparse neural labeling is Thy1-XFP transgenic mice, in which XFP is expressed under the control of neuron-specific elements from the *thy1* promoter (Feng et al., 2000). The design strategy of Thy1-XFP mice relies on a phenomenon called 'position effect variegation' that the transgene expression is varied between lines (Festenstein et al., 1996). Totally, 25 lines are reported and the fluorescent protein's expression in each Thy1-XFP mouse line was shown in a vested pattern. It is unable

to observe the neurons in the region that *thy1* gene is not expressed. In addition, genetic methods such as Thy1-XFP have disadvantage that it is difficult to change the color of fluorescent proteins etc for labeling unless generating new lines.

Compared to genetic methods, IUE-based approaches make experimental design much more flexible. To label single cells using IUE, a common approach is co-expression of a set of two plasmid such as CAG-loxP-STOP-loxP-XFP (1 mg/ml) and CAG-Cre in a very low concentration (e.g. 0.1 ng/ml) (Dhande et al., 2011). Using this type of method, only a small subset of cells is labeled. However, unfortunately with it, the labeling intensity is not usually bright enough for observation of the detailed cellular morphology such as dendritic spines and usually shows high background.

PASME is a recently reported technique that achieves sparse neural labeling by introducing the Thy1S-XFP expression vector or Thy1S-ER^{T2}CreER^{T2} expression vector together with the CAG-floxed-XFP expression vector into neurons by IUE (Ako et al., 2011). Due to the utilization of *thy1* promoter, the target neurons are limited to the cells that express *thy1* gene. In addition, the dendritic and axonal morphology could not be clearly seen in the neurons labeled by Thy1S-XFP. The relative high intensity labeling could be achieved only in the neurons transfected with Thy1S-ER^{T2}CreER^{T2} and CAG-floxed-XFP under the treatment of 4-OHT in postnatal mice.

Viral infection is another delivery system for transfection of genes into internal organ that IUE-based transient methods could not be applied for. Up to now, the sparse labeling via viral infection is usually performed through one of following two strategies: 1) by simply reducing the copy number of viral expression vector (Kim et al., 2013); 2) by utilizing a mutant Cre recombinase-mediated inversion system

that sparse gene delivery are achieved by Cre-induced inversion of two mutant loxP sites (lox66 and lox71) (Kim et al., 2012). Although these approaches achieve some level of sparseness, the low intensity of fluorescence limits their practicability in experiments requiring brightness.

The Supernova system solved all the problems mentioned above. First and foremost is the sparse labeling with extremely high fluorescent signals, which enabled morphological analysis on the detailed cellular component, such as dendritic spines and axonal branches. Second, the Supernova system can use both IUE and viral infection techniques, compared to genetic methods, which are more convenient with no restriction on the cell-type, target region, initial time point, and the color selection of fluorescent proteins for neural labeling. Third, using the Supernova system, the experimental turnover time is dramatically shortened from year to several weeks by comparing with the approaches based on transgenic animals. Therefore, a variety of experimental designs can be tested easily.

Manipulation of a target gene in sparsely labeled cells *in vivo*

To dissociate cell-autonomous and nonautonomous functions of a target gene in neural circuit formation and function, approaches for generation of isolated single mutant cells in an otherwise normal tissue, and simultaneously labeling them for morphological and physiological analysis are useful. MADM (mosaic analysis with double markers) and SLICK (single neuron labeling with inducible Cre-mediated knockout) are recently reported systems that are developed for such purpose.

The strategy of MADM system is generating genetically mosaic mice, in which isolated single mutant and wild-type cells are labeled with different fluorescent proteins in the same experimental

individual (Zong et al., 2005). A major limitation of the MADM system is that it requires two MADM transgenic mouse lines specific to the chromosome harboring gene of interest (Zong et al., 2005). Although, new mice that harbor MADM transgenes on different chromosomes are reported recently (Tasic et al., 2012), the effectiveness of using MADM system on the analysis of the cell-autonomous function of target gene is still restricted to the genes that located on mouse chromosome 6 distal to the ROSA26 locus, and mouse chromosome 11 distal to the *Hipp11* locus (Espinosa and Luo, 2008; Espinosa et al., 2009; Hippenmeyer et al., 2010; Liu et al., 2011; Muzumdar et al., 2007). Another disadvantage of MADM system is the time-consuming for generation mutant-MADM mice. At least, the crossing among four lines including a pair of knockin mice carrying MADM cassettes, heterozygous mice carrying a null mutation of interested gene, a Cre-driver line, are required. The preparation, selection and management of these mouse lines take time, space and efforts.

The strategy of SLICK is that the expression of cDNA encoding YFP and CreER, a tamoxifen-inducible form of Cre, are driven by separate copies of the Thy1 promoter that are linked together in opposite orientations (Young et al., 2008). The conditional knockout in sparse labeled neurons is performed by crossing SLICK mice with the mice having floxed allele of gene of interest. The utilization of Thy1 promoter restricted the application of SLICK system to only a defined population of neurons as Thy1-XFP mice. SLICK system is applicable in late embryonic, postnatal and adult stages, when Thy1 promoter is most active.

The Supernova system shares the same goal with MADM and SLICK systems that enable performing genetic manipulations specifically in fluorescent labeled individual cells. Here, I present three

ways to use the Supernova system to achieve gene manipulation at a single cell level. There are: (1) single-cell knockout, by transfecting Cre/loxP-based Supernova vectors into the cells in floxed mice; (2) single-cell gene knockdown, by over-expression of RNAi constructs against interested genes into the cells in wild-type mice; (3) single-cell genome editing, by introduction of TALEN-mediated Supernova gene manipulation vector sets into wild-type cells.

For conditional gene knockout in single-labeled cell, our Supernova system is much flexible. By using electroporation and viral infection, Cre/loxP-based Supernova vectors can be easily introduced into any type of cells, at any possible time point, with no restriction to species, as long as the floxed animal is available. Enhanced Cre expression guaranteed high genomic recombination. The high efficiency of Supernova system in deleting the floxed target gene from the chromosome is first confirmed by the disruption of functional N-methyl-D-aspartate receptor (NMDAR) in Supernova-labeled cortical neurons (Mizuno et al., 2014). Here, I further confirmed the consistency between Supernova-mediated single cell labeling and gene knockout utilizing $\alpha 2$ -Chn as a target gene (Figure 19-20). These facts demonstrate that Cre/loxP-based Supernova is a general method for labeled cell-specific gene knockout. Moreover, different from MADM and SLICK system, in which the color of marker is determined initially when the transgenic mice are generated, using the Supernova system, the color of fluorescent proteins could be freely selected according to the needs of the experiments. Fusion of PSD95, GAP43, nls etc to fluorescent proteins, could enable researchers to analyze the gene-defect-induced morphological changes via observing detailed cellular components.

The methods for genetic screening at a single cell level in wild-type animal would dramatically

change our way for studying the mechanism responsible for biological processes. Our RNAi- and TALEN-mediated Supernova systems are such approaches that can achieve single cell gene manipulation in wild type mice (Figure 19-20, 23-25). It is also applicable for investigation of gene function in single isolated neuron in species that traditional transgenic technology has not been previously feasible. Moreover, as known, the design of shRNA or TALENs against target gene is simple, because a lot of well-rounded design tools are provided on internet and so on. Followed by only one step cloning for constructing of shRNA or TALEN expression vectors, the constructed RNAi-mediated or TALEN-mediated Supernova system is ready for screening and identifying the cell-autonomous role of target genes in biological processes. Further, there are no limits of target genes, which are different from the MADM system. I need to mention that the efficiency of RNAi- and TALEN-mediated Supernova system for gene manipulation is case by case, which depends on the design of the sequences that for targeting the gene or genome. In the present study, I adapted the shRNA expression vector to Cre/loxP-mediated Supernova system. According to the differences between Cre/loxP- and Flpe/FRT-based Supernova labeling, the higher knockdown efficiency may be acquired, by adapting shRNA expression vector to Flpe/FRT-based System. Supernova system is also applicable for other approaches, such as regulating endogenous protein function in single cell, by over-expression of vectors which carry genes encoding dominant negative or constitutively active form of defined proteins.

In summary, the Supernova system was highly effective for sparse and bright cell labeling with an extremely low background. It achieved labeled cell-specific gene manipulation in wild-type mammals in vivo for the first time. Thus, the Supernova system is a promising tool to elucidate the cellular and

molecular mechanisms underlying neural circuit development and function.

EXPERIMENTAL PROCEDURES

Plasmid construction

- The construction of pK031.TRE-Cre and pK029.CAG-loxP-STOP-loxP-RFP-ires-tTA-WPRE were previously described (Mizuno et al., 2014).
- pK046.CAG-loxP-STOP-loxP-RFP-WPRE: To generate the pK046 vector, loxP-STOP-loxP sequence was amplified from the pBS302 vector (Gibco-BRL) using the primer pair HM010.F-loxP and HM007.R-loxP. The RFP sequence was amplified from the pK023.TurboRFP-N (Evrogen) using the primer pair HM026.F-RFP and HM030.R-RFP. The WPRE sequence was amplified from the pK021.Lenti-Synapsin-hChr2 (H134R)-EYFP-WPRE vector (Zhang et al., 2007) (Addgene) using the primer pair HM019.F-WPRE and HM020.R-WPRE. Obtained three products were ligated into the EcoRI/SalI, SalI/NotI, and NotI sites of the pCAGplay vector (Hitoshi et al., 1991; Kawaguchi and Hirano, 2006), respectively.
- pK038.CAG-loxP-STOP-loxP-EGFP-ires-tTA-WPRE: To generate the pK038 vector, EGFP and ires-tTA were cloned by PCR from pEGFP-N1 (Clontech) and pCAG-loxP-STOP-loxP-RFP-ires-tTA-WPRE vector using primer sets HM050.F-EGFP and HM055.R-EGFP, HM054.F-ires1 and HM035.R-tTA, respectively. Obtained two PCR products were combined and re-amplified using outside primers to generate EGFP-ires-tTA, which was cloned into SalI/NotI sites of the pCAG-loxP-STOP-loxP-RFP-ires-tTA-WPRE vector.
- pK039.CAG-loxP-STOP-loxP-AmCyan-ires-tTA-WPRE: To generate pK039 vector, the AmCyan was excised with SalI and StuI from pAmCyan (Clontech) and cloned into pCAG-loxP-STOP-loxP-

EGFP-ires-tTA-WPRE vector digested with SalI and EcoRV.

- pK036.TRE-Flpe-WPRE

To generate the pK036 vector, the coding sequences of Flpe was amplified from pK016.CAG-Flpe-ires-Puro (GeneBridge) using the primer pair AY101.F-Flpe and AY102.R-Flpe. The resulting product was ligated into BamHI/NotI sites of the pK026.TRE-Tight vector (Clontech). WPRE, excised with NotI from pK029.CAG-loxP-STOP-loxP-RFP-ires-tTA-WPRE vector, was ligated into NotI site of obtained pTRE-Flpe vector.

- pK037.CAG-FRT-STOP-FRT-RFP-ires-tTA-WPRE: pK037 vector was generated by replacing loxP-STOP-loxP sequence with the FRT-STOP-FRT sequence between EcoRI/SalI sites of pK029.CAG-loxP-STOP-loxP-RFP-ires-tTA-WPRE. FRT-STOP-FRT sequence was amplified from the pBS302 vector (Gibco-BRL) using the primer set HM009.F-FRT and HM008.R-FRT.

- pK068.CAG-FRT-STOP-FRT-EGFP-ires-tTA-WPRE: For the pK068 vector, EGFP-ires-tTA sequence was excised with SalI and NotI from pK038.CAG-loxP-STOP-loxP-EGFP-ires-tTA-WPRE vector and cloned into SalI /NotI sites of pK037.CAG-FRT-STOP-FRT-RFP-ires-tTA-WPRE vector.

- pK073.TRE-Dre-WPRE: The Dre sequences were amplified by PCR from pK055.CAG-Dre-ires-puro.gcc vector (a generous gift from Dr. Morimoto, NIG) using primer set WL006.F-Dre and WL007.R-Dre. Resulted product was cloned into the EcoRI/NotI sites of pK036.TRE-Flpe-WPRE vector to generate pK073.TRE-Dre-WPRE vector.

- pK129.CAG-Rox-STOP-Rox-RFP-ires-tTA-WPRE: For pK129 vector, the Rox-STOP-Rox was excised with BglIII and XhoI from pK078.JFRC176-10XUAS-rox-dSTOP-rox-myr::GFP (Addgene)

and ligated into BamHI/XhoI sites of pCAGplay vector (Hitoshi et al., 1991; Kawaguchi and Hirano, 2006). Obtained vector was then digested with EcoRI and XhoI and ligated into EcoRI/SalI sites of pK037.CAG-FRT-STOP-FRT-RFP-ires-tTA-WPRE vector by replacing FRT-STOP-FRT with Rox-stop-Rox.

- pK224.CAG-Rox-STOP-Rox-EGFP-ires-tTA-WPRE: For pK224, the Rox-STOP-Rox was excised with BglII and XhoI from pK078.JFRC176-10XUAS-rox-dSTOP-rox-myr::GFP (Addgene) and ligated into BamHI/XhoI sites of pCAGplay vector (Hitoshi et al., 1991; Kawaguchi and Hirano, 2006). EGFP-ires-tTA from the pK068.CAG-FRT-STOP-FRT-EGFP-ires-tTA-WPRE vector was excised with SalI and NotI and ligated into the XhoI/NotI sites of above obtained vector. WPRE, excised with NotI from pK046.CAG-loxP-STOP-loxP-RFP-WPRE, was ligated into NotI site of obtained pCAG-Rox-STOP-Rox-EGFP-ires-tTA vector.
- pK168.AAV-EF1 α -DIO-tTA-P2A-tRFP-WPRE: The tTA sequence was amplified from the pTet-Off-Advanced vector (Gossen and Bujard, 1992) using primers: 5'-TGCTAGCGCCACCATGTCTAGACTGGA-3' / 5'-TGGATCCCCCGGGGAGCATGTCAAGGT-3'. The P2A-tRFP sequence was amplified from TurboRFP (Evrogen, Moscow, Russia) using the primer pair: 5'-AGGATCCGGAAGCGGAGCTACTAACTTCAGCCTGCTGAAGCAGGCTGGAGACGTGGAGGAGAACCCTGGACCTATGAGCGAGCTGATCA-3' / 5'-AGGCGCGCCTCATCTGTGCCCCAGTTTG-3'. The pK168.AAV-EF1 α -DIO-tTA-P2A-tRFP-WPRE was generated by ligation of tTA and P2A-tRFP into the NheI/BamHI and BamHI/AscI sites

of the pAAV-EF1 α -DIO-EYFP vector (Addgene: 27056, Cambridge, MA, USA).

- pK170.AAV-TRE-Cre-WPRE: The Cre sequence was amplified from the pK067.CAG-nlsCre-WPRE. The pK170 was generated by ligation of Cre into the EcoRI/BglIII sites of the pK169.AAV-TRE-MCS-WPRE vector (a generous gift from Dr. Yu Hayashi).
- pK098.CAG-loxP-STOP-loxP-nlstagRFP-ires-tTA-WPRE: The encoding sequences of the nuclear localization signal (nls)-tagRFP were cloned by PCR from pK022.TagRFP-N (Evrogen) with the primer sets HM079.F-NLStagRFP and HM075.R-tagRFP. The PCR products were ligated into Sall/EcoRV sites of pK038.pCAG-LSL-EGFP-ires-tTA-WPRE vector by replacing EGFP.
- pK177.CAG-loxP-STOP-loxP-mir30 (GFP RNAi) and pK178.CAG-loxP-STOP-loxP-mir30 (GFP RNAi Scramble control): The shRNA against the coding region of GFP (441-461) and its scramble control were generated by PCR with the template oligonucleotide for GFP shRNA HM084: 5'-TGCTGTTGACAGTGAGCGAAGCCACAACGTCTATATCATGTAGTGAAGCCACAGATGTAC
ATGATATAGACGTTGTGGCTGTGCCTACTGCCTCGGA-3' and the template oligonucleotide for GFP shRNA scramble control HM085: 5'-TGCTGTTGACAGTGAGCGAGCTCATAGAAGCTCTACAATCTAGTGAAGCCACAGATGTAGATTGTAGAGCTTCTATGAGCGTGCCTACTGCCTCGGA-3' respectively, using the primers HM082.F-mir and HM083.R-mir. The amplified products were ligated into XhoI/EcoRI sites of pCAG-loxP-STOP-loxP-mir30 vector (Matsuda and Cepko, 2007; Addgene). The shRNA sense and antisense target sequences appear in underline. The insert sequences in the construct were verified by nucleotide sequencing using primers: HM088 and HM089.

- pK225.CAG-loxP-STOP-loxP-mir30 (LacZ RNAi) and pK226.CAG-loxP-STOP-loxP-mir30 (LacZ RNAi Scramble control): For single cell LacZ knockdown, the shRNA against the coding region of LacZ (651-671) and its scramble control were generated by PCR with the template oligonucleotide for

LacZ	shRNA	WL090	5'-
TGCTGTTGACAGTGAGCGAAAATCGCTGATTTGTGTAGTCTAGTGAAGCCACAGATGTAG			
<u>ACTACACAAATCAGCGATTTGTGCCTACTGCCTCGGA-3'</u>			
LacZ	shRNA	scramble	control
WL091:	5'-		
TGCTGTTGACAGTGAGCGAGGCAACTTCGGTTAGTATTTATAGTGAAGCCACAGATGTA			
TAAATACTAACCGAAGTTGCCGTGCCTACTGCCTCGGA-3'			

respectively, using the primers HM082.F-mir and HM083.R-mir. The sequence for LacZ shRNA scramble control are designed using internet tool termed siRNA Wizard-Generation of scrambled siRNA sequence. The amplified products were ligated into XhoI/EcoRI sites of pCAG-loxP-STOP-loxP-mir30 vector (Matsuda and Cepko, 2007; Addgene). The shRNA sense and antisense target sequences appear in underline. The insert sequences in the construct were verified by nucleotide sequencing using primers: HM088 and HM089.
- pK217.CAG-FRT-STOP-FRT-a2Chn TALEN Left and pK218.CAG-FRT-STOP-FRT-a2Chn TALEN Right: The a2Chn TALENs were constructed based on a two-step Golden Gate assembly method using the Platinum Gate TALEN Kit (Addgene, cat#1000000043). The design of a2Chn TALEN Left RVD is NI HD NI NI NI HD NI NN HD NI HD NI NG NN NN HD NI NN NG HD. The design of a2Chn TALEN Right RVD is NN NN HD HD NG NN NG NI NN HD HD NG HD NG NG NG HD NG HD NI. The predict cut site is at 237 of mouse a2-Chn exon6. The FRT-STOP-FRT was excised with

SpeI/SalI from pK037.CAG-FRT-STOP-FRT-RFP-ires-tTA-WPRE and ligated to the SpeI/XhoI sites

in obtained pK209.CMV- a2Chn TALEN Left and pK210.CMV- a2Chn TALEN Right.

All coding sequences in each construct were verified by nucleotide sequencing. The constructed plasmid and used primers are summarized in Table 1 and Table 2.

Table 1

Vector #	Vector Name
pK016	CAG-Flpe-ires-Puro (GeneBridge)
pK021	Lenti-Synapsin-hChr2 (H134R)-EYFP-WPRE
pK023	TurboRFP-N (Evrogen)
pK026	TRE-Tight vector (Clontech)
pK029	CAG-loxP-STOP-loxP-RFP-ires-tTA-WPRE
pK031	TRE-Cre
pK036	TRE-Flpe-WPRE
pK037	CAG-FRT-STOP-FRT-RFP-ires-tTA-WPRE
pK038	CAG-loxP-STOP-loxP-EGFP-ires-tTA-WPRE
pK039	CAG-loxP-STOP-loxP-AmCyan-ires-tTA-WPRE
pK046	CAG-loxP-STOP-loxP-RFP-WPRE
pK055	CAG-Dre-ires-puro.gcc vector
pK067	CAG-nlsCre-WPRE
pK068	CAG-FRT-STOP-FRT-EGFP-ires-tTA-WPRE
pK073	TRE-Dre-WPRE
pK078	JFRC176-10XUAS-rox-dSTOP-rox-myr::GFP (Addgene)
pK098	CAG-loxP-STOP-loxP-nlstagRFP-ires-tTA-WPRE
pK129	CAG-Rox-STOP-Rox-RFP-ires-tTA-WPRE
pK168	AAV-EF1 α -DIO-tTA-P2A-tRFP-WPRE
pK169	AAV-TRE-MCS-WPRE
pK170	AAV-TRE-Cre-WPRE
pK177	CAG-loxP-STOP-loxP-mir30 (GFP RNAi)
pK178	CAG-loxP-STOP-loxP-mir30 (GFP RNAi Scramble control)
pK217	CAG-FRT-STOP-FRT-a2Chn TALEN Left
pK218	CAG-FRT-STOP-FRT-a2Chn TALEN Right
pK224	CAG-Rox-STOP-Rox-EGFP-ires-tTA-WPRE
pK225	CAG-loxP-STOP-loxP-mir30 (LacZ RNAi)
pK226	CAG-loxP-STOP-loxP-mir30 (LacZ RNAi Scramble control)

Table 2

Primer #	Primer Sequence (from 5' to 3')
HM010	GGGAATTCTAATAACTTCGTATAGCATACATTATACGAAGTTATATTAAGGGTTCCGGATCCTCGGGGACACC
HM007	CCGTCGACATATAACTTCGTATAATGTATGCTATACGAAGTTATTAGGTCCCTCGACCTGCAGCCCAAGCTTA
HM026	CGAATTCTGCAGTCGACGGTACCGAGGGCC
HM030	GTCGCGGCCGCATCATCTGTGCCCCAGTTT
HM019	GCGGCCGCTCAACCTCTGGATTACAAAATT
HM020	GCGGCCGCTGCGGGGAGGCGGCCAAAGGG
HM050	CGGTCGACGCCACCATGGTGTAGCAAGGGCGAGGAGC
HM055	GGAATCCTTAATTAACCTGCATCTAGGATATCTTACTTGTACAGCTCGTCCATGCCGAGA
HM054	TCTCGGCATGGACGAGCTGTACAAGTAAGATATCCTAGATCGAGTTAATTAAGGATTCC
HM035	GGGCGGCCGCTTACTTAGTTACCCGGGGAGCATGTCAAG
AY101	GGAAGGATCCTTGTGCTGTCTCATCTTTGG
AY102	TTGCGGCCGCGGGCGGAATCTTAATTAACTC
HM008	GGGAATTCTAGAAGTTCCTATACTTTCTAGAGAATAGGAACCTCATTAAAGGGTTCCGGATCCTCGGGGACACCA
HM009	CCGTCGACATGAAGTTCCTATTCTCTAGAAAAGTATAGGAACCTCTAGGTCCCTCGACCTGCAGCCCAAGCTTA
WL006	CGAATTCGCC ACCATGGGTG CT
WL007	TGCGGCCGCT CACTTTCC TCTT
HM079	CCGTCGACCATGGGCCAAAGAAGAAGAGAAAGGTTTCGGTGTCTAAGGGCGAAG
HM075	CCGATATCTTCAATTAAGTTGTGCCCCAGTTTGCTAGG
HM082	CAGAAGGCTCGAGAAGGTATATTGCTGTTGACAGTGAGCG
HM083	CTAAAGTAGCCCTTGAATTCCGAGGCAGTAGGCA
HM088	GCGGCCGCATCGATGATATC
HM089	GATAGGCAGCCTGCACCTGAG
HM084	TGCTGTTGACAGTGAGCGAAGCCACAACGTCTATATCATGTAGTGAAGCCACAGATGTACATGATATAGACGTTGTGGCTGTGCCTACT GCCTCGGA
HM085	TGCTGTTGACAGTGAGCGAGCTCATAGAAGCTCTACAATCTAGTGAAGCCACAGATGTAGATTGTAGAGCTTCTATGAGCGTGCCTACT GCCTCGGA
WL090	TGCTGTTGACAGTGAGCGAAAATCGCTGATTTGTGTAGTCTAGTGAAGCCACAGATGTAGACTACACAAATCAGCGATTTGTGCCTACT GCCTCGGA
WL091	TGCTGTTGACAGTGAGCGAGGCAACTTCGGTTAGTATTTATAGTGAAGCCACAGATGTATAAATACTAACCGAAGTTGCCGTGCCTACT GCCTCGGA

Animals

All experiments of animal care and use were conducted according to Guidelines for Proper Conduct of Animal Experiments and were approved by the Institutional Animal Care and Use Committee of the National Institute of Genetics (NIG).

Genotypes of Emx1Cre KI- Δ Neo mice (Iwasato et al., 2000; Iwasato et al., 2008; Iwasato et al., 2004), CAG-loxP-CAT-loxP-GFP reporter mice (a kind gift of Dr. Jun-ichi Miyazaki) (Kawamoto et al., 2000), RNZ reporter mice (a kind gift of Dr. Shigeyoshi Itohara) (Kobayashi et al., 2013) and α 2-Chn flox mice (Iwata et al., 2014) were determined by PCR as previously reported.

Embryos for IUE and viral infection were obtained by mating one male with one female overnight, and the noon of a day, when a vaginal plug was found, was designated embryonic day (E) 0.5. The day of birth was counted postnatal day (P) 0.

In utero electroporation (IUE)

IUE was performed as described previously (Mizuno et al., 2007; Mizuno et al., 2014; Saito and Nakatsuji, 2001; Tabata and Nakajima, 2001). Briefly, timed pregnant mice were anesthetized with sodium pentobarbital (50 mg/kg body weight) in saline. After cleaning the abdomen with 70% ethanol, about 3 cm midline laparotomy was performed and the uterus was taken out. For DNA microinjection, glass capillary tubes (GC150TF-10; Harvard Apparatus) were pulled using a micropipette puller (PC-10; Narishige). A total of 0.5 μ l of DNA solution was injected into the right lateral ventricle of embryos using a mouth-controlled pipette system (Drummond Scientific). Square electric pulses (40 V; 50 ms) were delivered 5

times at a rate of 1 Hz by an electroporator (CUY21SC; NepaGene) to embryos through the uterus by holding them with forceps-type electrodes (CY650P10, Unique Medical Imada, Japan). The position of the electrodes for DNA transfection into neurons in the cortex and hippocampus was the same as previous reported (Saito and Nakatsuji, 2001; Nakahira and Yuasa, 2005). After electroporation, the uterus was repositioned in the abdominal cavity and the abdominal wall and skin were sutured with surgical sutures.

The plasmids for IUE were purified with NucleoBond Xtra Midi kit (Macherey-Nagel). The composition of DNA solution for each experiment was summarized as below.

- For Cre/loxP-based Supernova labeling, a DNA solution containing the pK031.TRE-Cre (5 ng/ μ l) and pK029.CAG-loxP-STOP-loxP-RFP-ires-tTA-WPRE (1 μ g/ μ l) or pK038.CAG-loxP-STOP-loxP-EGFP-ires-tTA-WPRE (1 μ g/ μ l) or pK039.CAG-loxP-STOP-loxP-AmCyan-ires-tTA-WPRE (1 μ g/ μ l) was used.
- For SnRFP Δ tTA labeling, a DNA solution containing the pK031.TRE-Cre (5 ng/ μ l) and pK046.CAG-loxP-STOP-loxP-RFP-WPRE (1 μ g/ μ l) was used.
- For Flpe/FRT-based Supernova labeling of cortical neurons, a DNA solution containing the pK036.TRE-Flpe-WPRE (5 ng/ μ l) and pK037.CAG-FRT-STOP-FRT-RFP-ires-tTA-WPRE (1 μ g/ μ l) or pK068.CAG-FRT-STOP-FRT-EGFP-ires-tTA-WPRE (1 μ g/ μ l) was used.
- For Flpe/FRT-based Supernova labeling of hippocampal CA1 neurons, a DNA solution containing the pK036.TRE-Flpe-WPRE (50 ng/ μ l) and pK037.CAG-FRT-STOP-FRT-RFP-ires-tTA-WPRE (1 μ g/ μ l) was used.
- For Dre/Rox-based Supernova labeling, a DNA solution containing the pK073.TRE-Dre-WPRE (5

ng/ μ l) and pK129.CAG-Rox-STOP-Rox-RFP-ires-tTA-WPRE (1 μ g/ μ l) or pK224.CAG-Rox-STOP-Rox-EGFP-ires-tTA-WPRE (1 μ g/ μ l) was used.

- For regular labeling experiments, a DNA solution containing the pK024.CAsalEGFP (1 μ g/ μ l) (Horikawa and Takeichi, 2001) (Figure 2-6, 8-10, 12), pK025.CAG-RFP vector (1 μ g/ μ l) (Mizuno et al., 2010) (Figure 5-6, 11, 15) was used.
- For Flpe/FRT-SnGFP and Dre/Rox-SnGFP labeling of cortical neurons in Emx1-Cre KI mice, pK046.CAG-loxP-STOP-loxP-RFP-WPRE (1 μ g/ μ l) was co-transfected as a control.
- For Supernova mediated sparse gene knockdown experiments using CAG-loxP-CAT-loxP-GFP reporter Tg mice, a DNA solution containing the pTRE-Cre (10 ng/ μ l), pK098.CAG-loxP-STOP-loxP-nlstagRFP-ires-tTA-WPRE (1 μ g/ μ l) and pK177.CAG-loxP-STOP-loxP-mir30 (GFP RNAi) (1 μ g/ μ l) or pK178.CAG-loxP-STOP-loxP-mir30 (GFP RNAi Scramble control) (1 μ g/ μ l) was used.
- For Supernova mediated sparse gene knockdown experiments using RNZ mice, a DNA solution containing the pTRE-Cre (10 ng/ μ l), pK039: pCAG-loxP-STOP-loxP-AmCyan-ires-tTA-WPRE (1 μ g/ μ l) and pK225: pCAG-loxP-STOP-loxP-mir30 (LacZ RNAi) (1 μ g/ μ l) or pK226: pCAG-loxP-STOP-loxP-mir30 (LacZ RNAi Scramble control) (1 μ g/ μ l) was used.
- For the experiment of TALEN-mediated a2-Chn gene manipulation by Supernova system, a DNA solution containing the pK036.TRE-Flpe-WPRE (50 ng/ μ l), pK037.CAG-FRT-STOP-FRT-RFP-ires-tTA-WPRE (1 μ g/ μ l), pK217.CAG-FRT-STOP-FRT-a2Chn TALEN Left (1 μ g/ μ l) pK218.CAG-FRT-STOP-FRT-a2Chn TALEN Right (1 μ g/ μ l) was used.

Virus preparation

The preparation of AAV was prepared using AAV-DJ/8 Helper Free Packaging System (Cell Biolabs, San Diego, CA, USA). The pAAV expression vector, together with pAAV-DJ (Agilent Technologies: 240071), pHelper (Agilent Technologies: 240071) was cotransfected into HEK293FT cells in Complete Medium with penicillin and streptomycin (DMEM containing 10% heat-inactivated FBS, 1 mM sodium pyruvate solution, 0.075% sodium bicarbonate solution). At 72 h after transfection, cells were gently scraped from the flask and centrifuged at 2,500 rpm for 30 min. The supernatant was filtered through a 0.45 µm membrane filter (Millipore, Bedford, MA, USA) and transferred to ultracentrifuge tubes. 2 ml of 20% sucrose/PBS was gently added to the bottom of the supernatant. Then, the supernatant was centrifuged at 22,000 rpm at 4°C for 2 hours in a Beckman ultracentrifuge. The virus pellet was resuspended in 100 µl cold PBS and stored at -80°C. The genomic titer of each virus was determined by quantitative PCR using the primer pair: 5'-GAGTTTCCCCACACTGAGTG-3' / 5'-GAGGCTTGAGAATGAACCAAGA-3'.

Virus injection

P10 mice were anesthetized with 2.5% isoflurane. The skin on injection point was opened. A hand drill (MINIMO, Tokyo, Japan) was used to drill the skull. For one mouse, 250 nl of AAV-DIO-RFP-tTA (1.0 x 10¹³ viral genomes per ml) mixed with 250 nl of AAV-TRE-Cre (1.0 x 10⁶ viral genomes per ml) were injected unilaterally into the right hippocampus. During the virus injection, the dose of isoflurane was then reduced to 1.5%. The injection site for labeling neurons in hippocampal CA1 regions was located approximately 1 mm lateral to the sagittal suture, half between the lambda and bregma, and -1.5 mm from

the dural surface. Virus delivery was performed at a rate of 100 nl per min using a programmable syringe pump (KD Scientific) with 34-gauge beveled NanoFil needle (World Precision Instruments, Sarasota, FL, USA).

Tissue processing and immunohistochemistry

Mice were anesthetized by an overdose of isoflurane. For immunohistochemistry and SeeDB procedure, mice were transcardially perfused with 10-30 ml of saline, followed by 20 ml of 4% paraformaldehyde (PFA) in 0.1M phosphate buffer (PB) pH 7.4. Brains were immersed into 4% PFA at 4°C for overnight and then transferred into 30% sucrose in 0.1M PB and store at 4°C for 2 days.

For neural labeling experiment, brains were cut on a freezing microtome (ROM-380; Yamato) into coronal sections at 100µm. Sections were rinsed in 0.1M PB and mounted with VECTASHIELD Hard Set Mounting Medium or 0.02% n-propyl gallate in 90% glycerol (Longin et al., 1993).

Immunohistochemistry of GFP and β -galactosidase (β -gal) were done on coronal sections sectioned frontally at 50µm. Briefly, sections were first permeabilized and blocked in 0.2% Triton X-100/5% normal goat or donkey serum (Sigma) in 0.1M PB for 1 hour at room temperature and then incubated at 4°C for overnight with primary antibodies. Next day, sections were rinsed in 0.1M PB and incubated with secondary antibodies in at 4°C for overnight. For GFP immunohistochemistry, anti-GFP rat antibody (1:1000, Nacalai Tesque) and Alexa 488 Donkey anti-rat IgG (1:1000, Invitrogen) was used. For β -gal immunohistochemistry, anti- β -gal mouse antibody (1:1000, Promega) and Alexa 568 goat anti-mouse IgG (1:1000, Invitrogen) was used. Sections were rinsed in 0.1M PB and mounted with or 0.02% n-propyl

gallate in 90% glycerol (Longin et al., 1993).

Immunohistochemistry of $\alpha 2$ -Chn were done on coronal sections sectioned frontally at 40 μ m. Tissue staining using the VECTASTAIN Elite ABC system. Briefly, sections were rinsed in 0.1% Triton X-100 in 1 \times PBS (PBT) twice and incubated in 3% H₂O₂/PBS at room temperature for 20 min. Then, sections were treated with pepsin (0.1 mg/ μ l) in 0.2N HCl/0.1M PB for 7 minutes at 37 $^{\circ}$ C. Next, sections were rinsed in PBT for three times and incubated with 10% normal goat serum (NGS) in PBT at room temperature for 1 hour. After blocking, sections were incubated with anti- $\alpha 2$ -chimaerin antibody (1: 20,000 dilution)/3% NGS in PBT(Iwasato et al., 2007) at 4 $^{\circ}$ C for overnight. Next day, sections were rinsed with PBS for three times and incubated in biotinylated goat anti-rabbit IgG (Vectastain Elite PK-6101)/3 % NGS in PBS (250 μ l/well) at 4 $^{\circ}$ C for overnight. Then, sections were rinsed with PBS and incubated in StrABC/HRP (250 μ l/well) at room temperature for 1 hour with shaking. Before the detection, sections were blocked in 10% NGS in PBT at room temperature for 30 min with shaking. After incubation in Fluorophore Amplification Reagent working solution for 8 min at room temperature, sections was washed and further stained with DAPI (Roche, USA) for nuclear staining. Sections were mounted with or 0.02% n-propyl gallate in 90% glycerol (Longin et al., 1993).

Optical clearing using SeeDB

Perfused and fixed brain were cleared with the SeeDB according to the standard protocol reported previously (Ke et al., 2013). In brief, the brains were serially incubated in 20ml of 20%, 40% and 60%, (weight/volume) fructose in DW, each for 8 hours in 50 ml conical tubes with overhead tube rotator at 4

rpm at 25°C. Samples were then incubated in 80% fructose for 12 hours, 100% fructose for 12 hours and finally in SeeDB containing 80.2% weight/weight fructose for 24 hours with rotation at 25°C. All fructose solutions contained 0.5% α -thioglycerol.

Two-photon imaging

For imaging, SeeDB-cleared whole brain samples were put into a Tissue-TEK II (No.2, Sakura Finetek, Japan) and covered by a micro cover glass (24×60 mm, thickness No.1 0.12-0.17mm, Matsunami, Japan). The SeeDB solution was used for immersion (Figure 9B right panel). Imaging was performed using a LSM 7MP multiphoton microscope (Zesis) with a HighQ-2 laser, a BiG detector (Zesis), and a 20× objective lens (1.05 numerical aperture (NA)). RFP in callosal projection neuron were excited, and emitted fluorescence was filtered (575-620 nm). Sequential z-images consisted of optical sections (512×512 pixels; 1.19 μ m/pixels) with 1.74 μ m intervals. Laser power was manually adjusted to give constant fluorescent intensities at all depths. The whole cellular morphology of single L2/3 callosal projection neuron was reconstructed from totally 23×1 blocks (1 block = 607.28 μ m×607.28 μ m, Z_{\max} = 1.5mm from the surface) images from the electroplated side to contralateral side where the axons projected. Acquired three-dimensional images were analyzed using the IMARIS Filament Tracer software (Bitplane).

Image analysis and quantification

Fluorescent images were acquired using a TCS SP5 confocal microscope (Leica). For quantification the sparseness and brightness between Cre/loxP-SnRFP and Cre/loxP-SnRFP Δ tTA, Cre/loxP-SnRFP and

Flpe/FRT-SnRFP mediated neural labeling (Figure 1, 2, 7), Z-stacked-images consisted of optical sections (1024×1024 pixels, physical length $387.50 \times 387.50 \mu\text{m}$) with $1.20 \mu\text{m}$ intervals using $40 \times$ objective lens (0.85 NA) was used. The sparseness was quantified as the percentage of the number of RFP-positive neurons to the number of GFP-positive neurons, which was labeled by pK024.CAG-GFP for normalizing the transfection efficiency. For quantification of brightness, I distinguished RFP^{high} neurons as neurons labeled with RFP at high intensity, which show clear dendritic morphology from other RFP-positive neurons. The brightness was termed as the ratio of RFP^{high} neurons to RFP-positive neurons. For visualizing dendritic spines of Supernova-labeled neurons, sequential z-images consisted of optical sections (1024×1024 pixels) with $0.5 \mu\text{m}$ intervals using 63x oil immersion objective (1.4 NA) with 10x zoom was imaged.

For examination of the genomic recombination efficiency of Cre/loxP-mediated Supernova system in floxed mouse lines, Cre/loxP-SnRFP was electroporated into hippocampal CA1 region in $\alpha 2$ -Chn^{flx/flx} and $\alpha 2$ -Chn^{flx/+} mouse. The whole view of hippocampus was imaged as z-stacked-images consisted of optical sections (1024×1024 pixels) with $7 \mu\text{m}$ intervals using $10 \times$ objective lens (0.40 NA). The images used for quantification was one-step image (no z-ztack) (2048×2048 pixels) that taken by $40 \times$ objective lens (0.85 NA). I counted the percentage of cells that shows $\alpha 2$ -Chn single to the cell visualized by DAPI staining in both Cre/loxP-SnRFP labeled RFP positive cells and RFP-negative cells that around these labeled cells in the same image (Figure 13). And I also quantified the $\alpha 2$ -Chn single intensity in Cre/loxP-SnRFP labeled cells and RFP negative cells in $\alpha 2$ -Chn^{flx/flx} and $\alpha 2$ -Chn^{flx/+} mice. The lowest raw intensity of $\alpha 2$ -Chn signal in Cre/loxP-SnRFP labeled cell in $\alpha 2$ -Chn^{flx/flx} mice was considered as the background. The average of raw intensity of $\alpha 2$ -Chn signals in all RFP negative cells obtained from $\alpha 2$ -

Chn^{fl_{ox}/fl_{ox}} and α 2-Chn^{fl_{ox}/+} mice was considered to be 100% and was used to normalize the raw intensity of α 2-Chn signal in Cre/loxP-SnRFP labeled cells.

For quantification of the efficiency of RNAi-mediated gene knockdown in Supernova labeled neurons, Z-stacked-images consisted of optical sections (1024 \times 1024 pixels,) with 1.20 μ m intervals using 40 \times objective lens (0.85 NA) was used. The background intensity of each channel (channel 1 for reporter gene expression; channel 2 for Supernova labeling intensity) was quantified in an area without neural labeling in the same image. The knockdown efficiency = (Raw intensity of reporter gene - channel 1 background)/(Raw intensity of Supernova labeling intensity- channel 2 background) \times 100%. For both knockdown group (n=5 mice) and control group (n=5 mice), three images from each individual was taken and quantified.

Finally, for the experiment of TALEN-mediated gene manipulation using Supernova System, one-step image (no z-stack) (2048 \times 2048 pixels) that was taken by 40 \times objective lens (0.85 NA) was used. The cells in each image were divided into three groups depending on the α 2-Chn signals. Because hippocampal CA1 pyramidal neurons ubiquitously express very high level of α 2-Chn during early postnatal period, thus α 2-Chn^{high} cells refer to cells that show high intensity of α 2-Chn signals, and the intensity of the signal are similar with that in surround RFP-negative cells (control cells). α 2-Chn^{negative} refers to cells in which the α 2-Chn signals would not be detected. α 2-Chn^{low} cells refer to cells, in which the α 2-Chn signals can be visualized, but the intensity of α 2-Chn signals are weaker than that in surround RFP-negative cells (control cells). The percentage of α 2-Chn^{high}, α 2-Chn^{low} and α 2-Chn^{negative} in SnRFP labeled cells and RFP-negative cells (control cells) were counted.

Statistics

Microsoft Excel and SPSS statistics version 19 were used to conduct the statistical analyses. For parametrical statistics, two-tailed unpaired Student's t-test for two independent samples or analysis of variance (ANOVA) for multiple independent samples was used. The differing means were identified using the Tukey-Kramer post hoc test after ANOVA. $P < 0.05$ was considered significant. Values are given as mean \pm standard errors (SE). Asterisks in figures indicate as follows: * for $p < 0.05$, ** for $p < 0.01$, *** for $p < 0.001$.

ACKNOWLEDGMENTS

First, I would like to express deepest appreciation to my supervisor, Professor Takuji Iwasato, who gave me the chance for studying neuroscience. Without his invaluable guidance, understanding, patience and encouragement, this study would not have been possible. Thank you for believing in me, even when I did not believe myself.

I would also like to express my sincere gratitude to Dr. Hidenobu Mizuno, who helped to get me started on the path to neuroscience. His encouragement and faith in me throughout have been extremely helpful. He was always available for my questions and he was positive and gave generously of his time and vast knowledge. Thank you for your helpful discussions, precise directions, technical supports and constant encouragement on this project.

I owe a deep sense of gratitude to Dr. Ryohei Iwata for his keep interest on me at every stage of my research. Your prompt inspirations, timely suggestions with kindness, enthusiasm and dynamism, especially, your technical assistance on viral infection and TALEN experiments have enabled me to complete my thesis.

I also appreciate my Progress Committee Members, Professors Yumiko Saga, Hiroyuki Araki, Tatsumi Hirata, Emiko Suzuki, Hiromi Hirata, and previous member, Professor Yasushi Hiromi for their input, valuable discussions and critical reading of the manuscripts.

I am very grateful for the friendship of Iwasato lab members, Dr. Shota Katori, Takuya Sato, Satoko Kouyama, Minako Kanbayashi.-I thank you all for the moral support, encouragements, that I will forever treasure. Especially, I profusely thank Dr. Ayumi Suzuki, Shingo Nakazawa and all of my friends

for listening and giving me words of encouragement, helping me survive all the stress and not letting me give up. You made my years at NIG a delight!

Thanks are due to all the staffs in NIG and SOKENDAI for their kind help and co-operation throughout my study period.

Thanks are also due to my former laboratory colleagues in Hokkaido University, Professor Naoshi Hiramatsu and Dr. Osamu Nishimiya for their constant encouragement and supports.

And appreciates are further extended to JSPS, JASSO and Iwatani Naoji Foundation for the financial supports.

Last and not least, I would like to thank my beloved family for letting me be the person I am today. Without your untiring love, constant guidance, encouragement moral and financial supports, I could not have made this far. I love you all!

REFERENCES

- Ako, R., Wakimoto, M., Ebisu, H., Tanno, K., Hira, R., Kasai, H., Matsuzaki, M., and Kawasaki, H. (2011). Simultaneous visualization of multiple neuronal properties with single-cell resolution in the living rodent brain. *Molecular and Cellular Neuroscience* 48, 246-257.
- Anastassiadis, K., Fu, J., Patsch, C., Hu, S., Weidlich, S., Duerschke, K., Buchholz, F., Edenhofer, F., and Stewart, A.F. (2009). Dre recombinase, like Cre, is a highly efficient site-specific recombinase in *E. coli*, mammalian cells and mice. *Disease Models & Mechanisms* 2, 508-515.
- Chung, K., Wallace, J., Kim, S.-Y., Kalyanasundaram, S., Andalman, A.S., Davidson, T.J., Mirzabekov, J.J., Zalocusky, K.A., Mattis, J., and Denisin, A.K. (2013). Structural and molecular interrogation of intact biological systems. *Nature* 497, 332-337.
- Dacey, D.M., and Lee, B.B. (1994). The 'blue-on' opponent pathway in primate retina originates from a distinct bistratified ganglion cell type. *Nature* 367, 731-735.
- David, S., and Aguayo, A.J. (1981). Axonal elongation into peripheral nervous system "bridges" after central nervous system injury in adult rats. *Science* 214, 931-933.
- Dhande, O.S., Hua, E.W., Guh, E., Yeh, J., Bhatt, S., Zhang, Y., Ruthazer, E.S., Feller, M.B., and Crair, M.C. (2011). Development of single retinofugal axon arbors in normal and $\beta 2$ knock-out mice. *The Journal of Neuroscience* 31, 3384-3399.
- Ehrengruber, M.U., Hennou, S., Büeler, H., Naim, H.Y., Déglon, N., and Lundstrom, K. (2001). Gene transfer into neurons from hippocampal slices: comparison of recombinant Semliki Forest Virus, adenovirus, adeno-associated virus, lentivirus, and measles virus. *Molecular and*

Cellular Neuroscience 17, 855-871.

Espinosa, J.S., and Luo, L. (2008). Timing neurogenesis and differentiation: insights from quantitative clonal analyses of cerebellar granule cells. *The Journal of Neuroscience* 28, 2301-2312.

Espinosa, J.S., Wheeler, D.G., Tsien, R.W., and Luo, L. (2009). Uncoupling dendrite growth and patterning: single-cell knockout analysis of NMDA receptor 2B. *Neuron* 62, 205-217.

Feng, G., Mellor, R.H., Bernstein, M., Keller-Peck, C., Nguyen, Q.T., Wallace, M., Nerbonne, J.M., Lichtman, J.W., and Sanes, J.R. (2000). Imaging Neuronal Subsets in Transgenic Mice Expressing Multiple Spectral Variants of GFP. *Neuron* 28, 41-51.

Festenstein, R., Tolaini, M., Corbella, P., Mamalaki, C., Parrington, J., Fox, M., Miliou, A., Jones, M., and Kioussis, D. (1996). Locus control region function and heterochromatin-induced position effect variegation. *Science* 271, 1123-1125.

Gianino, S., Stein, S.A., Li, H., Lu, X., Biesiada, E., Ulas, J., and Xu, X.M. (1999). Postnatal growth of corticospinal axons in the spinal cord of developing mice. *Developmental brain research* 112, 189-204.

Golgi, C. (1873). Sulla struttura della sostanza grigia del cervello. *Gazzetta Medica Italiana Lombardia* 33, 244-246.

Hall, C., Michael, G.J., Cann, N., Ferrari, G., Teo, M., Jacobs, T., Monfries, C., and Lim, L. (2001). α 2-chimaerin, a Cdc42/Rac1 regulator, is selectively expressed in the rat embryonic nervous system and is involved in neuriteogenesis in N1E-115 neuroblastoma cells. *The Journal of Neuroscience* 21, 5191-5202.

- Hama, H., Kurokawa, H., Kawano, H., Ando, R., Shimogori, T., Noda, H., Fukami, K., Sakaue-Sawano, A., and Miyawaki, A. (2011). Scale: a chemical approach for fluorescence imaging and reconstruction of transparent mouse brain. *Nat Neurosci* 14, 1481-1488.
- Hippenmeyer, S., Youn, Y.H., Moon, H.M., Miyamichi, K., Zong, H., Wynshaw-Boris, A., and Luo, L. (2010). Genetic mosaic dissection of *Lis1* and *Ndel1* in neuronal migration. *Neuron* 68, 695-709.
- Hitoshi, N., Ken-ichi, Y., and Jun-ichi, M. (1991). Efficient selection for high-expression transfectants with a novel eukaryotic vector. *Gene* 108, 193-199.
- Honig, M.G., and Hume, R.I. (1989). Dil and diO: versatile fluorescent dyes for neuronal labelling and pathway tracing. *Trends in neurosciences* 12, 333-341.
- Horikawa, K., and Armstrong, W. (1988). A versatile means of intracellular labeling: injection of biocytin and its detection with avidin conjugates. *Journal of neuroscience methods* 25, 1-11.
- Iwasato, T., Datwani, A., Wolf, A.M., Nishiyama, H., Taguchi, Y., Tonegawa, S., Knöpfel, T., Erzurumlu, R.S., and Itohara, S. (2000). Cortex-restricted disruption of NMDAR1 impairs neuronal patterns in the barrel cortex. *Nature* 406, 726-731.
- Iwasato, T., Erzurumlu, R.S., Huerta, P.T., Chen, D.F., Sasaoka, T., Ulupinar, E., and Tonegawa, S. (1997). NMDA receptor-dependent refinement of somatotopic maps. *Neuron* 19, 1201-1210.
- Iwasato, T., Inan, M., Kanki, H., Erzurumlu, R.S., Itohara, S., and Crair, M.C. (2008). Cortical adenylyl cyclase 1 is required for thalamocortical synapse maturation and aspects of layer IV barrel development. *The Journal of Neuroscience* 28, 5931-5943.

- Iwasato, T., Kato, H., Nishimaru, H., Ishikawa, Y., Inoue, H., Saito, Y.M., Ando, R., Iwama, M., Takahashi, R., and Negishi, M. (2007). Rac-GAP α -chimerin regulates motor-circuit formation as a key mediator of EphrinB3/EphA4 forward signaling. *Cell* 130, 742-753.
- Iwasato, T., Nomura, R., Ando, R., Ikeda, T., Tanaka, M., and Itohara, S. (2004). Dorsal telencephalon-specific expression of Cre recombinase in PAC transgenic mice. *Genesis* 38, 130-138.
- Iwata, R., Ohi, K., Kobayashi, Y., Masuda, A., Iwama, M., Yasuda, Y., Yamamori, H., Tanaka, M., Hashimoto, R., Itohara, S., et al. (2014). RacGAP α 2-Chimaerin Function in Development Adjusts Cognitive Ability in Adulthood. *Cell Reports* 8, 1257-1264.
- Kaplitt, M.G., Leone, P., Samulski, R.J., Xiao, X., Pfaff, D.W., O'Malley, K.L., and Doring, M.J. (1994). Long-term gene expression and phenotypic correction using adeno-associated virus vectors in the mammalian brain. *Nature genetics* 8, 148-154.
- Kawaguchi, S.-y., and Hirano, T. (2006). Integrin α 3 β 1 suppresses long-term potentiation at inhibitory synapses on the cerebellar Purkinje neuron. *Molecular and Cellular Neuroscience* 31, 416-426.
- Kawamoto, S., Niwa, H., Tashiro, F., Sano, S., Kondoh, G., Takeda, J., Tabayashi, K., and Miyazaki, J.-i. (2000). A novel reporter mouse strain that expresses enhanced green fluorescent protein upon Cre-mediated recombination. *FEBS Letters* 470, 263-268.
- Ke, M.-T., Fujimoto, S., and Imai, T. (2013). SeeDB: a simple and morphology-preserving optical clearing agent for neuronal circuit reconstruction. *Nat Neurosci* 16, 1154-1161.
- Kim, J.-Y., Ash, R.T., Ceballos-Diaz, C., Levites, Y., Golde, T.E., Smirnakis, S.M., and Jankowsky, J.L. (2013). Viral transduction of the neonatal brain delivers controllable genetic mosaicism for

- visualizing and manipulating neuronal circuits in vivo. *The European journal of neuroscience* 37, 1203-1220.
- Kim, J., Zhao, T., Petralia, R.S., Yu, Y., Peng, H., Myers, E., and Magee, J.C. (2012). mGRASP enables mapping mammalian synaptic connectivity with light microscopy. *Nature methods* 9, 96-102.
- Kobayashi, Y., Sano, Y., Vannoni, E., Goto, H., Ikeda, T., Suzuki, H., Oba, A., Kawasaki, H., Kanba, S., Lipp, H.-P., et al. (2013). Genetic dissection of medial habenula–interpeduncular nucleus pathway function in mice. *Frontiers in Behavioral Neuroscience* 7.
- Langevin, L.M., Matter, P., Scardigli, R., Roussigné, M., Logan, C., Blader, P., and Schuurmans, C. (2007). Validating in utero electroporation for the rapid analysis of gene regulatory elements in the murine telencephalon. *Developmental Dynamics* 236, 5, 1273-1286.
- Liang, P., Moret, V., Wiesendanger, M., and Rouiller, E.M. (1991). Corticomotoneuronal connections in the rat: Evidence from double-labeling of motoneurons and corticospinal axon arborizations. *The Journal of Comparative Neurology* 311, 356-366.
- Liu, C., Sage, J.C., Miller, M.R., Verhaak, R.G., Hippenmeyer, S., Vogel, H., Foreman, O., Bronson, R.T., Nishiyama, A., and Luo, L. (2011). Mosaic analysis with double markers reveals tumor cell of origin in glioma. *Cell* 146, 209-221.
- Longin, A., Souchier, C., Ffrench, M., and Bryon, P. (1993). Comparison of anti-fading agents used in fluorescence microscopy: image analysis and laser confocal microscopy study. *Journal of Histochemistry & Cytochemistry* 41, 1833-1840.
- Mizuno, H., Hirano, T., and Tagawa, Y. (2007). Evidence for activity-dependent cortical wiring: formation

- of interhemispheric connections in neonatal mouse visual cortex requires projection neuron activity. *The Journal of Neuroscience* 27, 6760-6770.
- Mizuno, H., Hirano, T., and Tagawa, Y. (2010). Pre - synaptic and post - synaptic neuronal activity supports the axon development of callosal projection neurons during different post - natal periods in the mouse cerebral cortex. *European Journal of Neuroscience* 31, 410-424.
- Mizuno, H., Luo, W., Tarusawa, E., Saito, Y.M., Sato, T., Yoshimura, Y., Itohara, S., and Iwasato, T. (2014). NMDAR-regulated dynamics of layer 4 neuronal dendrites during thalamocortical reorganization in neonates. *Neuron* 82, 365-379.
- Muzumdar, M.D., Luo, L., and Zong, H. (2007). Modeling sporadic loss of heterozygosity in mice by using mosaic analysis with double markers (MADM). *Proceedings of the National Academy of Sciences* 104, 4495-4500.
- Parrish, J.Z., Emoto, K., Kim, M.D., and Jan, Y.N. (2007). Mechanisms that regulate establishment, maintenance, and remodeling of dendritic fields. *Annu Rev Neurosci* 30, 399-423.
- Peel, A.L., and Klein, R.L. (2000). Adeno-associated virus vectors: activity and applications in the CNS. *Journal of neuroscience methods* 98, 95-104.
- Saito, T., and Nakatsuji, N. (2001). Efficient gene transfer into the embryonic mouse brain using in vivo electroporation. *Developmental biology* 240, 237-246.
- Scott, E.K., and Luo, L. (2001). How do dendrites take their shape? *Nature neuroscience* 4, 359-365.
- Sohal, V.S., Zhang, F., Yizhar, O., and Deisseroth, K. (2009). Parvalbumin neurons and gamma rhythms enhance cortical circuit performance. *Nature* 459, 698-702.

- Tabata, H., and Nakajima, K. (2001). Efficient in utero gene transfer system to the developing mouse brain using electroporation: visualization of neuronal migration in the developing cortex. *Neuroscience* 103, 865-872.
- Tasic, B., Miyamichi, K., Hippenmeyer, S., Dani, V.S., Zeng, H., Joo, W., Zong, H., Chen-Tsai, Y., and Luo, L. (2012). Extensions of MADM (mosaic analysis with double markers) in mice. *PLoS ONE* 7, e33332.
- Tomer, R., Ye, L., Hsueh, B., and Deisseroth, K. (2014). Advanced CLARITY for rapid and high-resolution imaging of intact tissues. *Nat Protocols* 9, 1682-1697.
- Wong, R.O., and Ghosh, A. (2002). Activity-dependent regulation of dendritic growth and patterning. *Nature reviews neuroscience* 3, 803-812.
- Young, P., Qiu, L., Wang, D., Zhao, S., Gross, J., and Feng, G. (2008). Single-neuron labeling with inducible Cre-mediated knockout in transgenic mice. *Nature neuroscience* 11, 721-728.
- Zhang, F., Wang, L.-P., Brauner, M., Liewald, J.F., Kay, K., Watzke, N., Wood, P.G., Bamberg, E., Nagel, G., Gottschalk, A., et al. (2007). Multimodal fast optical interrogation of neural circuitry. *Nature* 446, 633-639.
- Zong, H., Espinosa, J.S., Su, H.H., Muzumdar, M.D., and Luo, L. (2005). Mosaic analysis with double markers in mice. *Cell* 121, 479-492.

FIGURE LEGENDS

Figure 1. The design of Supernova system

(A) Schematic representation of the vector sets. The Supernova RFP (SnRFP) consists of two vectors: tetracycline response element (TRE)-Cre (TRE-Cre) and CAG-loxP-STOP-loxP-RFP-ires-tTA-WPRE (LSL-RFP-tTA).

(B) The strategy of Supernova system. (1) Initially, the leakage of TRE occasionally drives very weak Cre expression, only in a small portion of cells that are transfected with both two vectors. Cre subsequently excises the LSL cassette in a few copies of the LSL-RFP-tTA vector, initiating the transcription of RFP and tetracycline transactivator (tTA). (2) Through binding with TRE, tTA further facilitates the expression of Cre. This positive feedback loop of tTA-TRE leads to a high expression level of both Cre and RFP.

Figure 2. Supernova system achieved sparse neural labeling with high fluorescent intensity

(A) Schematic representation of the vector sets. As a control for examining the efficacy of TRE-tTA enhancement, the ires-tTA cassette was deleted from the *LSL-RFP-tTA* vector (SnRFP Δ tTA).

(B) TRE-tTA cycles facilitated RFP expression in SnRFP-labeled neurons. Layer 4 (L4) cortical neurons at postnatal day 16 (P16) labeled with SnRFP (upper panel) and SnRFP Δ tTA (lower panel) by in utero electroporation (IUE) at embryonic day 14.5 (E14.5). The fluorescent images were acquired using a confocal microscope under low laser power to avoid the saturation of fluorescent signals in cell bodies of labeled neurons.

(C) The sparseness of Supernova labeling. $8.18\% \pm 0.92\%$ (n=4 mice) of CAG-GFP positive neurons are

SnRFP-positive. Similarly, $8.60\% \pm 1.21\%$ (n=4 mice) of GFP-expressing cells expressed RFP in SnRFP Δ tTA labeling. All values represent mean \pm SEM. (NS): not significant, unpaired Student's *t*-test.

(D) The brightness of Supernova labeling. The average brightness of RFP signals in the cell bodies of SnRFP-labeled neurons (1.07 ± 0.11 , n = 4 mice, total 86 cells) was significantly higher than that in SnRFP Δ tTA labeled neurons (0.86 ± 0.06 , n = 4 mice, total 124 cells). The intensity of GFP signals in the same individual RFP-positive neurons was used to normalize the electroporation efficiency. All values represent mean \pm SEM. (*) $P < 0.05$, unpaired Student's *t*-test.

Figure 3. Supernova system achieved sparse neural labeling with high fluorescent intensity

(A) RFP expression enhanced by TRE-tTA cycles enabled clear visualization of dendrites in SnRFP-labeled neurons. The same samples used in Figure 2B were re-photo using a confocal microscope under relative high laser power to detect the dendrites of labeled neurons. Arrows: RFP^{high} neurons in which the whole dendritic morphology could be clearly visualized. Arrow heads: RFP^{low} neurons in which only the cell body can be identified.

(B) The high intensity of SnRFP labeling. The brightness was defined as the ratio between the number of RFP^{high} neurons and total RFP-positive neurons. $53.69\% \pm 4.47\%$ (n=3 mice) of SnRFP-labeled neurons were RFP^{high} neurons, while only $24.87\% \pm 1.33\%$ (n=3 mice) of SnRFP Δ tTA labeled neurons were RFP^{high} neurons, indicating that the RFP expression was amplified by TRE-tTA cycles. All values represent mean \pm SEM.

Figure 4. The developmental time course of Supernova labeling

(A) SnRFP could be observed two days after transfection. SnRFP and CAG-GFP was co-transfected into cortical neurons by IUE at E14.5 and the coronal sections were made from the E16.5 mouse brain. Arrows: the leading processes of labeled neuron.

(B) Images of SnRFP-labeled cortical neurons during early postnatal period. CAG-GFP indicated regular labeling. At P0, SnRFP was already bright enough to visualize dendritic morphology of labeled neurons.

(C) The sparseness of Supernova system was not changed during the first postnatal week. The ratio of RFP-positive neurons to GFP-positive neurons was quantified, with $4.50\% \pm 0.40\%$ (n=3 mice) at P0, $4.73\% \pm 0.33\%$ (n=4 mice) at P4 and $5.63\% \pm 0.75\%$ (n=5 mice) at P8. The ratio of RFP^{high} to total RFP-positive neurons was $59.77\% \pm 9.29\%$ (n=5 mice) in P8 brain, which were similar to results of previous quantification in Figure 1D. All values represent mean \pm SEM, one-way ANOVA, (NS) not significant.

Figure 5. The color variation of Supernova labeling

(A) Schematic representation of the expanded “Supernova” vector sets. Restriction sites (SalI/ EcoRV) were introduced into the original *LSL-RFP-tTA* vector, thus the target gene X (e.g., fluorescent protein) can be easily adapted into Supernova systems by subcloning into SalI/ EcoRV sites of the *LSL-Gene X-tTA* vector.

(B) Sparsely labeled cortical neurons with various fluorescent proteins. Supernova Amcyan (SnAmyan), SnGFP and SnRFP were delivered into layer V, layer IV and layer II/III cortical neurons by IUE at E13.5, E14.5 and E15.5, respectively. CAG-LSL-GFP or CAG-LSL-RFP vector was co-electroporated to indicate

transfected neurons. The coronal sections were made from P8 brains.

Figure 6. High intensity of Supernova labeling enabled clear visualization of dendrites.

Supernova labeling (right panel) is sparse and bright enough to visualize the morphology of labeled neurons in a single cell level. Compare to the regular labeling (middle panel) with CAG-RFP or CAG-GFP (middle panels and merge in left panels). SnAmcyan, SnGFP and SnRFP were introduced into cortical neurons in different cortical layers by IUE at E13.5, E14.5 and E15.5, respectively. Coronal sections of the P8 mouse brains were made. The CAG-RFP or CAG-GFP vector was co-transfected to indicate the transfected neurons.

Figure 7. High intensity of Supernova labeling enabled clear visualization of dendritic spines.

SnAmcyan, SnGFP, SnRFP-labeled cortical neurons. Coronal brain sections were prepared from 1 month-old mice.

Figure 8. Visualization of individual corticospinal axons by Supernova labeling

(A) Schematic representation of the corticospinal tract, which arises in the deep layer of motor cortex, crosses the midline at medulla, and extends to the spinal cord. Right panel, the coronal view of spinal cord.

(B) SnRFP and CAG-GFP were transfected into cortical neurons in the motor cortex by IUE at E13.5.

Sagittal sections (100 μ m thick) were made from the P5 mouse brain.

(C) Coronal sections at cervical enlargement of the spinal cord showed single corticospinal axons. Lower

panel: higher magnification images of the rectangle in the upper panel.

Figure 9. The Supernova vector sets based on Flpe/FRT.

(A) Schematic representation of Flpe/FRT-based SnRFP (Flpe/FRT-SnRFP). As a control for examining the efficacy of TRE-tTA enhancement, the ires-tTA was deleted from the *FSF-RFP-tTA* vector (Flpe/FRT-SnRFP Δ tTA).

(B) Images of L2/3 labeled by Flpe/FRT-SnRFP (upper panel) and Flpe/FRT-SnRFP Δ tTA (lower panel).

Briefly, Flpe/FRT-SnRFP and Flpe/FRT-SnRFP Δ tTA were electroporated into L2/3 cortical neurons by IUE at E15.5. CAG-GFP was co-transfected to indicate the transfected neurons. Brains were sampled at P16.

Figure 10. Flpe/FRT-based Supernova system achieved sparse and high intensity neural labeling.

(A) Higher magnification images of Figure 9B. The fluorescent images were acquired using a confocal microscope under low laser power to avoid the saturation of fluorescent signals in cell bodies of labeled neurons.

(B) The sparseness of Flpe/FRT-based Supernova labeling. $1.67\% \pm 0.17\%$ (n=5 mice) of CAG-GFP positive neurons are Flpe/FRT-SnRFP-positive, while only $0.48\% \pm 0.10\%$ (n=5 mice) of GFP-expressing cells expressed RFP in Flpe/FRT-SnRFP Δ tTA labeling. All values represent mean \pm SEM. (***) $p < 0.001$, unpaired Student's *t*-test.

(C) TRE-tTA cycles facilitated RFP expression in Flpe/FRT-SnRFP-labeled neurons. The average brightness of RFP signals in the cell bodies of Flpe/FRT-SnRFP-labeled neurons (2.035 ± 0.19 , n = 4 mice,

total 155 neurons) was significantly higher than that in SnRFP Δ tTA labeled neurons (0.26 ± 0.02 , n = 4 mice, total 81 cells). The intensity of GFP signals in the same individual RFP-positive neurons was used to normalize the electroporation efficiency. All values represent mean \pm SEM. (***) P<0.001, unpaired Student's *t*-test.

Figure 11. The number of Flpe/FRT-SnGFP labeled neurons could be adjusted.

(A) Images of L2/3 cortical neurons labeled by Flpe/FRT-SnGFP. The concentration of TRE-Flpe vector in DNA solution was 5ng/ μ l (upper panel) and 500ng/ μ l (lower panel), separately. CAG-RFP was co-transfected to indicate the transfected cells. Coronal sections were made from P8 brains.

(B) The quantification of cell numbers that were labeled with Flpe/FRT-SnGFP. $1.43\% \pm 0.09\%$ (n=5 mice) of RFP positive neurons were labeled by Flpe/FRT-SnGFP, when 5ng/ μ l was used as the final concentration of TRE-Flpe vector. In contrast, almost all of RFP positive neurons ($98.71\% \pm 2.46\%$, n=5 mice) were labeled by Flpe/FRT-SnGFP, when the final concentration of TRE-Flpe vector were increased to 500ng/ μ l. All values represent mean \pm SEM. (***) P<0.001, unpaired Student's *t*-test.

Figure 12. Flpe/FRT-based Supernova system shows more excellent properties in sparseness and brightness than those of Cre/loxP-based Supernova system in neural labeling.

(A) Schematic representation of Supernova vector sets based on Cre/loxP and Flpe/FRT.

(B) L2/3 cortical neurons labeled by Cre/loxP-based Supernova RFP (Cre/loxP-SnRFP, upper panel) and Flpe/FRT-based Supernova RFP (Flpe/FRT-SnRFP, lower panel). Electroporation was performed at E15.5

and coronal sections were made from the P6 mouse brain. The fluorescent images were acquired using a confocal microscope.

(C) Compared to Cre/loxP-SnRFP, Flpe/FRT-SnRFP achieved better sparseness in neural labeling. In (B) $14.84\% \pm 3.27\%$ (n=4 mice) of GFP positive neurons were labeled by Cre/loxP-SnRFP. This ratio was significantly lower when Flpe/FRT-SnRFP was used for labeling, which was $1.95\% \pm 0.23\%$ (n=4 mice).

All values represent mean \pm SEM, (**) $0.001 < P < 0.01$, unpaired Student's *t-test*.

(D) Flpe/FRT-SnRFP labeling shows less background than Cre/loxP-SnRFP labeling. The percentage of RFP^{high} neurons to total RFP-positive neurons is much higher in Flpe/FRT-SnRFP labeling ($90.00\% \pm 7.93\%$, n=4 mice), comparing to that in Cre/loxP-based SnRFP labeling ($55.99\% \pm 3.60\%$, n=4 mice). All values represent mean \pm SEM, (**) $0.001 < P < 0.01$, unpaired Student's *t-test*.

Figure 13. High fluorescent intensity of Flpe/FRT-SnRFP labeling enabled visualization of single dendritic spines.

Flpe/FRT-SnRFP was introduced into hippocampal CA1 pyramidal neurons by IUE at E14.5. The brain was dissected at P14. Coronal sections were made, followed by DAPI-staining to reveal the hippocampal structure. DG: dentate gyrus.

Figure 14. Imaging and reconstruction of Flpr/FRT-SnRFP labeled callosal projection neuron in intact whole brain.

(A) Optical clearing of the P5 mouse brain using the SeeDB method ((Ke et al., 2013).

(B-D) Fluorescence imaging and reconstruction of individual callosal projection neuron. (B) Flpe/FRT-SnRFP was electroporated into the right hemisphere of cerebral cortex at E15.5. At P12, the brain was perfused, fixed and proceed with SeeDB. Fine morphological architecture and fluorescent signal is preserved in SeeDB cleared brain. Two-photon microscopy was utilized to capture the images of a labeled neuron (arrowhead) from the dorsal cortical surface. (C) Z-stacked two-photon images of Flpe/FRT-SnRFP labeled callosal projection neuron. (D) 3D reconstruction of labeled callosal projection neuron (right panel) and its collosal fibers (left panel).

Figure 15. Supernova systems based on Flpe/Frt and Dre/Rox enabled sparse neural labeling in

Emx1Cre KI mice

(A-B) Schematic representation of the Supernova vector set, in which the Cre/loxP was replaced by another recombinase system, Flpe/FRT or Dre/Rox.

(C) Comparing to Cre-dependent neural labeling by CAG-LSL-RFP in Emx1Cre knock-in (KI) mice, Flpe/FRT-based SnGFP (Flpe/FRT-SnGFP) and Dre/Rox-based SnGFP (Dre/Rox-SnGFP) labeled only a small portion of cortical neurons with their dendritic morphology was clearly visible. Briefly, vectors for Flpe/FRT-SnGFP and Dre/Rox-SnGFP, together with CAG-LSL-RFP were delivered into cortical neurons of Emx1Cre KI mice by IUE at E14.5, separately. The brains were dissected at P8, and coronal sections were made.

(D) The high intensity of Flpe/FRT-SnRFP and Dre/Rox-SnRFP labeling was maintained even in adult (3-month-old) mice, and enabled clear visualization of whole cellular morphology including dendritic spines.

Vectors for Flpe/FRT-SnRFP and Dre/Rox-SnRFP were delivered into cortical neurons of Emx1Cre KI mice by IUE at E14.5, separately. Three-month-old mouse brains were fixed and cut into coronal sections.

(E) Schematic image shows the Cre-expression in Emx1Cre KI mice (Iwasato et al., 2000; Iwasato et al., 2008; Iwasato et al., 2004). Cx, cortex; O, olfactory bulb; H, hippocampus; C, cerebellum; B, brainstem; S, spinal cord.

Figure 16. Co-expression of multiple proteins in a single cell

(A) Schematic representation of a Cre/loxP-based Supernova vector set for co-expression of two genes, the nuclear localization signal (nls)-RFP (nlsRFP) and GFP in a single cell.

(B) Utilizing the Cre/loxP-based Supernova system, nlsRFP and GFP was co-expressed in a small population of cortical neurons by IUE at E14.5. Coronal brain sections were made at P4.

(C) Schematic representation of an Flpe/FRT-based Supernova vector set for co-expression of two genes, the RFP and GFP, in a single cell.

(D) Using the Flpe/FRT-based Supernova system, RFP and GFP are co-expressed in isolated sparse neurons. Coronal brain sections were made at P16.

Figure 17. AAV-mediated Supernova system enabled visualization of isolated single neuron in the hippocampus.

(A) Schematic representation of the Supernova vector set that designed for adeno-associated virus (AAV) infection. In the cells transfected with both vectors, leakage from TRE drives weak expression of Cre,

which arouse Cre-dependent inversion of RFP-P2A-tTA in *AAV-DIO-RFP-tTA* vector. TRE-tTA cycles further enhance the expression of both Cre and RFP.

(B) Time schedule of viral infection.

(C) Typical morphologies of sparsely labeled hippocampal CA1 pyramidal neurons (P30). AAV-based SnRFP (AAV-SnRFP) was injected into the mouse hippocampus at P10. Twenty days after transfection, the brain was dissected. After sectioning, DAPI-staining was performed to visualize the hippocampal structure.

Upper: low-power images of a coronal section through P30 hippocampus transfected with AAV-SnRFP.

Lower: higher-magnification of the square in the upper panel. DG: dentate gyrus.

(D) Spines of the dendrites (arrowhead in C lower panel) of AAV-SnRFP labeled hippocampal CA1 pyramidal neurons.

Figure 18. The efficacy and specificity of Cre/loxP-based Supernova system in the excision of a floxed fragment from chromosome.

(A) Schematic image showing Cre/loxP-SnRFP induced GFP expression in CAG-loxP-CAT-loxP-GFP reporter mouse.

(B) Genomic recombination is restricted in SnRFP-labeled neurons. Cre/loxP-SnRFP was transfected into L2/3 cortical neurons of GFP reporter mice by IUE at E15.5. Coronal sections were made from the P8 brain, followed by immunohistochemistry to enhance the GFP signals. In P8 brain section, almost all of SnRFP-labeled neurons (359/397 cells, n=3 mice) expressed GFP. Notably, all of RFP^{high} neurons were labeled by GFP (291/291 cells, n=3 mice). On the contrary, all GFP positive neurons were labeled by SnRFP (359/359

cells, n=3 mice).

Figure 19. Labeled cell-specific $\alpha 2$ -Chn KO via Cre/loxP-based Supernova system in $\alpha 2$ -Chn flox/flox mice.

(A) Schematic images for Supernova-mediated knockout (KO) of $\alpha 2$ -chimaerin ($\alpha 2$ -Chn) in a $\alpha 2$ -Chn floxed mouse line, in which the essential exon encoding $\alpha 2$ -Chn is flanked by two loxP sites.

(B) Single cell $\alpha 2$ -Chn KO in SnRFP-labeled hippocampal CA1 neurons. Cre/loxP-SnRFP was electroporated into hippocampal CA1 region at E14.5. Brain was sampled at P14. $\alpha 2$ -Chn immunohistochemistry and DAPI-staining were performed to visualize $\alpha 2$ -Chn expression and soma of cells, respectively, in hippocampal CA1 region. Left panel shows the hippocampus of $\alpha 2$ -Chn floxed mouse electroporated with SnRFP. Two sets of enlarged example images are shown in the right. DG: dentate gyrus.

(C) Quantification of Supernova-dependent $\alpha 2$ -Chn knockout efficiency. Almost all of CA1 hippocampal cells ($97.70\% \pm 0.09\%$, n=3 mice) express $\alpha 2$ -Chn, while only $5.93\% \pm 3.00\%$ (n=3 mice) of weak SnRFP labeled neurons were shown $\alpha 2$ -Chn signals. All values represent mean \pm SEM, (**) $0.001 < P < 0.01$, unpaired Student's *t*-test.

Figure 20. Comparison of $\alpha 2$ -Chn protein expression level in Cre/loxP-SnRFP labeled hippocampal neurons in $\alpha 2$ -Chn flox/+ mice and α -Chn flox/flox mice.

(A) Experimental protocol.

(B) Representative images of Cre/loxP-SnRFP labeled hippocampal CA1 neurons in $\alpha 2$ Chn flox/+ mice

and $\alpha 2$ -Chn flox/flox mice. Cre/loxP-SnRFP was electroporated into hippocampal CA1 region at E14.5. Brain was sampled at P14. $\alpha 2$ -Chn immunohistochemistry was performed to visualize $\alpha 2$ -Chn expression.

(C) The $\alpha 2$ -Chn protein expression levels in RFP-positive cells in $\alpha 2$ -Chn flox/flox mice were significantly lower than those in $\alpha 2$ flox/+ mice and $\alpha 2$ -Chn flox/flox mice, excluding the possibility that high RFP expression may impede the expression of $\alpha 2$ -Chn in the experiments for Figure 14. One-way ANOVA, (***) $p < 0.001$.

Figure 21. RNAi-mediated Supernova achieved labeled cell-specific gene knockdown in GFP reporter mice

(A) Schematic representation of a Supernova vector set that is designed for single cell GFP knockdown. shRNA against GFP was expressed by *LSL-mir30*, which is a Cre-dependent shRNA expression vector (Matsuda and Cepko, 2007).

(B) Illustrate showing strategy for examination of Supernova-mediated GFP knockdown.

(C) CAG-LSL-mir30 (GFP RNAi) (lower panels) or CAG-LSL-mir30 (GFP RNAi scramble sequence) (upper panels) was co-electroporated with Supernova nlsRFP (Sn-nlsRFP) into CAG-loxP-CAT-loxP-GFP GFP reporter mouse cortex by IUE at E14.5. Brain was harvested at P8, sectioned and stained with an anti-GFP antibody.

(D) The GFP singles in GFP RNAi-expressing neurons were significantly lower than those in cells expressing GFP RNAi scramble sequence. GFP knockdown efficiency was determined by relative GFP fluorescent intensity that is normalized by nlsRFP intensity. (**) $0.001 < P < 0.01$, unpaired Student's *t-test*.

Figure 22. RNAi-mediated Supernova achieved labeled cell-specific gene knockdown in RNZ reporter mice

- (A) Schematic representation of a Supernova vector set that is designed for single cell LacZ knockdown.
- (B) Illustration showing strategy for examination of Supernova-mediated LacZ knockdown in RNZ mice.
- (C) CAG-LSL-mir30 (LacZ RNAi) (lower panels) or CAG-LSL-mir30 (LacZ RNAi scramble sequence) (upper panels) was co-transfected with SnAmcyan into the RNZ transgenic reporter mouse cortex by IUE at E14.5. Coronal sections were made from the mouse brain at P8 and stained with an anti- β -Gal antibody.
- (D) LacZ knockdown efficiency was quantified as the fluorescent intensity ratio of an anti- β -Gal antibody to Amcyan. The β -gal expression level was significantly reduced in SnAmcyan labeled neurons co-expressed with LacZ RNAi, compared to that co-expressed with LacZ RNAi scramble sequence. (***) $p < 0.001$, unpaired Student's *t*-test.

Figure 23. A design of TALEN-mediated Supernova system for genome editing of $\alpha 2$ -Chn gene in single wild-type cells.

- (A) $\alpha 2$ -Chn TALENs were designed to target the exon 6 of $\alpha 2$ -Chn gene in mouse genome.
- (B) Schematic representation of a Supernova vector set that is designed for $\alpha 2$ -Chn gene manipulation in a single cell level.

Figure 24. Labeled cell-specific $\alpha 2$ -Chn gene manipulation in wild type mice by TALEN-mediated

Supernova system.

(A) Confocal images of the hippocampus in wild-type mice that are electroporated with the Supernova $\alpha 2$ -Chn TALEN vector set. The vector set shown in Figure 18B was electroporated into hippocampal CA1 region at E14.5. Brains were sampled at P14. $\alpha 2$ -Chn immunostaining and DAPI-staining were performed to visualize $\alpha 2$ -Chn expression and cell body of cells, respectively, in hippocampal CA1 region. DG: dentate gyrus.

(B) Representative images of CA1 neurons transfected with the Supernova $\alpha 2$ -Chn TALEN vector set. Cells in hippocampal CA1 region were divided into three groups depending on the intensity of anti- $\alpha 2$ -Chn signals: $\alpha 2$ -Chn^{high}, $\alpha 2$ -Chn^{low} and $\alpha 2$ -Chn^{negative}. Most of RFP-negative neurons are expressing high level of $\alpha 2$ -Chn protein ($\alpha 2$ -Chn^{high} cell). In majority of RFP-positive neurons, the $\alpha 2$ -Chn protein expression is undetectable ($\alpha 2$ -Chn^{negative} cell, RFP-labeled cell in upper panel of B). A small portion of RFP-positive neurons shows reduced $\alpha 2$ -Chn protein expression ($\alpha 2$ -Chn^{low} cell, RFP-labeled cell in lower panel of B).

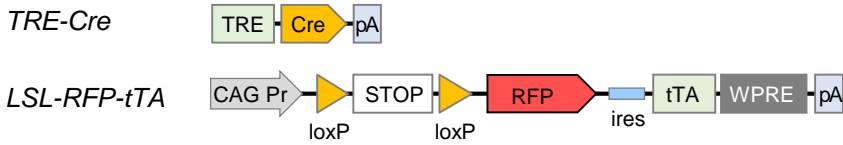
(C) The percentages of $\alpha 2$ -Chn^{high}, $\alpha 2$ -Chn^{low} and $\alpha 2$ -Chn^{negative} cells in RFP-negative neurons (left panel) and RFP-positive neurons (right panel).

Figure 25. High fluorescent protein expression does not affect the expression of $\alpha 2$ -Chn protein.

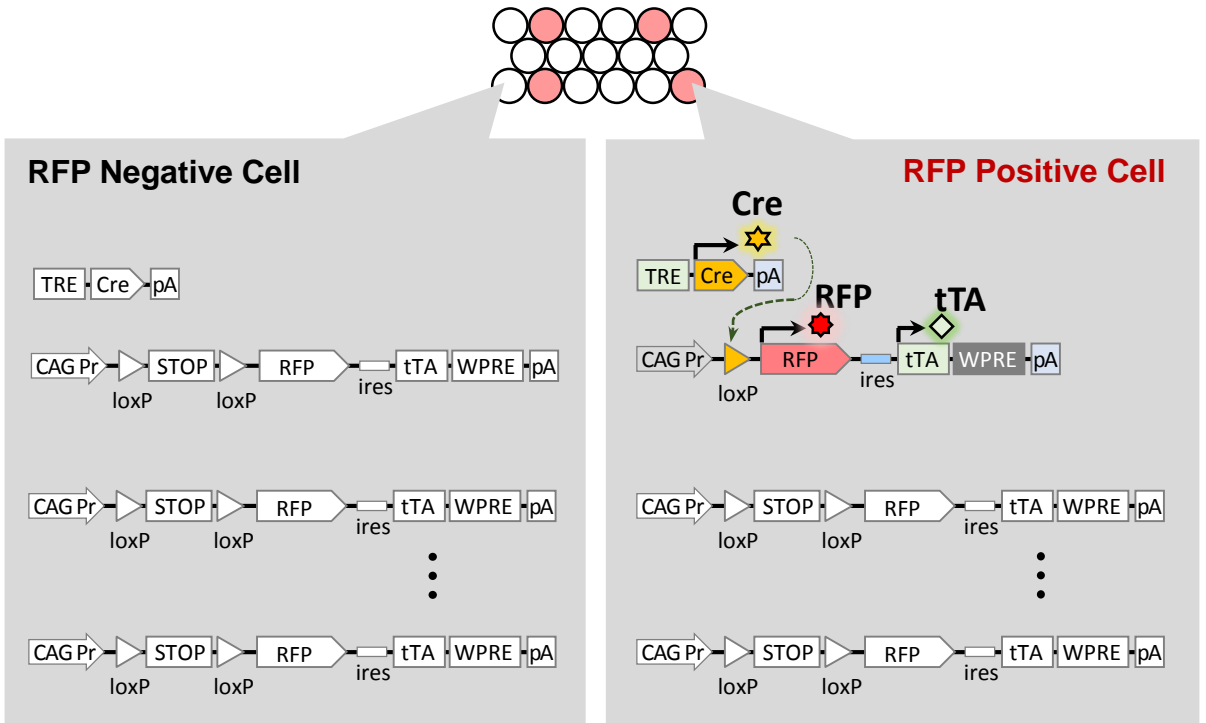
Two set of example images of Flpe/FRT-SnRFP labeled hippocampal CA1 neurons showing $\alpha 2$ -Chn protein expression. Briefly, Flpe/FRT-SnRFP was introduced into hippocampal CA1 neurons by IUE at E14.5. Coronal sections from P14 brains were prepared and stained with an anti- $\alpha 2$ -chimaerin antibody. Arrowheads: the RFP-positive cells that labeled by Flpe/FRT-SnRFP.

Figure 1

A Supernova RFP (SnRFP)



B (1) Leakage of TRE drives the weak expression of Cre



(2) The expression of RFP is facilitated by the positive feedback of the tTA–TRE cycles

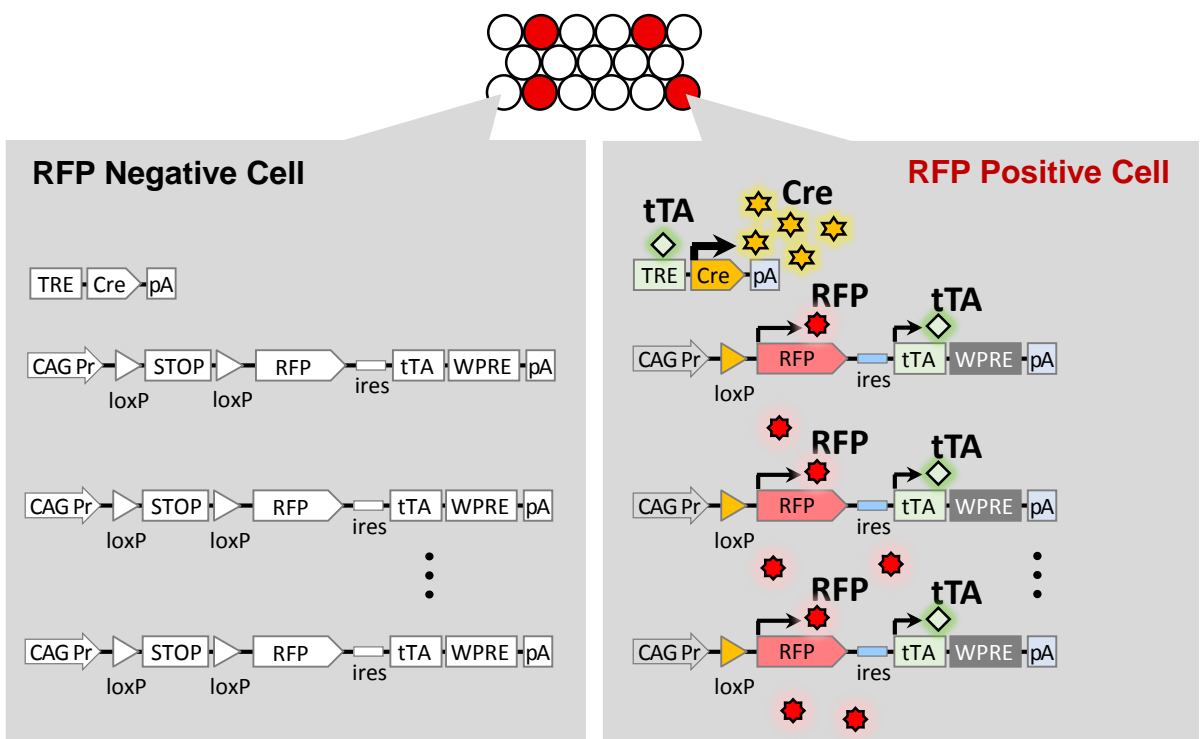
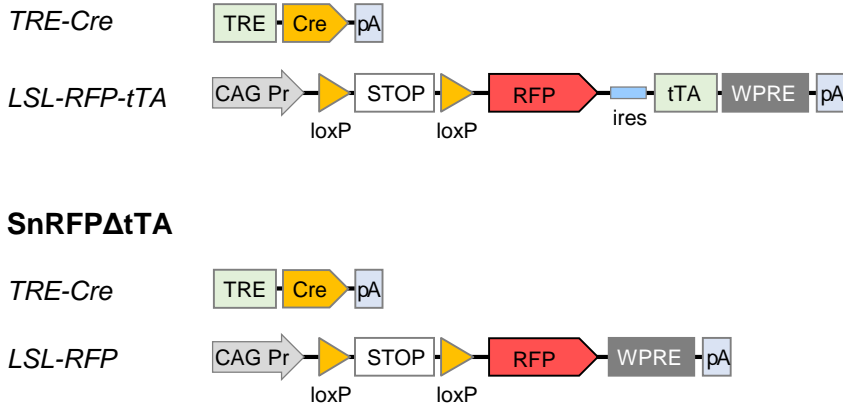


Figure 2

A Supernova RFP (SnRFP)



B IUE E14.5, L4 cortical neuron

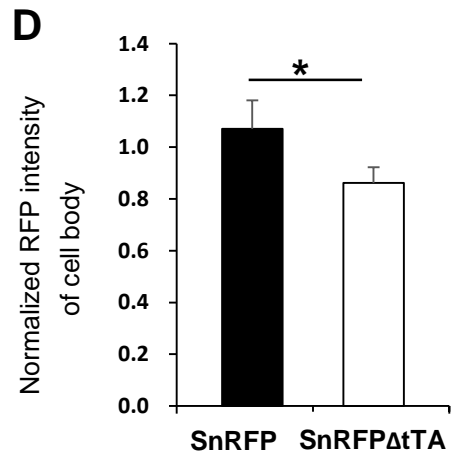
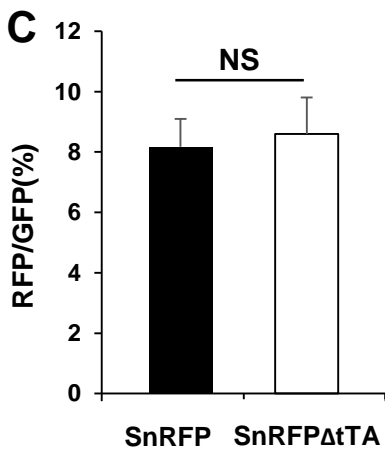
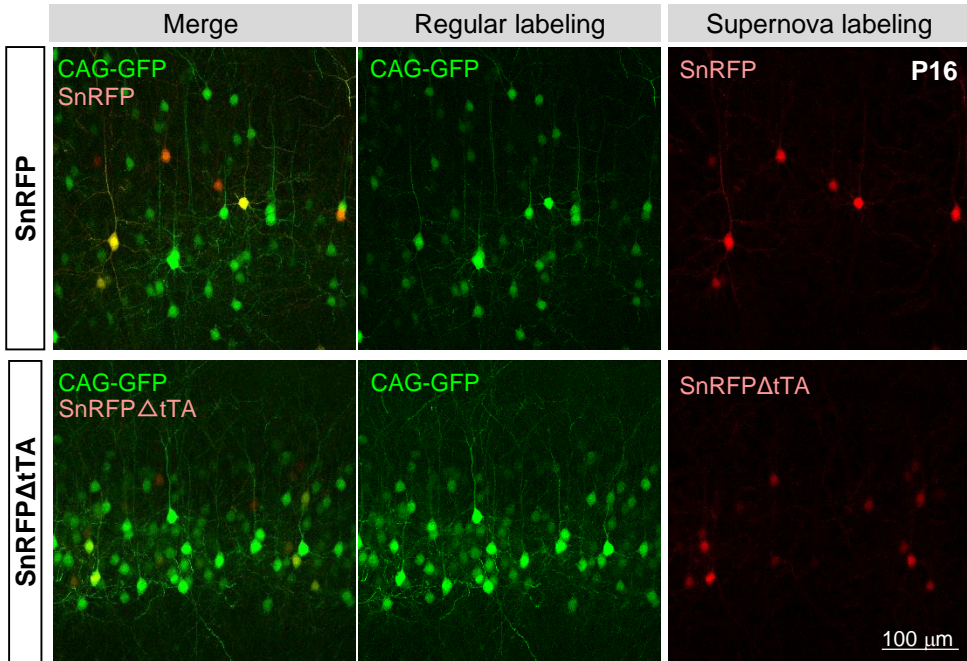
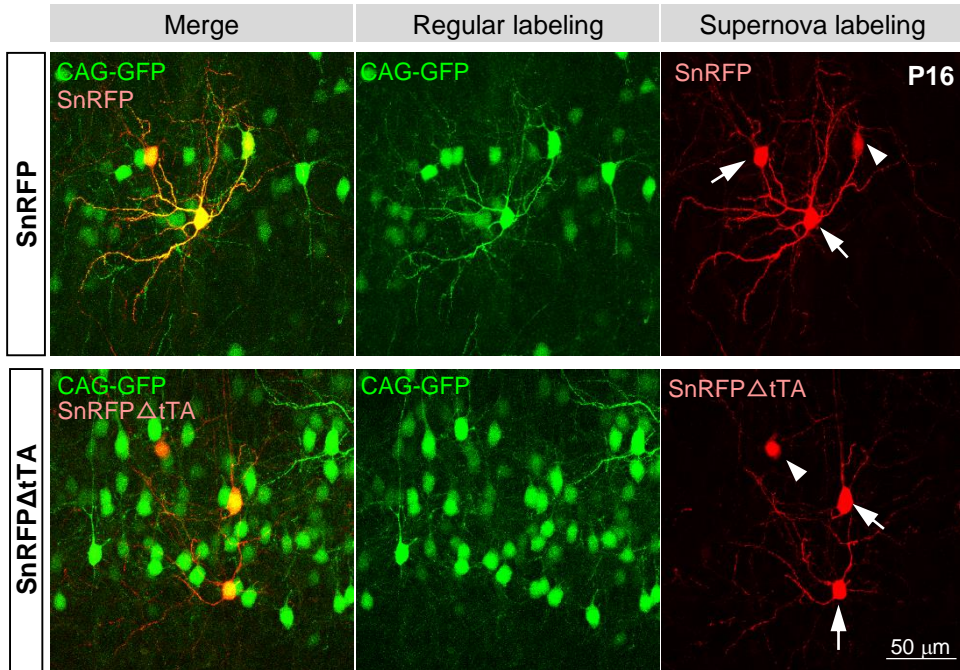


Figure 3

A

IUE E14.5, L4 cortical neuron



B

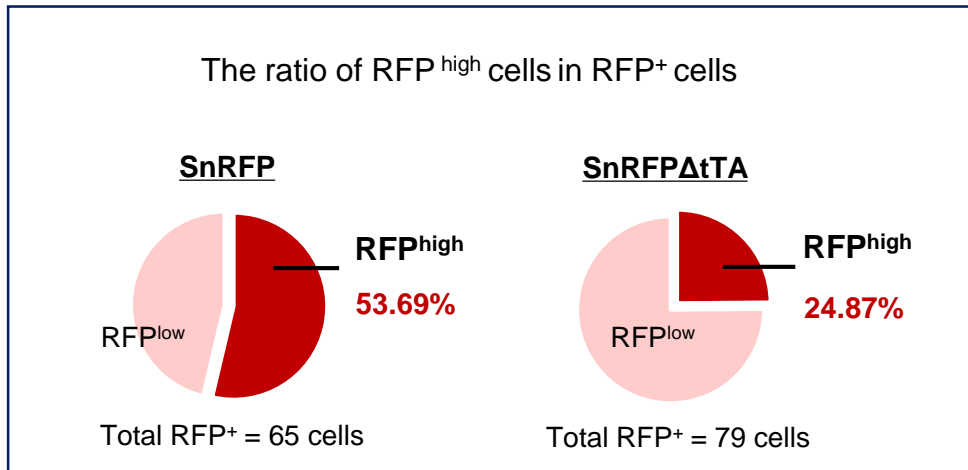


Figure 4

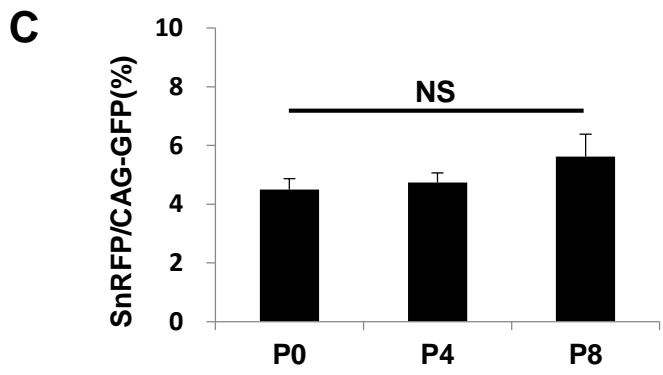
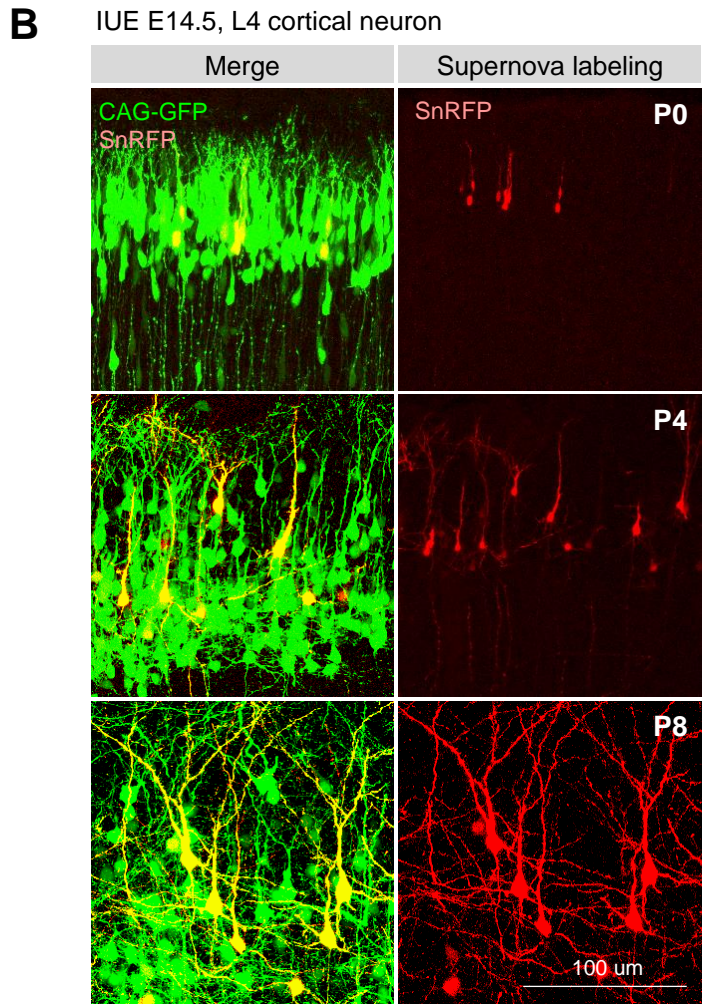
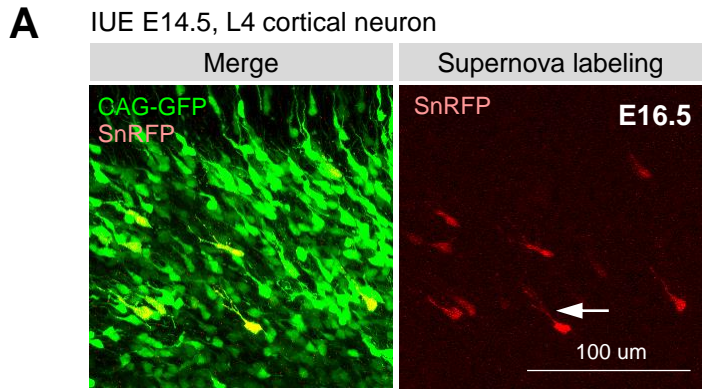


Figure 5

A Cre/loxP-based Supernova labeling

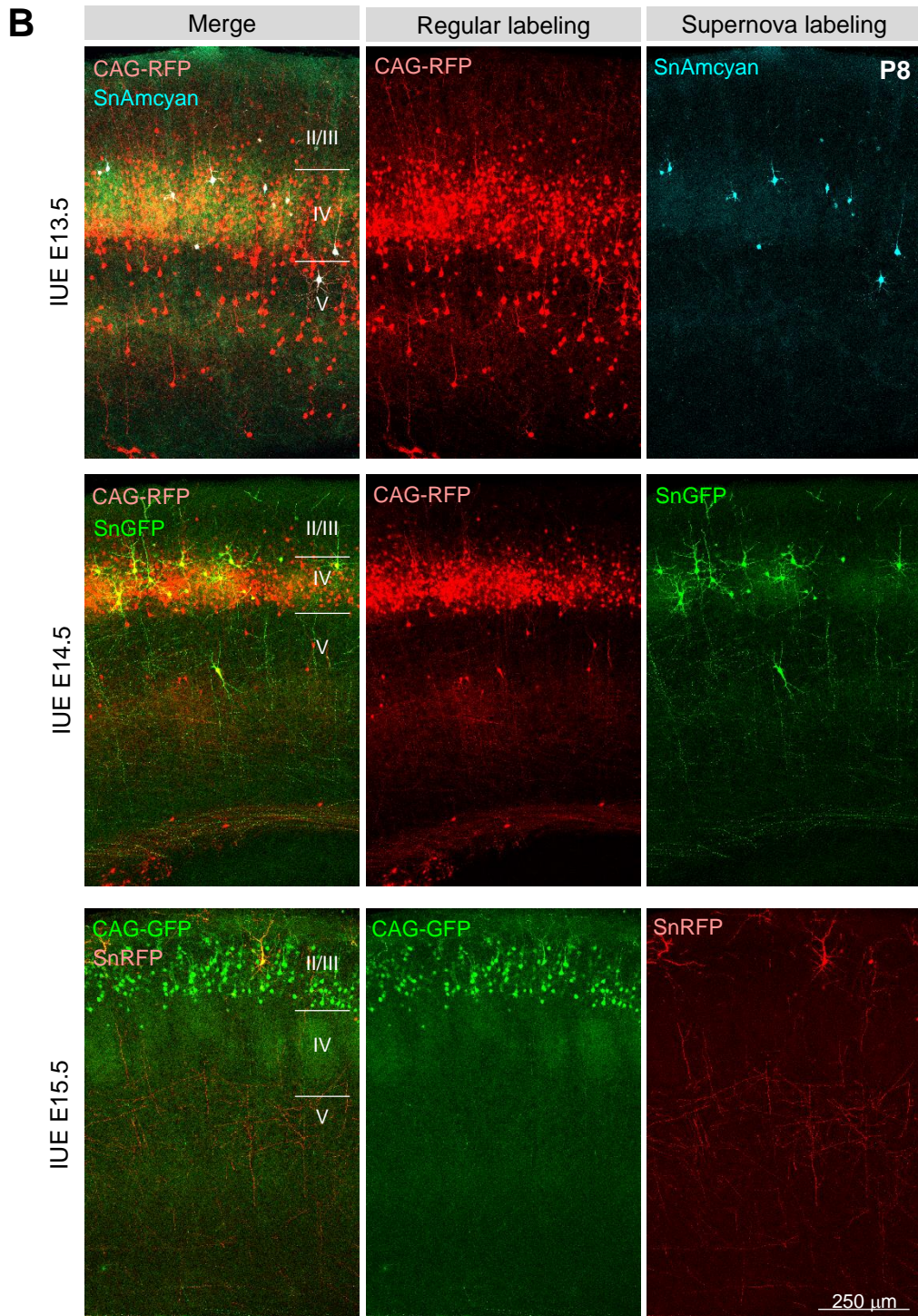
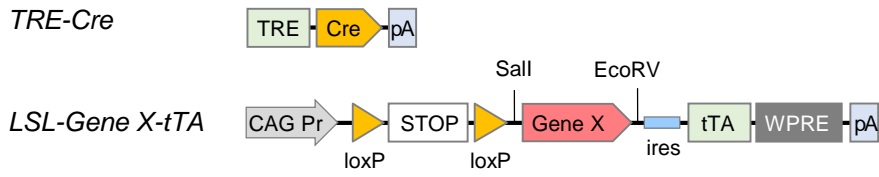


Figure 6

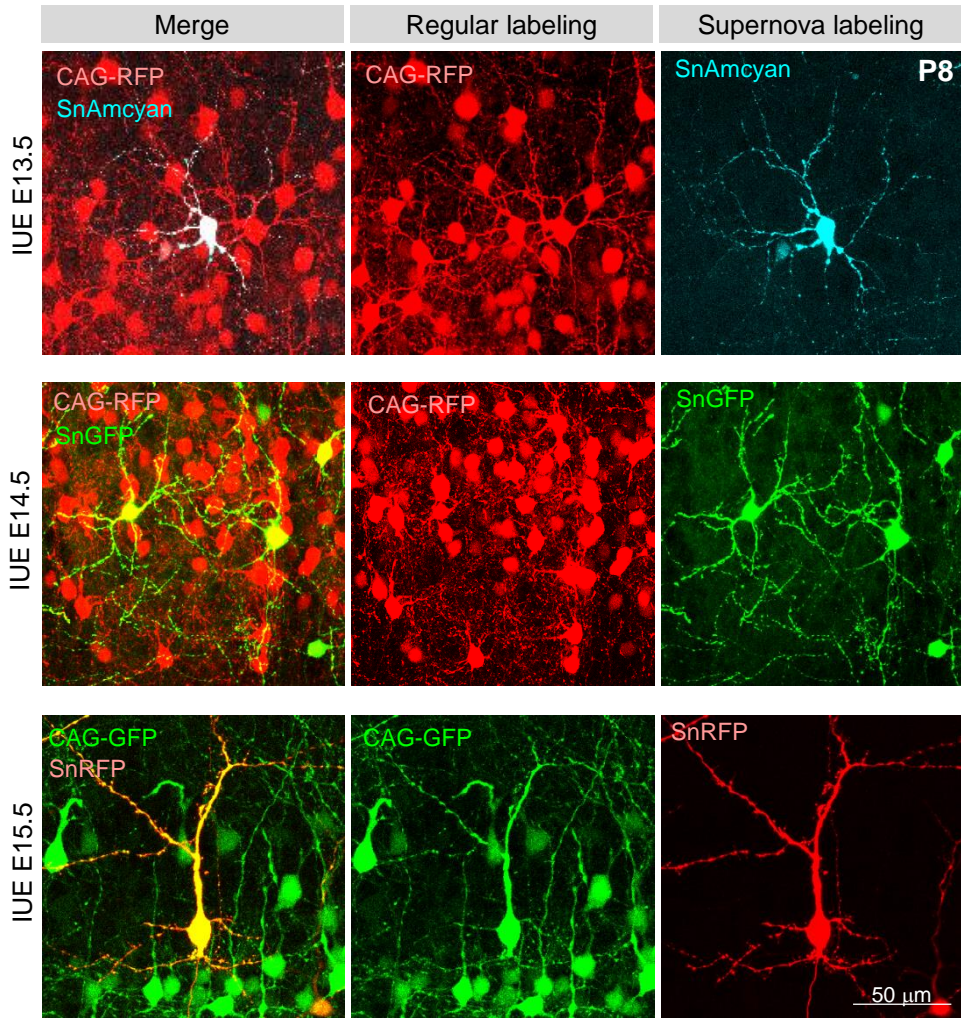


Figure 7

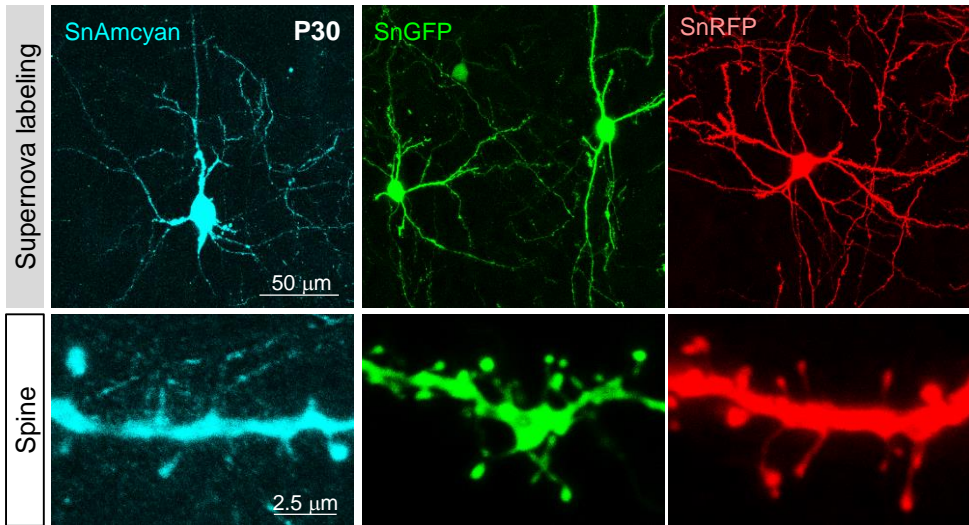
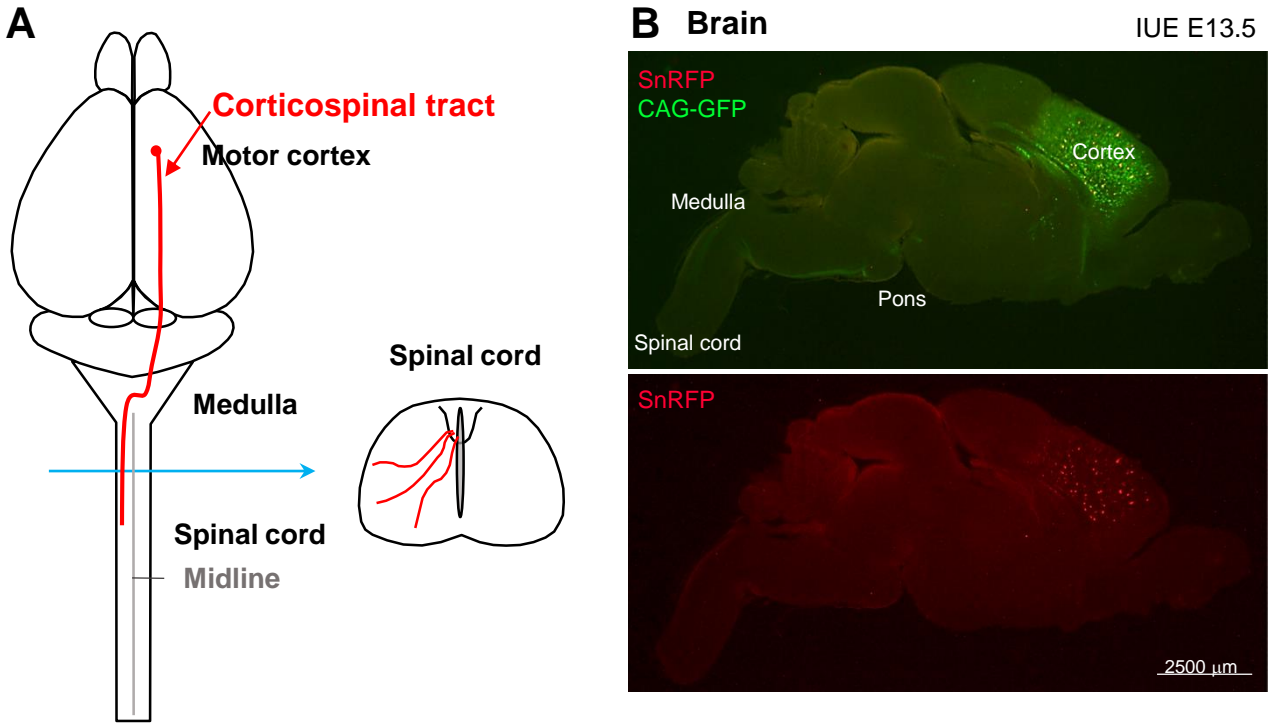


Figure 8



C Cervical enlargement of Spinal Cord

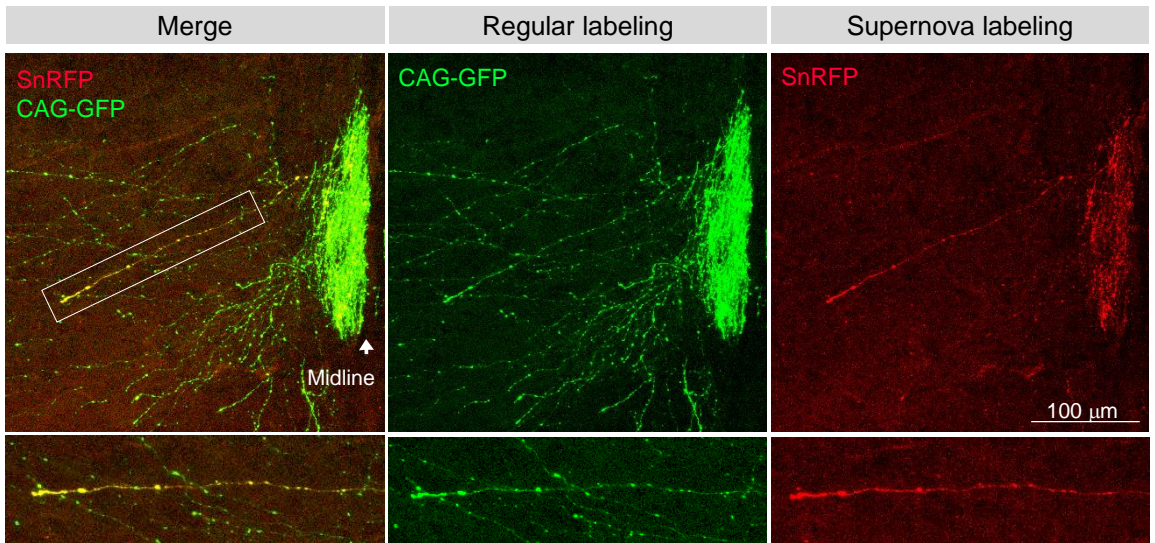
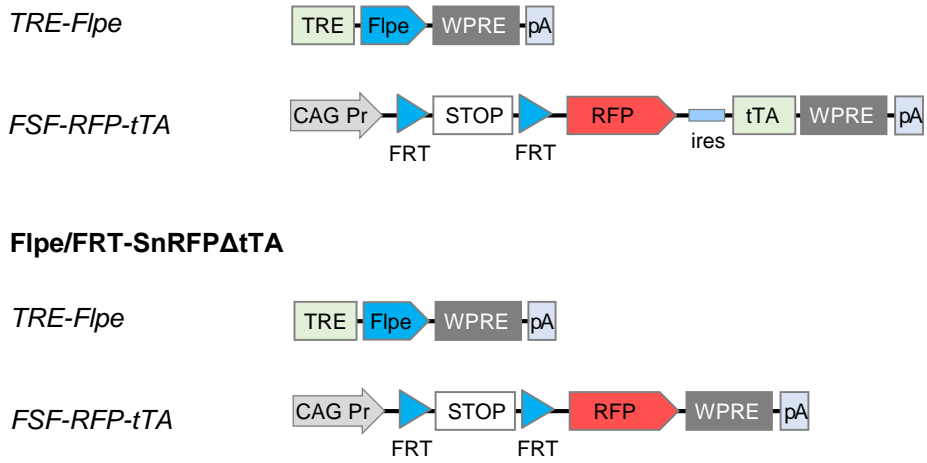


Figure 9

A Flpe/FRT-based Supernova RFP (Flpe/FRT-SnRFP)



B IUE E14.5, L4 cortical neuron

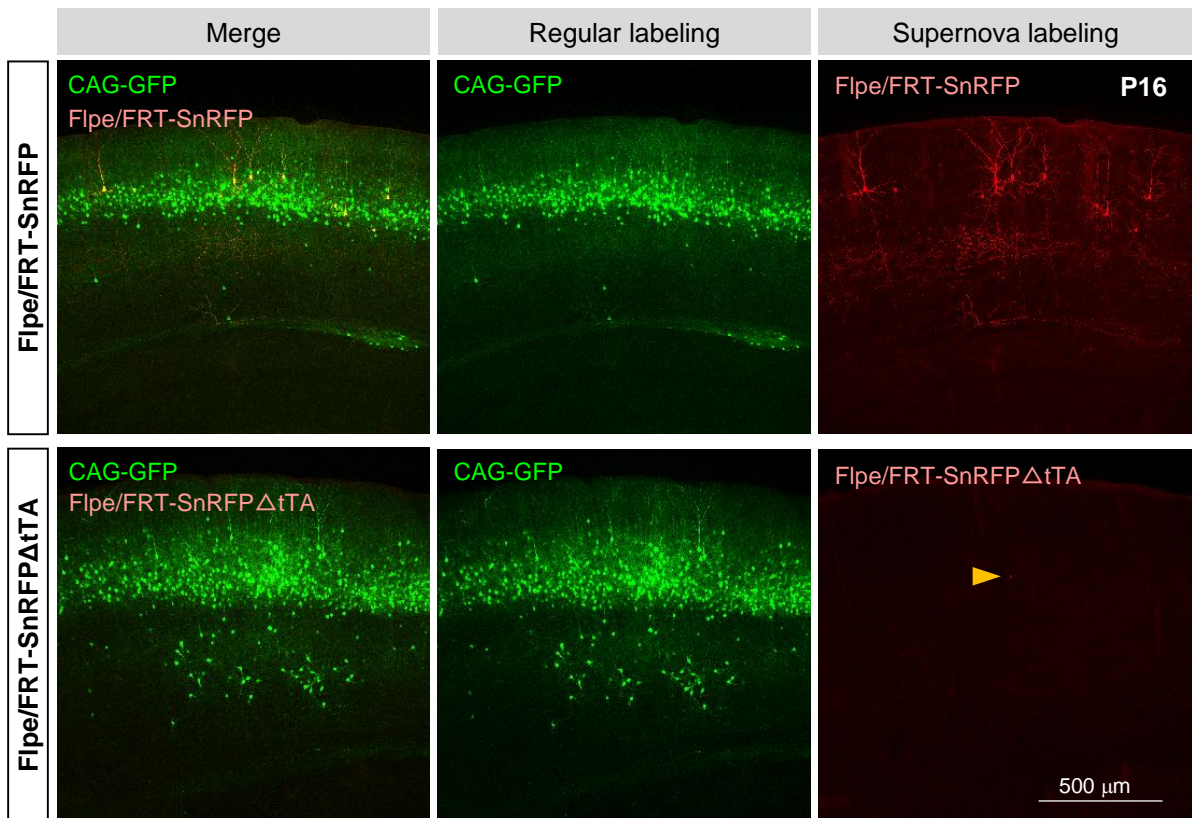


Figure 10

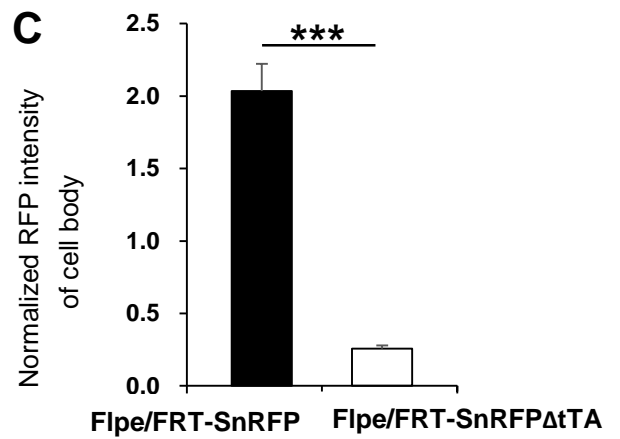
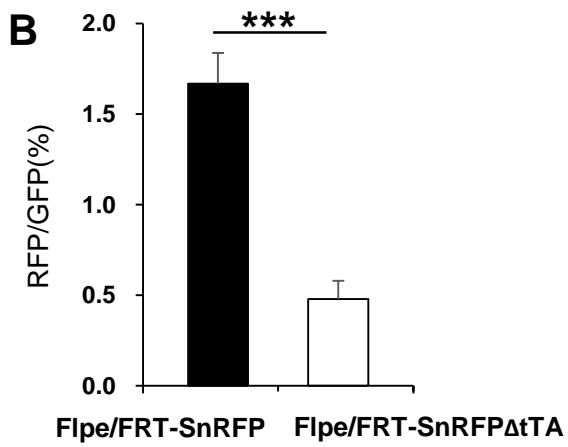
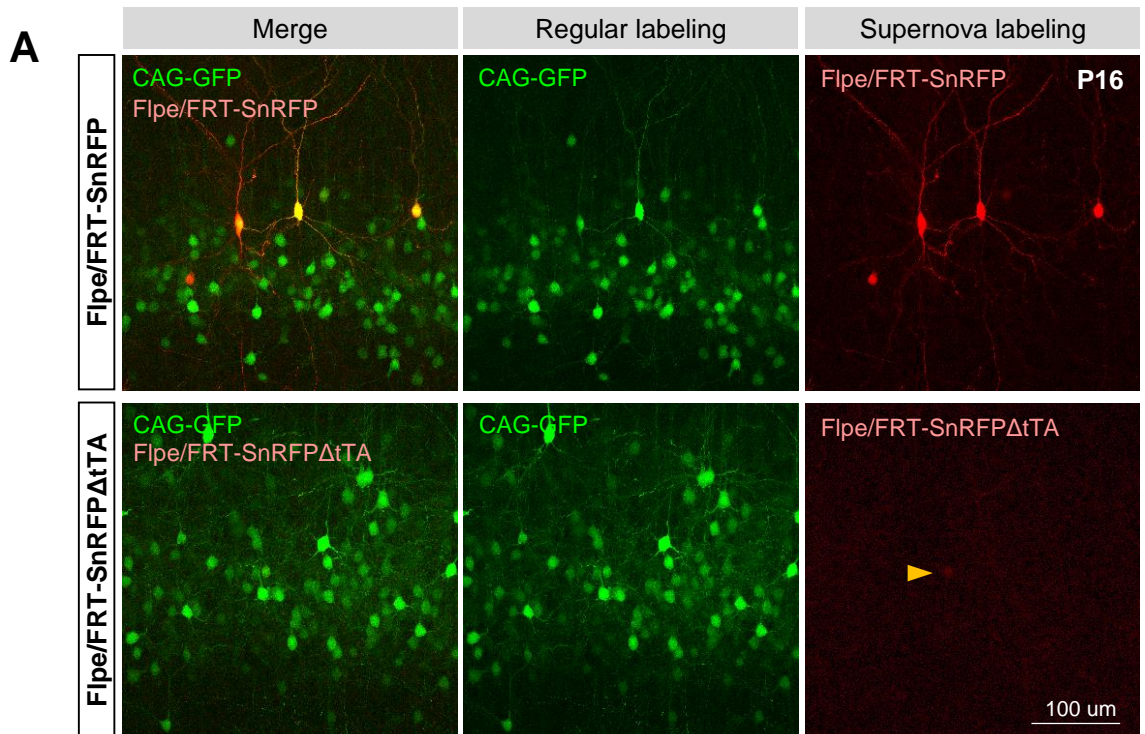


Figure 11

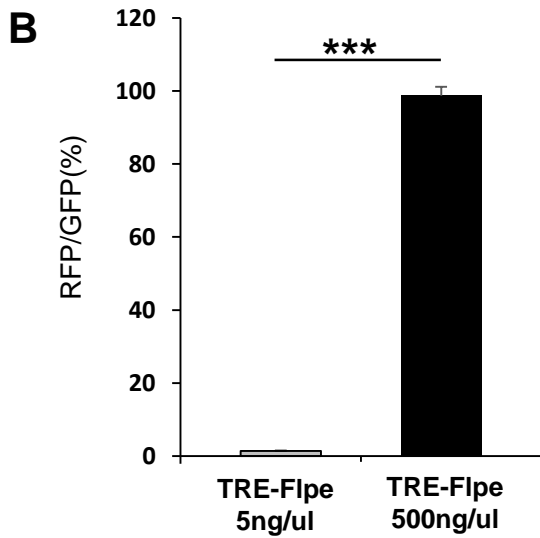
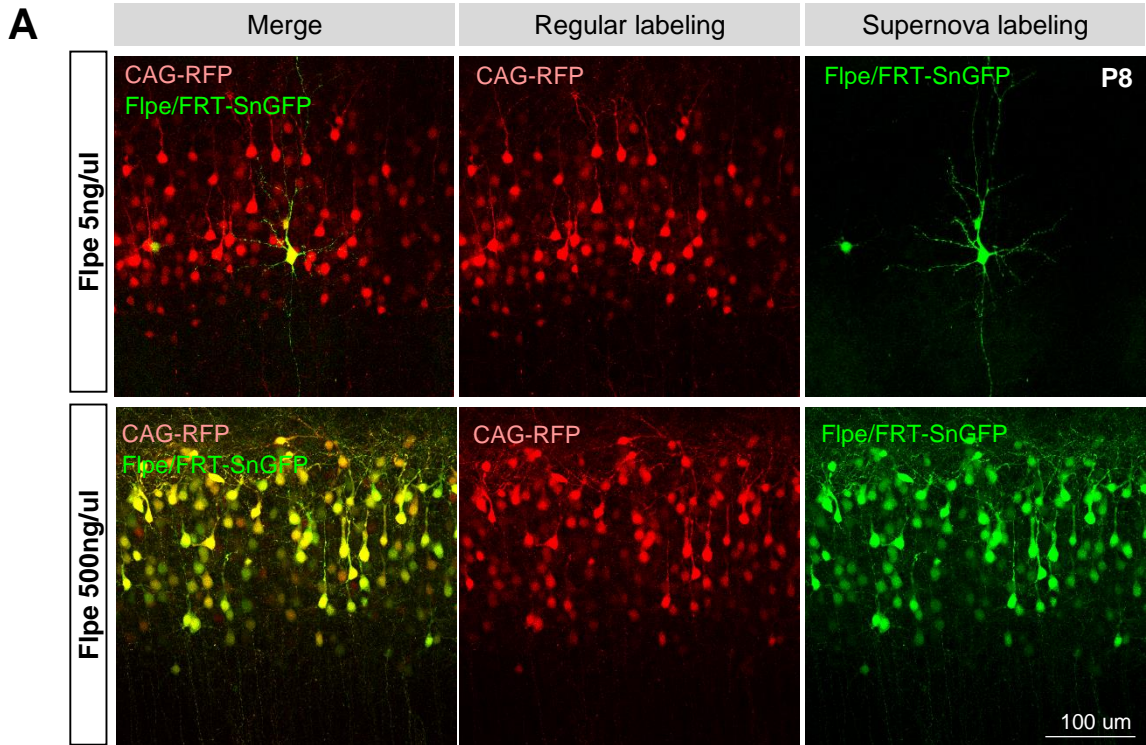
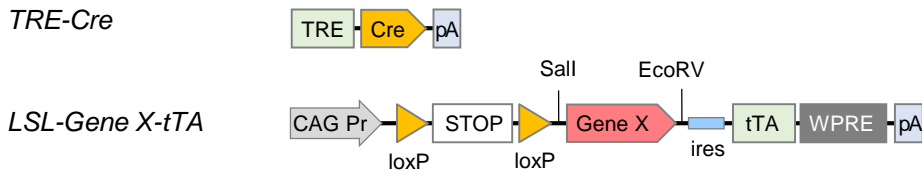
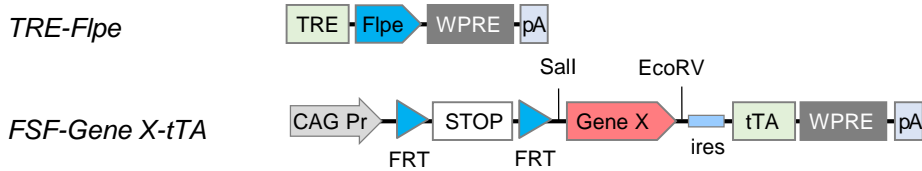


Figure 12

A Cre/loxP-based Supernova labeling



Flpe/FRT-based Supernova system



IUE E15.5, L2/3 cortical neuron

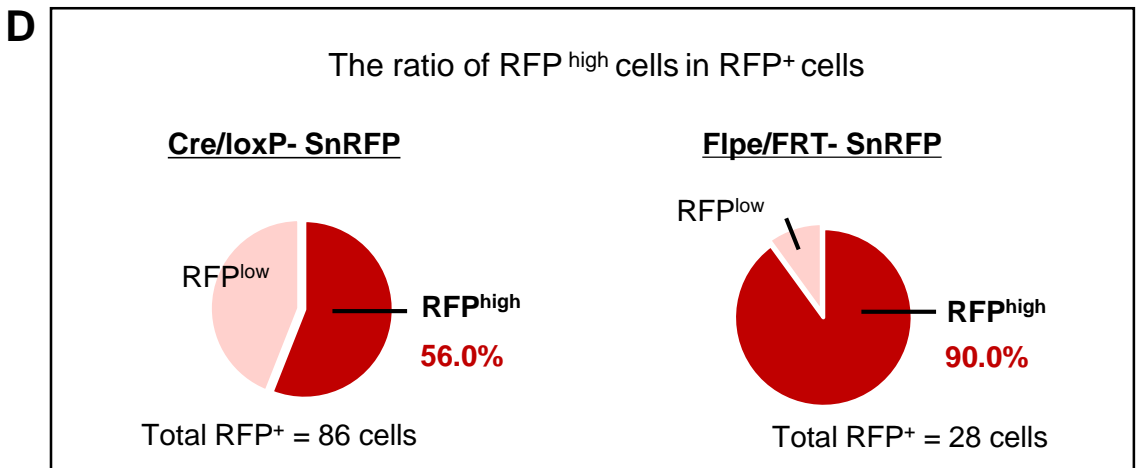
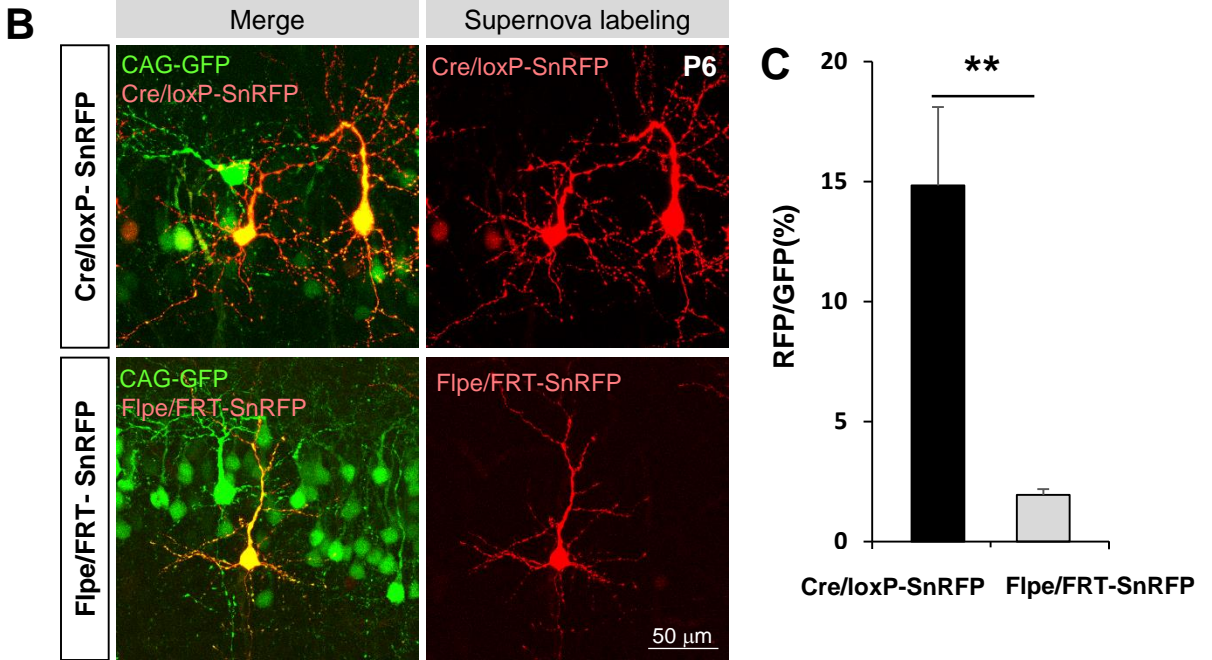


Figure 13

IUE E14.5, Hippocampal CA1 neuron

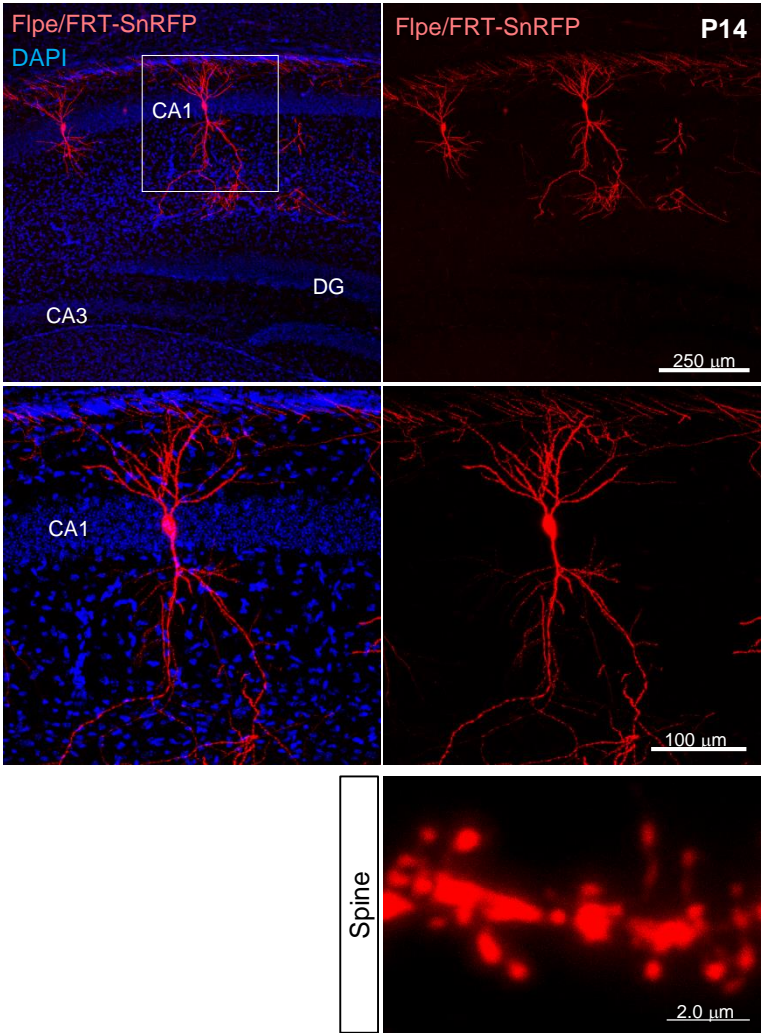


Figure 14

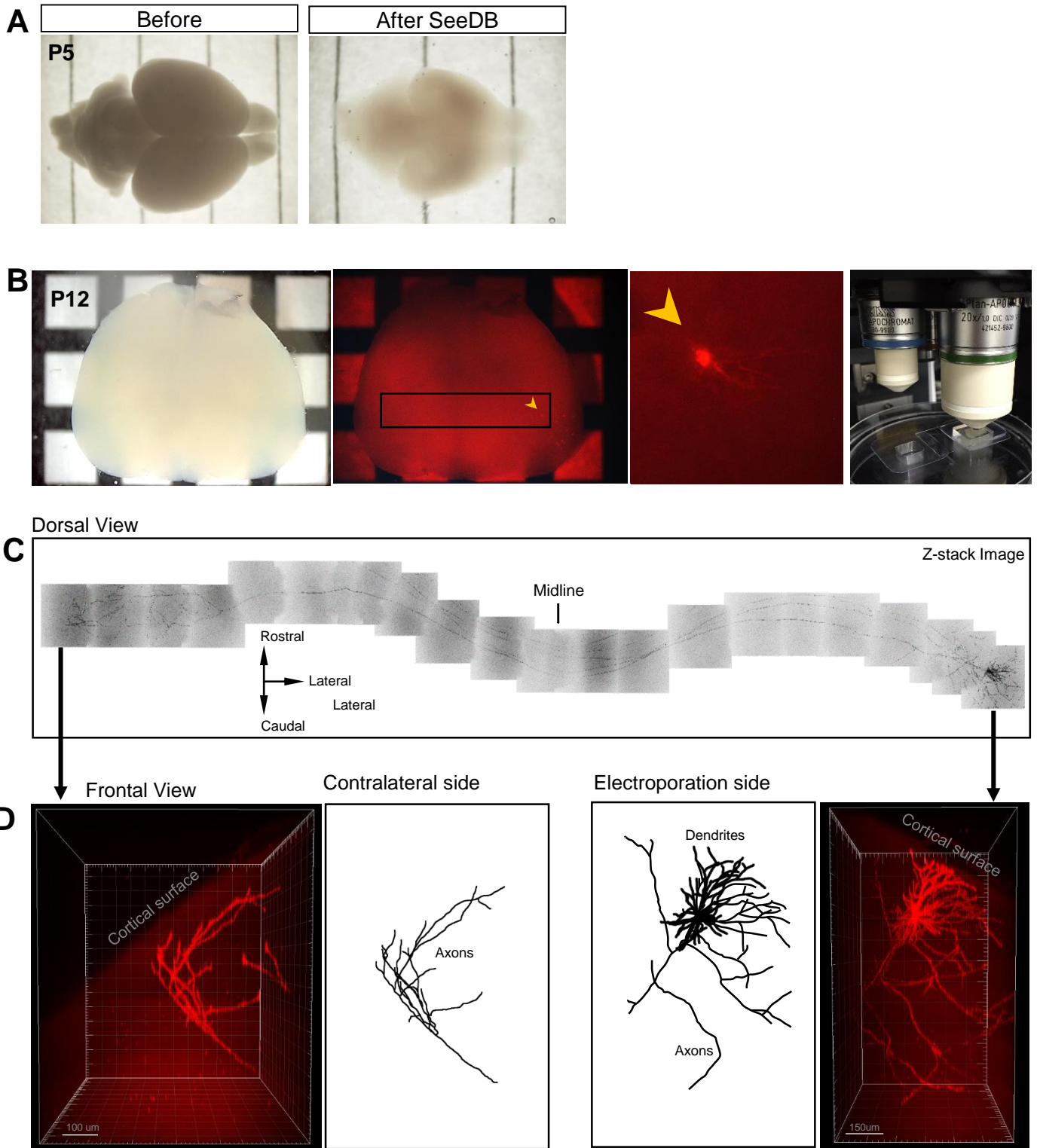
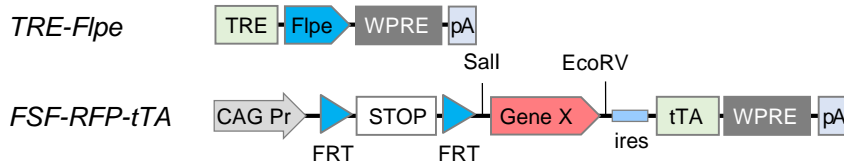
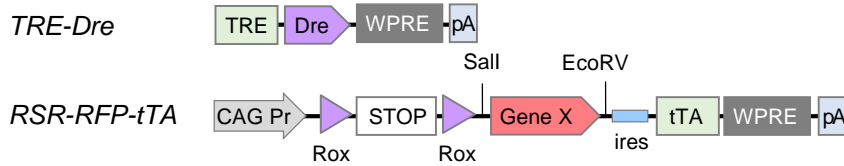


Figure 15

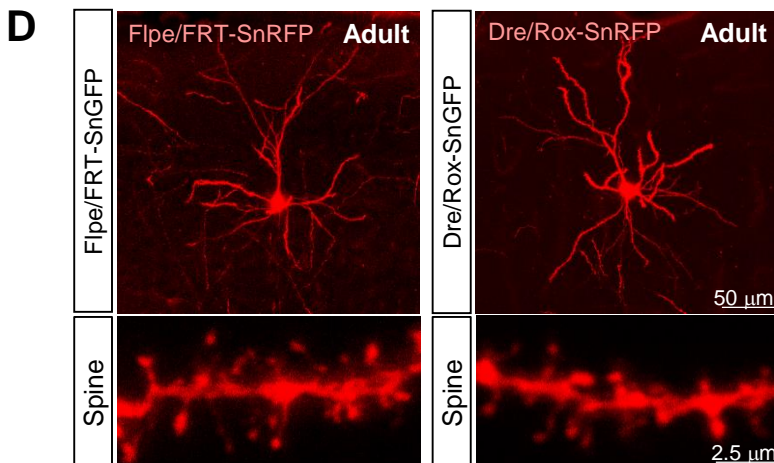
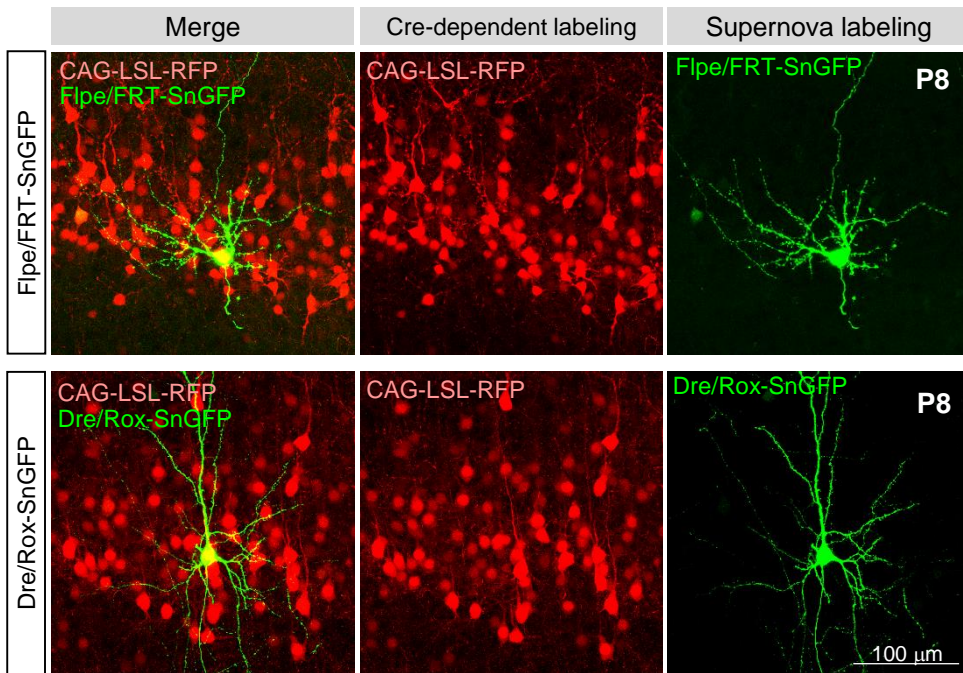
A Flpe/FRT-based Supernova system



B Dre/Rox-based Supernova system



C Emx1Cre KI mouse, IUE E14.5, Cortical



E Emx1Cre KI mouse

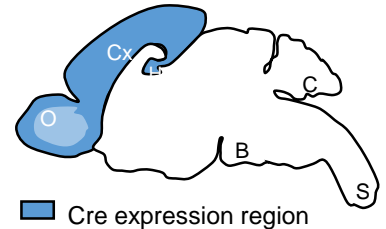


Figure 16

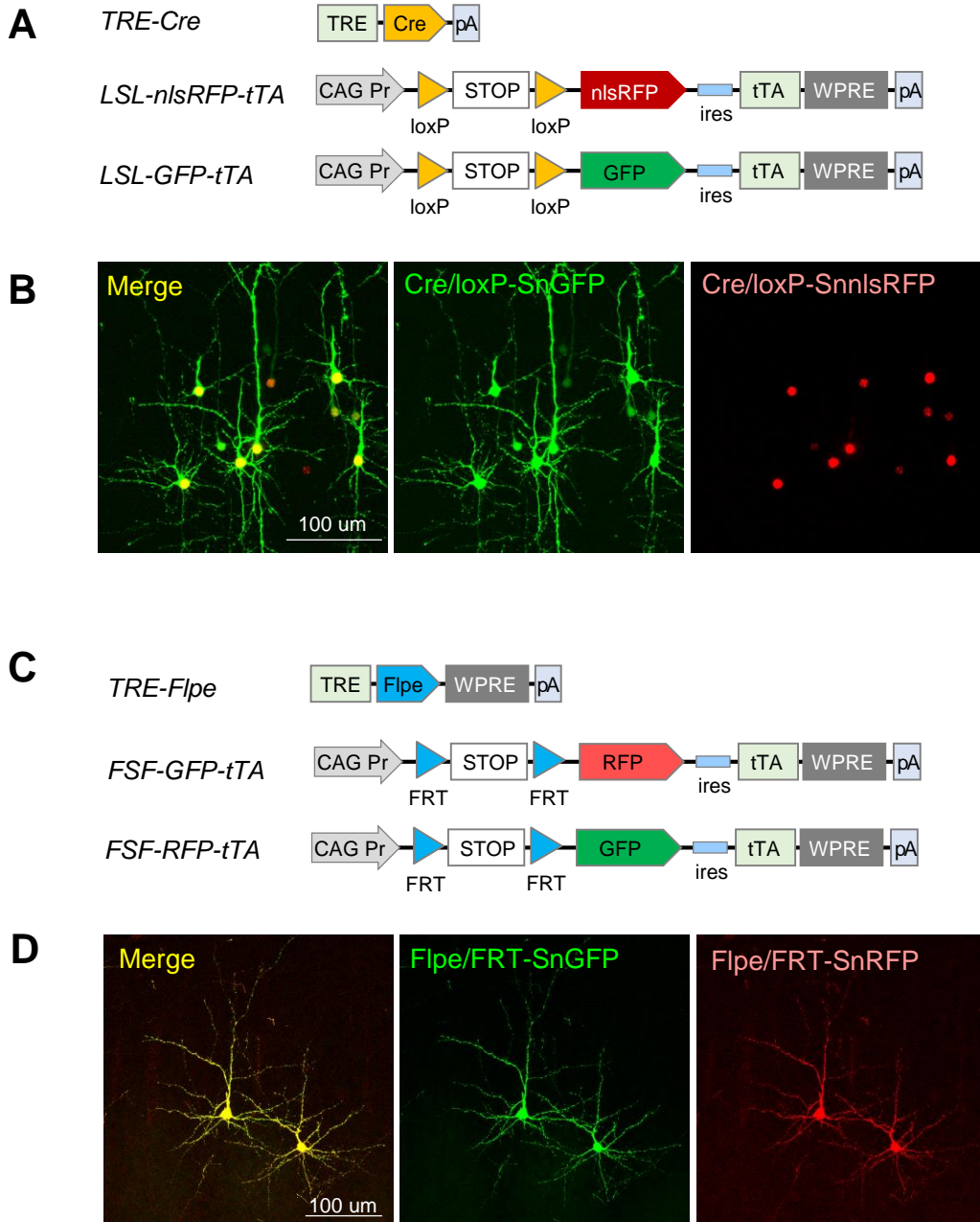
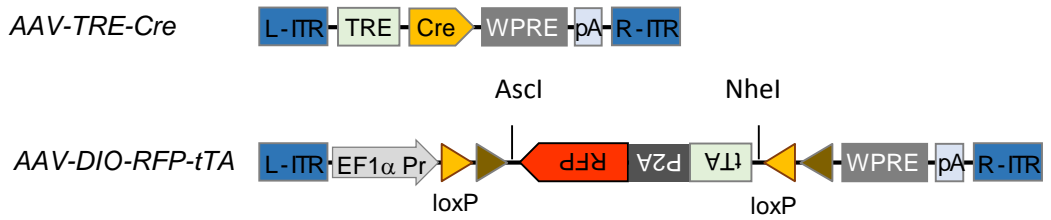
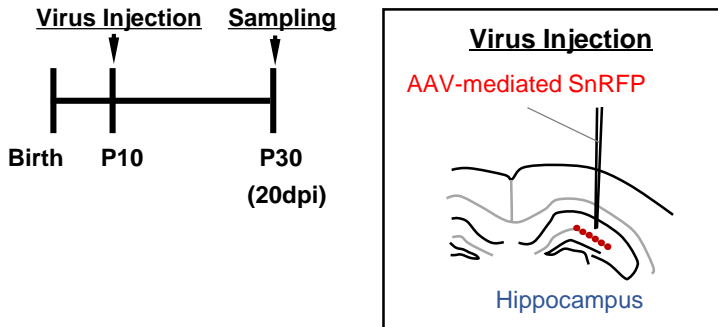


Figure 17

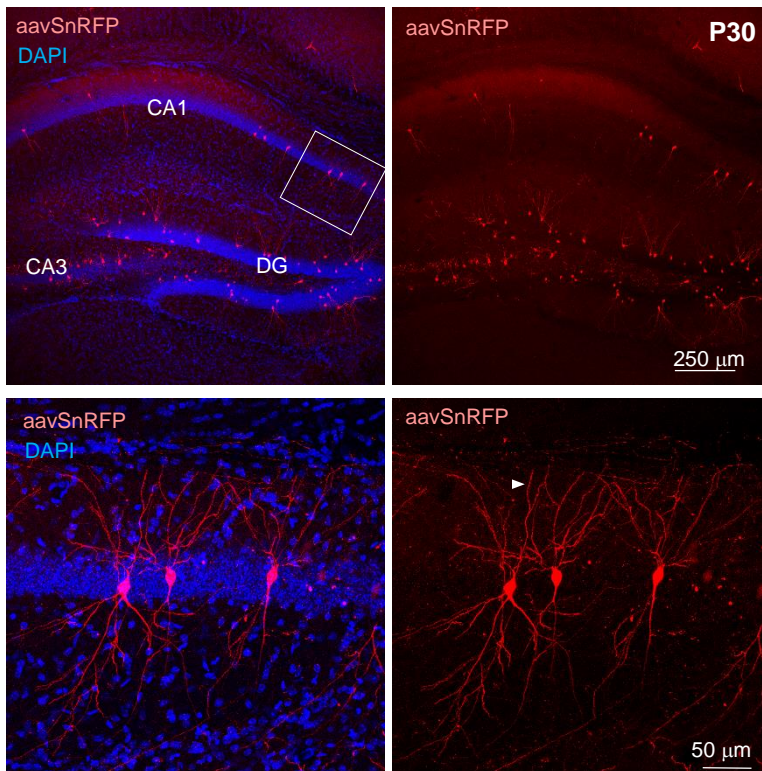
A AAV-supernova system



B



C



D

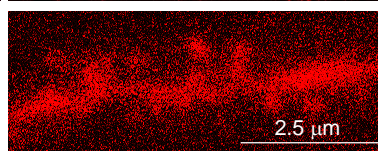
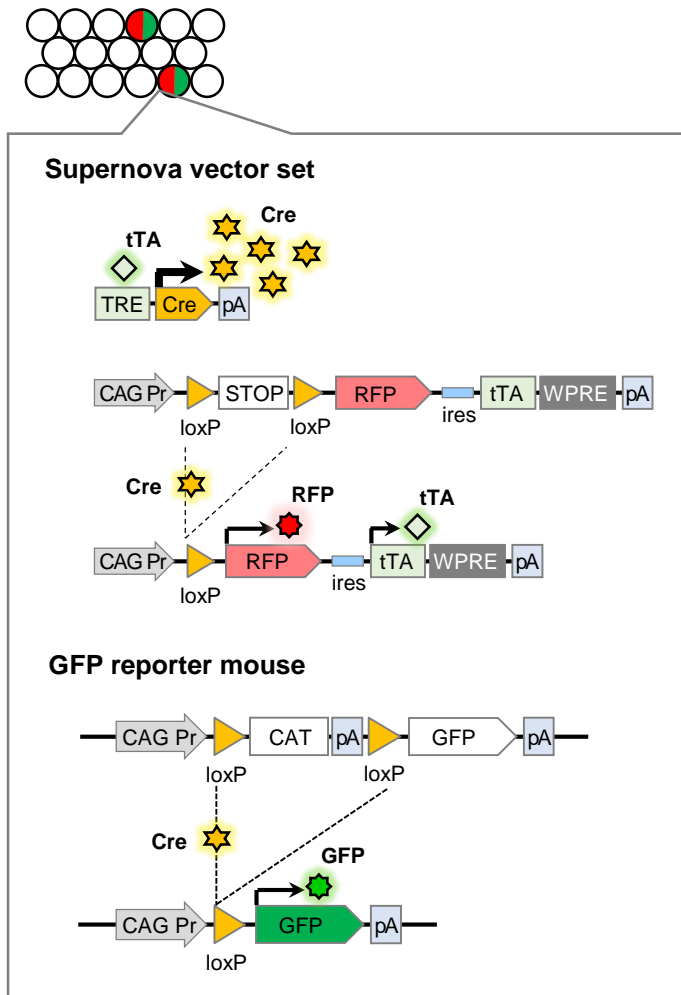
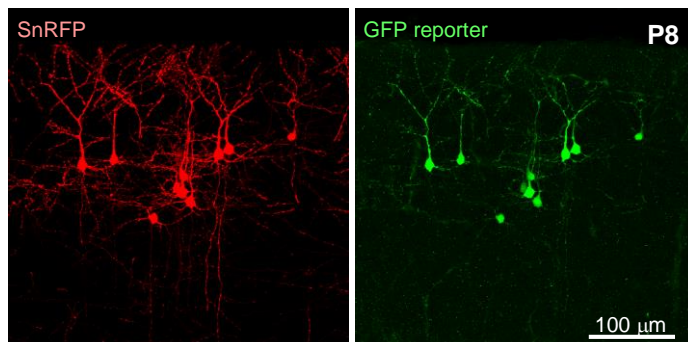


Figure 18

A IUE Cre/loxP-SnRFP to cells in GFP reporter mice

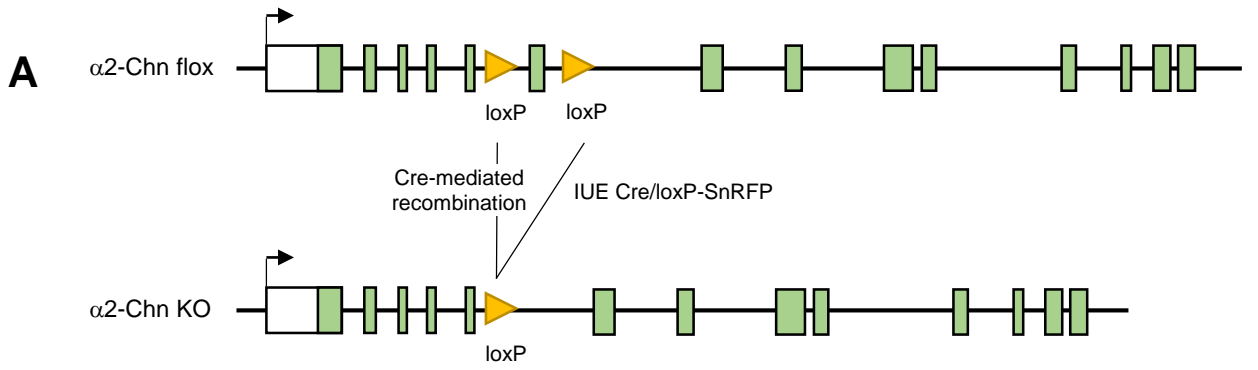


B IUE E15.5, L2/3 cortical neuron



GFP / RFP = 90.43% (359/397) cells
 GFP / RFP^{high} = 100% (291/291) cells
 RFP / GFP = 100% (359/359) cells
 (n=6 mice)

Figure 19



IUE E14.5, Hippocampal CA1 neuron

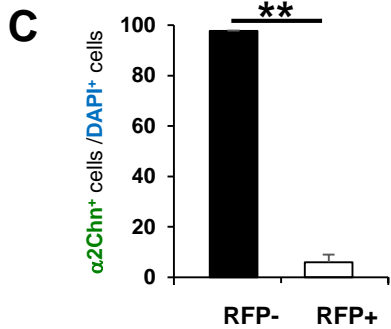
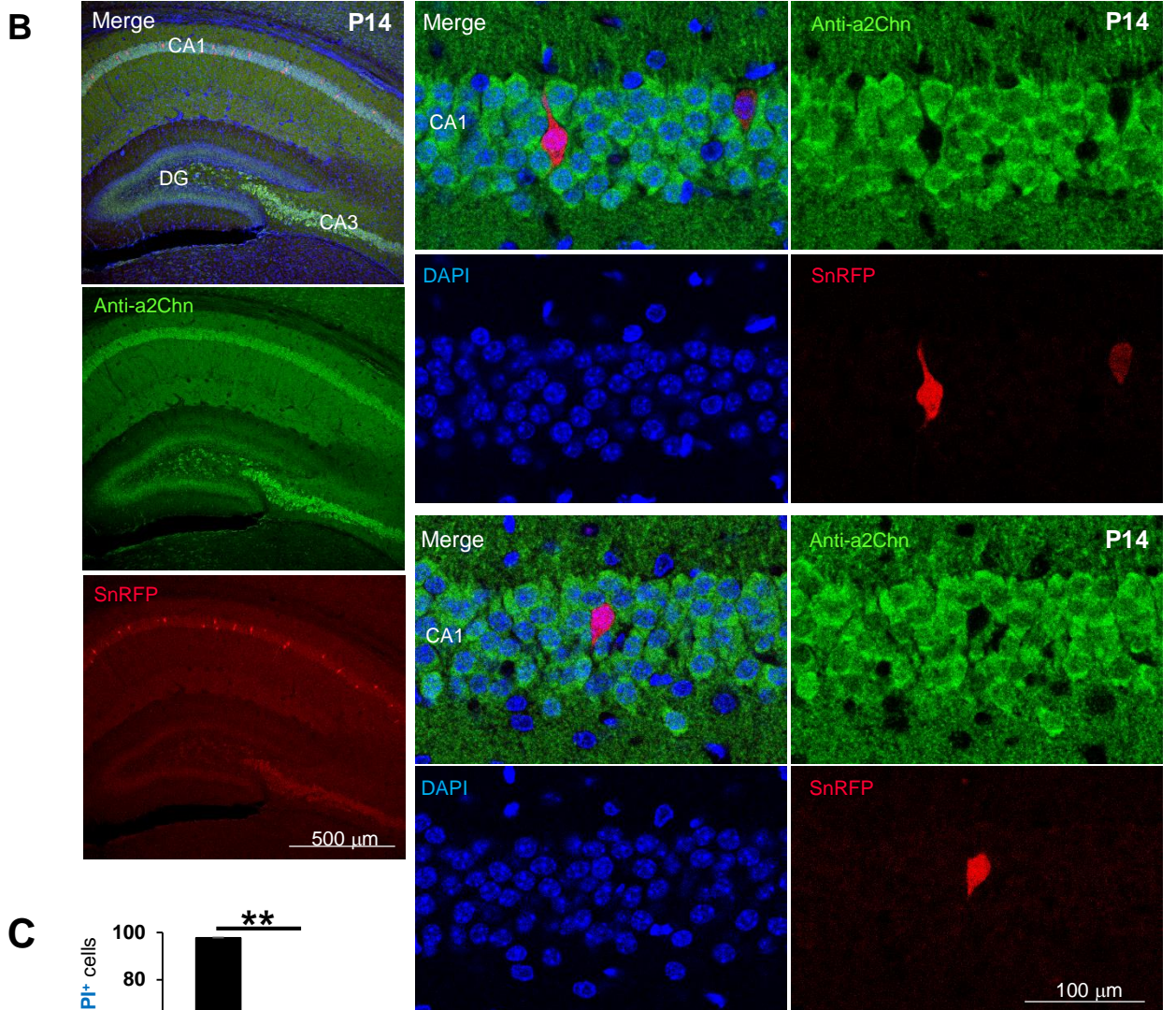


Figure 20

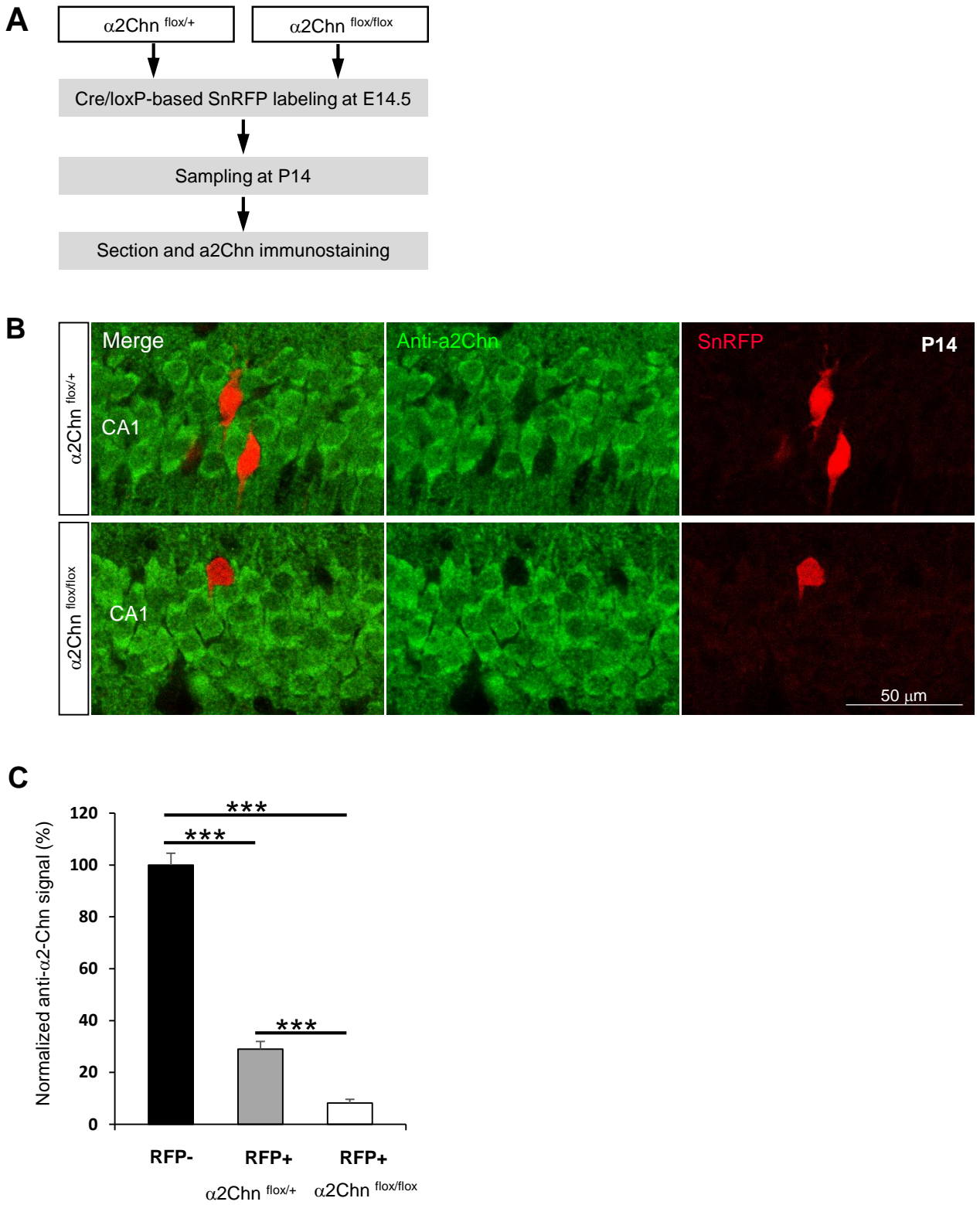


Figure 21

A Supernova vector sets for single cell GFP knockdown

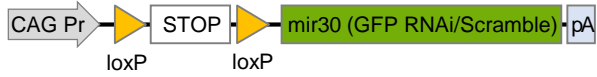
TRE-Cre



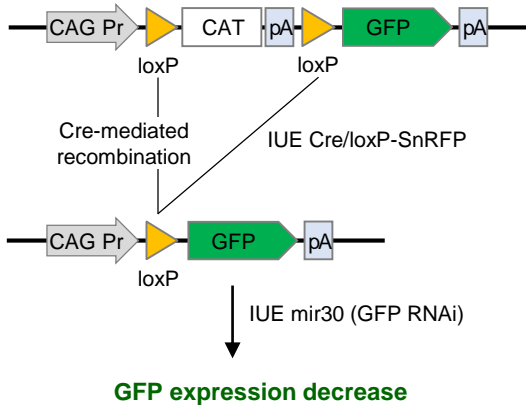
LSL-nlsRFP-tTA



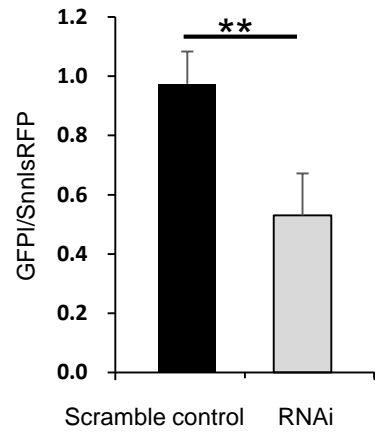
LSL-mir30 (GFP RNAi/Scramble)



B CAG-loxP-CAT-loxP-GFP reporter mice



D



C

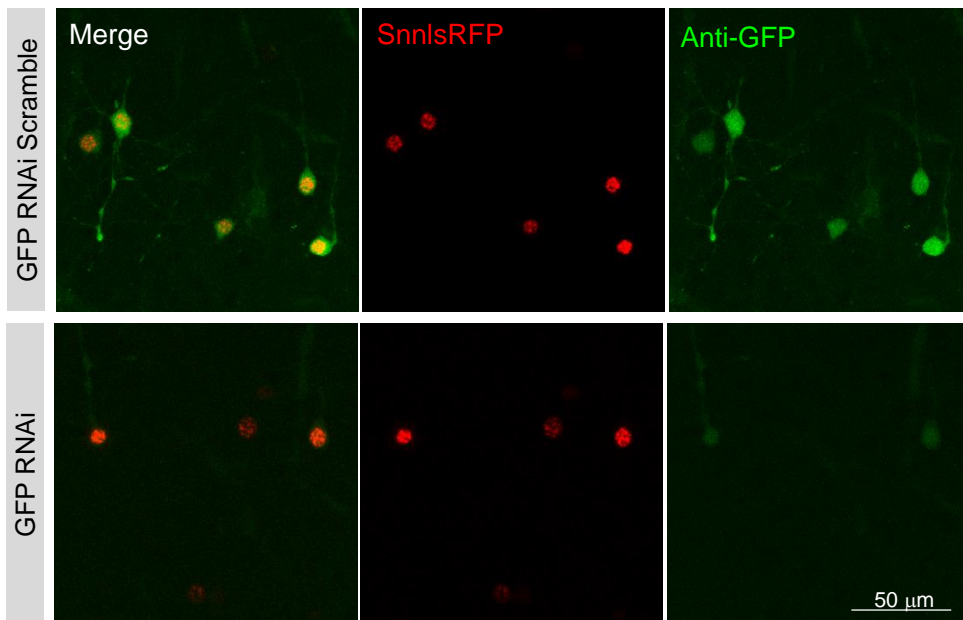


Figure 22

A Supernova vector sets for single cell LacZ knockdown

TRE-Cre



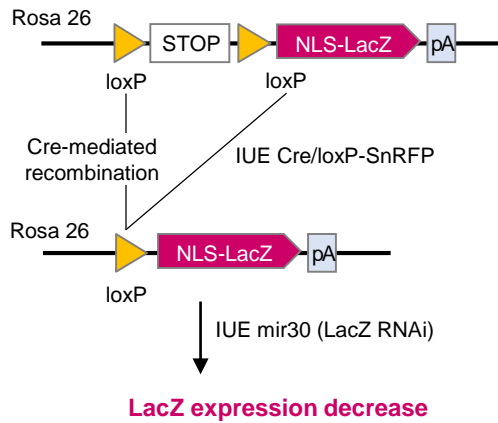
LSL-Amcyan-tTA



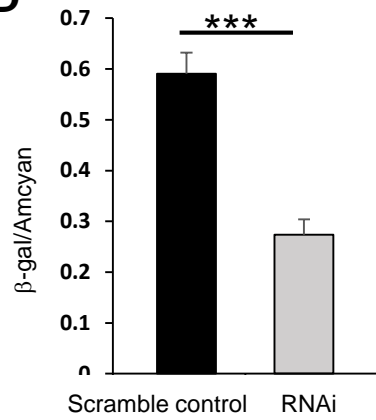
LSL-mir30 (LacZ RNAi/Scramble)



B RNZ reporter mice



D



C

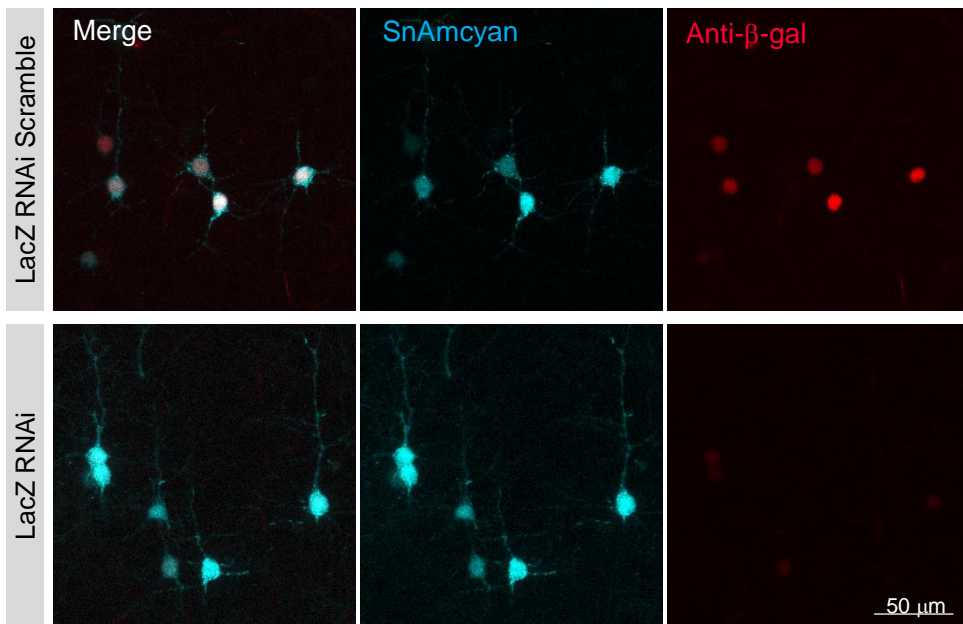
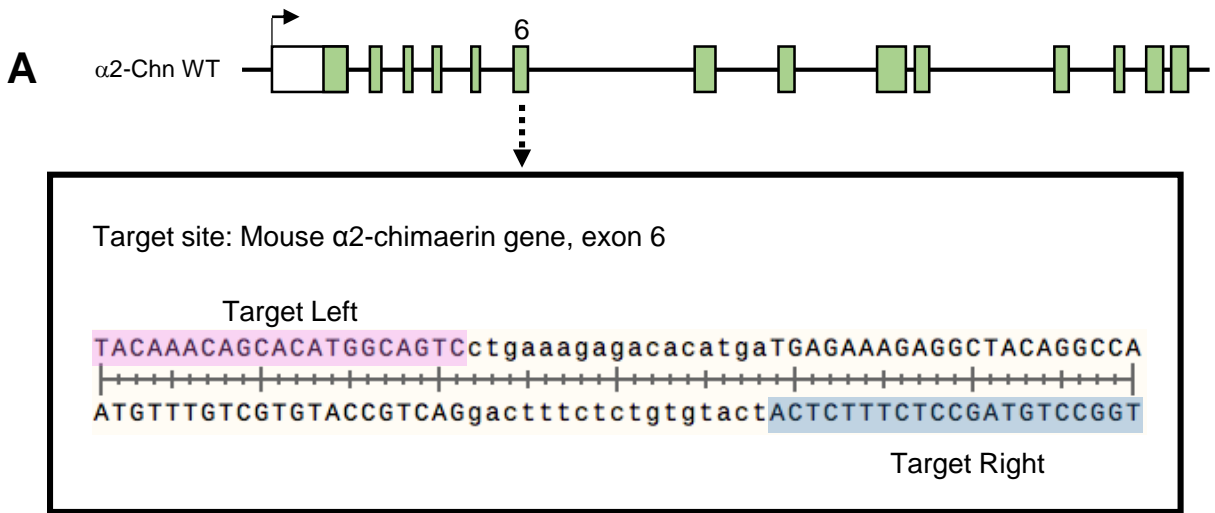


Figure 23



B Flpe/FRT-based Supernova system

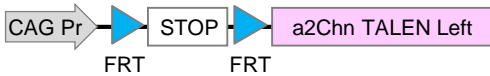
TRE-Flpe



FSF-RFP-tTA



FSF-a2Chn TALEN Left



FSF-a2Chn TALEN Right

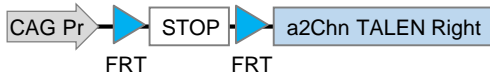
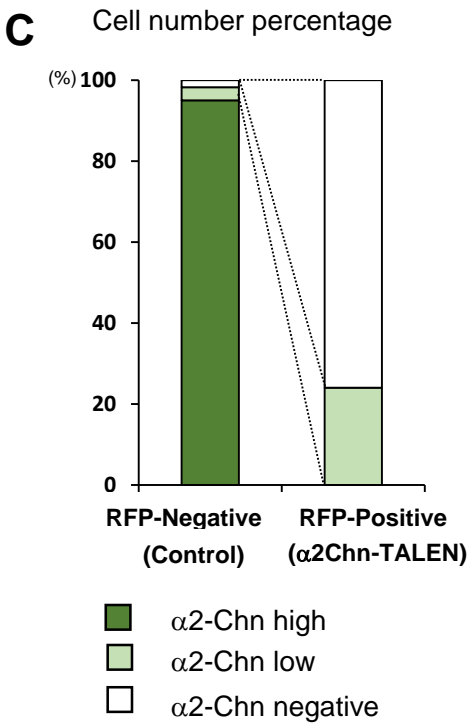
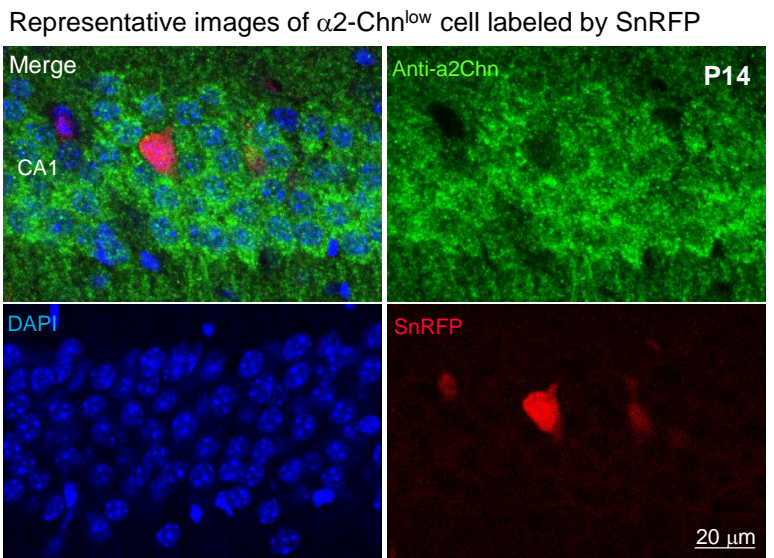
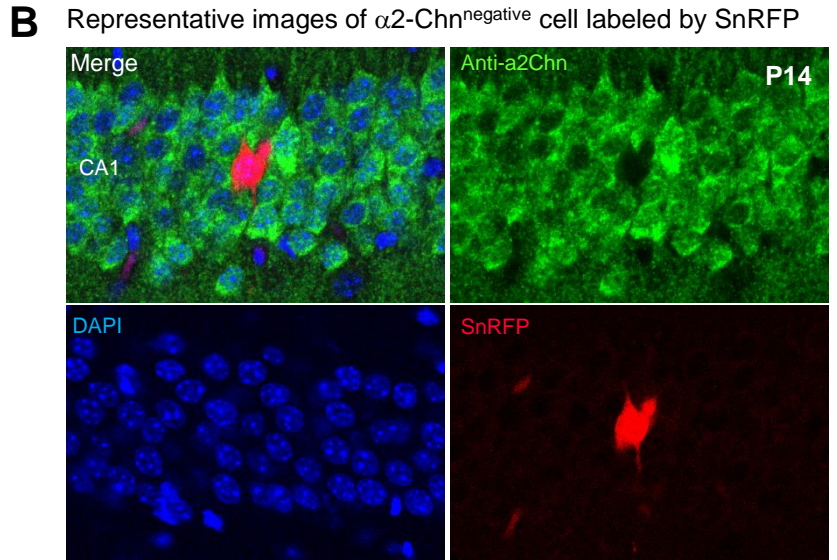
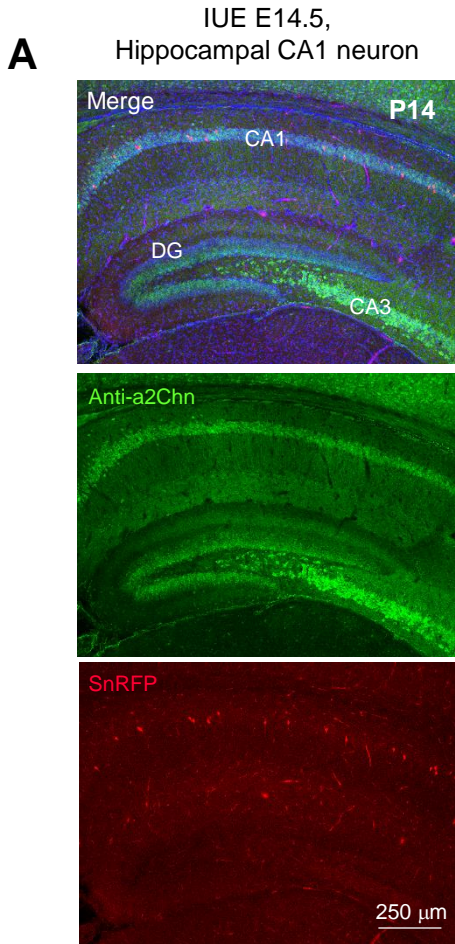


Figure 24



D

	RFP-negative cells (Control)	RFP-positive cells ($\alpha 2\text{-Chn-TALEN}$)
$\alpha 2\text{-Chn}^{\text{high}}$	1354	0
$\alpha 2\text{-Chn}^{\text{low}}$	47	15
$\alpha 2\text{-Chn}^{\text{neg}}$	25	38
Total cells	1426	53

Figure 25

